Fatigue in hopper dredgers

# Fatigue assessment of trailing suction hopper dredgers

## A study on the contribution of the dredging cycle to the fatigue damage in the bottom door openings

L. Blekman

Delft University of Technology

TU Delft

BUREAU VERITAS

TU Delft

BUREAU VERITAS

# Fatigue assessment of trailing suction hopper dredgers

## A study on the contribution of the dredging cycle to the fatigue damage in the bottom door openings

by

L. Blekman

to obtain the degree of Master of Science
at the Delft University of Technology,
to be defended publicly on Friday February 23, 2018 at 15:00 AM.


| | | |
|---|---|---|
| Student number: | 4400496 | |
| Project duration: | March 2, 2017 – February 23, 2018 | |
| Thesis committee: | Prof. dr. ir. M. Kaminski, | TU Delft, supervisor |
| | Dr. Ir. J.H. den Besten, | TU Delft |
| | Dr. Ir. R. Helmons, | TU Delft |
| | Ir. N. Daniels, | Bureau Veritas |




TU Delft

# Abstract

Since the 19th century hopper dredgers have been used for civil operations such as land reclamation and water way maintenance. In the past 25 years a trend of scale enlargement of hopper dredgers driven by economic and productivity reasons is seen. Scaling of the designs has effect on strength and fatigue assessment as well on settling of particles which affect the rate op production. This thesis is focussed on the fatigue assessment of the the hopper dredger. Cracked damages in coaming and bottom door areas have been found in relatively large hopper dredgers that are classed by Bureau Veritas. According to Bureau Veritas rules for steel ships fatigue assessment is required if the ship has length greater than 170 m but damages have also been observed in hopper dredgers with a smaller length. This indicates that the hopper dredger design demands for a specific fatigue assessment procedure. The hopper dredger has a unique characteristic load profile consisting of loading and unloading cargo several times a day in combination with small wave heights due to reduced freeboard regulations. Special interest is given on the effect of the loading and unloading cycle in the corners of the bottom discharge openings. It is suspected that the effect of this characteristic cycle may be underestimated and requires an alternative assessment procedure. The main question is what the contribution of this cycle is and how it should be assessed. The relatively low frequency of the cycle raises the suspicion of low-cycle fatigue and this phenomenon is therefore investigated.

The main parameters regarding the current fatigue requirements are evaluated for use within a simplified fatigue assessment of a hopper dredger. A modern representative hopper dredger design is analysed from load profile determination up to fatigue life prediction. A finite element model is used to establish the structural response of the ship to the hopper dredger specific load profile. High multi-axial stresses are found in the bottom door opening corners. Principal hot spot stress ranges in details of the bottom opening corners are calculated and used for a sensitivity analysis of parameters in the simplified fatigue analysis. It is seen that a fully loaded hopper approaches the structural strength limits of the design and results in significantly large stress ranges in structural details found in the assessed bottom opening corners.

It is concluded that the loading and unloading cycle has a major contribution to the fatigue damage in the bottom opening corners. In fact 97% of the fatigue damage is induced by the dredging cycle and therefore this cycle could be seen as the sole cause for fatigue cracks in the bottom opening corner structural details. The high stress ranges confirm the suspicion of a low-cycle fatigue phenomenon and therefore further research is done on how to approach this type of fatigue. A method is proposed to take into account bi-axial cyclic plasticity and material hardening based on the use of a maximum principal hot spot stress range. Linear-elastic stresses are corrected to pseudo elastic stresses and effects of SN-curve selection, material selection, bi-axiallity and residual stress are analysed. Based on the found pseudo hot spot stress ranges it is concluded that the linear-elastic stresses in the analysed hopper are not high enough to demand for such a low-cycle fatigue assessment approach. The bi-axial ratio between the two multi-axial plane stress components has no effect on this conclusion.

# Acknowledgements

This report documents the final phase of my studies to obtain a Master of Science degree at Delft University of Technology. Several people have supported me in multiple ways throughout the process and therefore I want to share my gratitude. I have learnt a ton in the performance of this project and enlarged my knowledge theoretically and gained experience on the execution of such a project.

First of all I want to thank my graduation committee for the support in the realisation of this thesis. Feedback during progress meetings has helped my to find a coarse within the extensive subject of this thesis. Special thanks goes to Henk den Besten who made time to sit with me and discuss my questions anytime I was stuck in the process.

Secondly, I want to thank Bureau Veritas for the opportunity to work on this project and providing me with the proper tools in the performance of it. In addition I want to thank the colleagues at Bureau Veritas for their support and making the office a pleasant place to work. Especially Nick Daniels, Gerhard Vreugdenhil, Sietse Bolt and Thijs Noyon for their review of my work, support and input during weekly progress meetings. Nick, thanks for supervising me, joining me during out of office meetings and reviewing my thesis work and writing.

Finally I would like to thank my friends and family for their understanding throughout this on occasionally tense period. Thanks to the GOTM for giving me the sometimes needed distraction. A special thanks goes to Liona Kuikhoven who helped me tremendously during times of disability and giving me great support through difficult phases. Now we are finally both on the other side of the medal.

*L. Blekman*
*Delft, February 2018*

# Contents

# Nomenclature

| | | |
|---|---|---|
| S | Spectral moment | [MPa] |

**Acronyms**

| | |
|---|---|
| BV | Bureau Veritas |
| HWBM | Horizontal wave bending moment |
| HWBM | Verital wave bending moment |
| IIW | International institute of welding |
| SWBM | Still water bending moment |

**Greek Symbols**

| | | |
|---|---|---|
| $\alpha$ | Indicates an angle | [deg] |
| $\beta$ | Magnification factor of standard deviation | [-] |
| $\delta$ | Scale parameter of Weibull long term distribution | [-] |
| $\Delta\sigma$ | Stress range | [MPa] |
| $\epsilon$ | Strain | [mm/mm] |
| $\epsilon_1$ | First principal strain | [mm/mm] |
| $\epsilon_2$ | Second principal strain | [mm/mm] |
| $\epsilon'_f$ | Fatigue ductility coefficient | [-] |
| $\gamma$ | Shape parameter of Weibull long term distribution | [-] |
| $\gamma_w$ | Walker mean stress correction material paramter | [-] |
| $\lambda$ | Bi-axiality ratio | [-] |
| $\nu$ | Poison's ratio | [-] |
| $\omega(s)$ | Normalized warping function | [-] |
| $\rho$ | Density | $[kg/mm^3]$ |
| $\sigma$ | Stress | [MPa] |
| $\sigma_1$ | First principal stress | [MPa] |
| $\sigma_2$ | Second principal stress | [MPa] |
| $\sigma'_f$ | Fatigue strength coefficient | [-] |
| $\sigma_n$ | Nominal stress | [MPa] |
| $\lambda$ | Rayleigh coefficient | [-] |

**Roman Symbols**

| | | |
|---|---|---|
| $f_s$ | Correction factor taking into acount supporting member of a cruciform joint | [-] |

| | | |
|---|---|---|
| $f_w$ | Correction factor taking into stress gradient along the weld of a cruciform joint | [-] |
| $K_t$ | Geomteric stress concentration factor | [-] |
| $K_w$ | Weld notch stress concentration factor | [-] |
| $N_f$ | Cycles to failure according to applicable SN-curve | [-] |
| $R_r$ | Probability of occurance | [-] |
| $T_{average}$ | Average wave period | [s] |
| A | Surface area | [$mm^2$] |
| a | Acceleration | [$mm/s^2$] |
| b | Fatigue strength exponent | [-] |
| c | fatigue ductility exponent | [-] |
| D | Fatigue damage | [-] |
| d | Weir level height | [mm] |
| E | Young's Modulus | [MPa] |
| e | Shear centre | [mm] |
| F | Force | [N] |
| g | Gravitational acceleration | [$mm/s^2$] |
| HB | Brinell Hardness | [-] |
| I | Area moment of inertia | [$mm^4$] |
| K | SN-curve characteristic values | [-] |
| K' | Cyclic strength coefficient | [MPa] |
| L | Length of ship | [m] |
| M | Moment | [Nmm] |
| m | Slope of SN-curve | [-] |
| N | Number of cycles to failure | [-] |
| n' | Cyclic hardening exponent | [-] |
| P | Pressure | [MPa] |
| R | Stress ratio | [-] |
| S | Indicates stress | [MPa] |
| T | Draught | [$m$] |
| t | Thickness | [mm] |
| x | x coordinate | [mm] |
| y | y coordinate | [mm] |
| z | z coordinate | [mm] |

**Subscripts**

| | |
|---|---|
| 0.5net | Indicates half of the net value |
| 1 | Indicates first value |
| 2 | Indicates second value |
| 97.7 | Indicates 97.7 probability of survival |
| amp | Indicates cyclic amplitude |
| b | Indicates bending component |
| beam | Value associated with beam characteristics |
| c | Indicates cut plate edge |
| ca | Corrosion addition |
| cargo | Indicates cargo characteristic value |
| cor | Including corrosion correction |
| dr | Value associated with dredging cycle stress range |
| eff | Effective value |
| em | Value associated with empty hopper load condition |
| eq | Indicates equivalent value |
| fl | Value associated with fully loaded hopper load condition |
| gross | Gross value |
| horizontal | Indicates horizontal direction |
| hs | Indicates structural hot spot stress |
| i | Indicates specific load case |
| Inertial | Indicates accelaration component |
| j | Indicates specific load case |
| lca | Indicates BV wave load case a |
| lcb | Indicates BV wave load case b |
| lcc | Indicates BV wave load case c |
| lcd | Indicates BV wave load case d |
| le | Indicates linear elastic value |
| m | Indicates membrane component |
| max | Indicates maximum value |
| mean | Mean value |
| min | Indicates minimum value |
| n | Value at node |
| na | Value associated with navigation condition |
| net | Net value |

| | |
|---|---|
| neutral | indicates neutral position |
| pl | Indicates plastic component |
| pseudo | Indicates pseudo value |
| R | Indicates reaction force |
| ref | Reference value |
| res | Indicates residual stress |
| sd | Specific density |
| shear | indicates shear component |
| shear | indicates shear component |
| shift | Indicates shifted location |
| stdv | Standard deviation |
| tuning | Tuned value |
| vertical | Indicates vertical direction |
| w | Indicates welded joint |
| wave | Indicates wave component |
| wl | Indicates weld leg dimensions |
| x | Indicates valuie in positive x-axis direction |
| y | Indicates valuie in positive y-axis direction |
| yield | Associated with yield characteristics of material |
| z | Indicates valuie in positive z-axis direction |

# List of Figures

# List of Tables

# 1 Introduction

*To clarify the purpose of this thesis, this chapter presents the context of the problem which this thesis deals with. This will give insight on why the research is performed and what the desired end-product is of all the activities performed in the context of this thesis. The main subject of this report is the procedure of fatigue analysis in trailing suction hopper dredgers. The research is based on damages that are found in hopper dredgers and therefore these damages are first analysed in this chapter to establish the magnitude of the problem. With this information a research question and additional sub-questions are formulated. These questions cover the knowledge gap and form the thesis outline to fill this gap.*

## 1.1. Trailing suction hopper dredger

As explained in the introduction of this chapter the main subject of research is the trailing suction hopper dredger. This self-propelled dredging vessel is used for a wide variety of maritime construction and maintenance projects. Activities such as construction and maintenance of harbours and waterways are examples of typical every day operations of the hopper dredger. This ship is used for land reclamation and beach nourishment where the excavated material is used to construct civil structures. The operating activities of a hopper dredger require the dredger to be able to excavate, store, transport and discharge materials like sand, clay and gravel. Hopper dredgers are in most cases custom build ships which leads to a wide variety of designs. Of course there are differences in size, but also in the configuration of the dredging installation and the design of the hull. In **figure 1.1** a schematic illustration of a trailing suction hopper dredger is presented.

### 1.1.1. Loading

For Land reclamation project soil is required to build civil structures or when a harbour needs to be deepened soil needs to be excavated and transport elsewhere. Therefore one of the main functions of a hopper dredger is to excavate soil and load the hopper. When the hopper dredger has reached the dredging area the dragheads are lowered to the seabed. Liquid soil types like silt and soft clay, cohesive soil types like firm clay and rock and non-cohesive soil types like sand and gravel are excavated. The mixture is sucked up with the suction pipe powered by a dredge pump. It is then stored in the cargo hold of the hopper dredger where the solid particles can settle and the density in the hopper can increase. An overflow pipe discharges the excessive water using two types of systems. A constant volume system is a system where the volume in the hopper is constant and the overflow is fixed. Using this system the density in the hopper is proportional to the draught. Loading is stopped when the dredging mark is reached. The second system, a constant tonnage system, enables the adjustment of the overflow level so that more soil can settle and the water can be discharged.

### 1.1.2. Unloading

After loading the hopper navigates to the discharge area. When the reclamation or dump site is reached the material can be discharge in multiple ways. This is either done by pumping to the required destination, 'rainbowing'(ejecting the mixture through air to the deposit site) or by dumping the sediment. Two types of hull mechanisms are used for dumping of dredged sediment. This could be done by splitting the hull, and therefore opening the bottom of the cargo hold, to discharge to the seabed. The second type of mechanism is opening the doors in the bottom of the hopper. If the hopper is equiped with bottom door it is not able to split

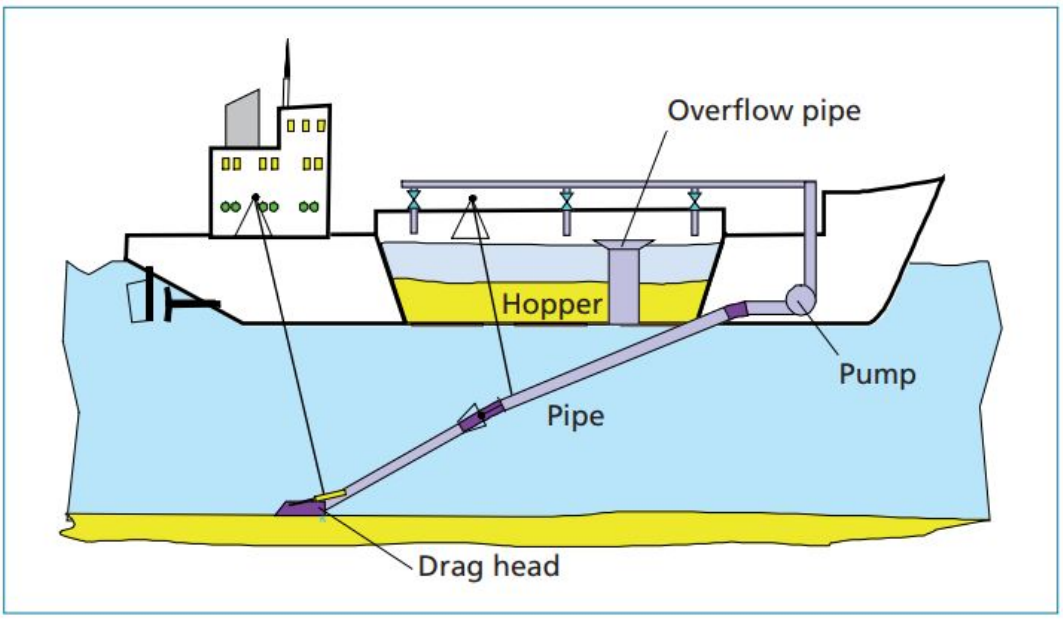


Figure 1.1: Schematic drawing of a hopper dredger [19]

open. The unloading time depends on the hull design configuration and the dredged material. Discharged time is reduced if jets are installed inside the hopper to loosen the soil for a better discharge flow through the doors. If for example small rocks or gravel is dredged the solid material could also be discharged dry in a port which does however increase the discharge time.

### 1.1.3. Hull design

In this section the hull designs of hopper dredgers with bottom doors will be further elaborated. The earlier mentioned split hopper dredgers in section 1.1.2 will not be included in the subject of fatigue in hopper dredgers. The main reason for this is the fact that the damages which are found in hopper dredgers are mostly found on hopper dredgers that discharge through bottom doors which are not used in split hopper type dredgers.

Hopper dredgers can be built as single or double well ships [81]. In this thesis these will be called respectively hull designs with a V-shape or a W-shaped cross section. In the past, around 1970, hopper dredgers where equipped with two parallel hopper well lines which are separated with a so called cellular keel construction, the cellular keel. This is a construction spanning the end bulkhead and dividing the bottom door lines which can be seen in **figure 1.2a**. This layout has the advantage that more bottom openings are possible to open for discharge. Another typical design is the v-shaped hopper dredger where bottom door opening corners are positioned in one row along the length of the ship. This design is presented in **figure 1.2b**.
When the hopper is filled and the ship is above discharge location the hopper is unloaded through bottom doors. From an economic point of view this process has to be done as quick as possible with as little sediment left as possible. Bottom door patterns determine the discharge speed. Increasing this speed can be done by increasing the number of wells and the size of the wells keeping in mind the strength integrity of the hull. Here one of the main concerning areas in the hopper hull design arises: the corners of the bottom door openings. Why this is will be further explained in section 1.3. One of the factors contributing to the force magnitude on these structural details is the design configuration. Multiple configurations are given by Bureau Veritas rules [9]. The dumping systems in the hopper well have to meet some requirements for optimal design [81]:

- Fast discharge. Seek for a plane symmetrical flow.
- No protruding parts in door opening.
- Proper sealing of bottom doors.
- No influence on ship resistance.
- Easy maintenance.

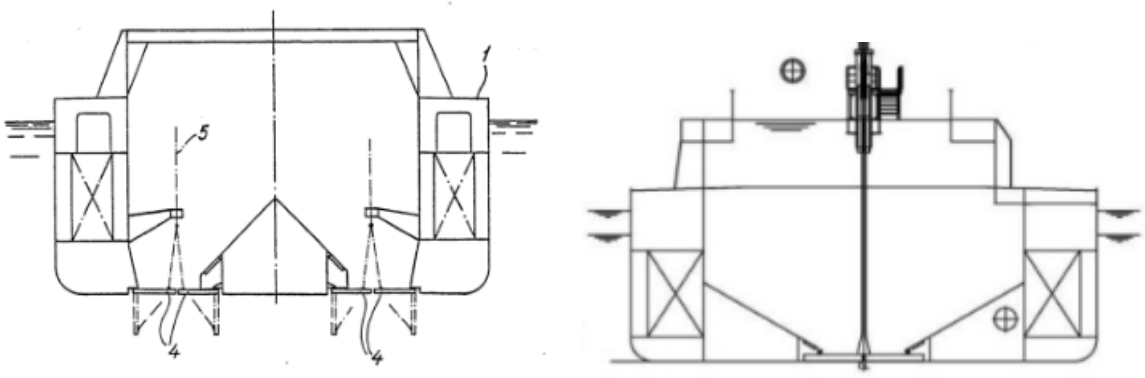


(a) (b)

Figure 1.2: **(a)** Midship cross section W-shaped hopper dredger, **(b)** Midship cross section V-shaped hopper dredger

- Shallow water discharge.

The structural design of the hull is pushed to its limits by increasing bottom door size and quantity to decrease the discharge time. In addition, hopper coamings are raised to enclose more volume in the hopper which leads to limitations regarding stability and hull strength [34]. Stability is effected due to a higher centre of mass and additional global and local loads require impractical dimension of the ship.

With the loading and unloading cycle of the hopper dredger it shows itself different from other bulk cargo ships. Instead of loading and unloading ones a week a hopper dredger could be loading and discharging up to six times a day. This frequent hopper loading changes the load condition of the hopper. It has a major contribution to the minimum and maximum longitudinal bending moment in the ship. The fluctuation between the bending moments is cause for difference in structural response of the ship. which is interesting in terms of fatigue.

## 1.2. Classification of hopper dredgers

This thesis is performed in co-operation with Bureau Veritas Rotterdam. This company is a classification society and does the classification for a wide variety of products and services. In Rotterdam, ship and offshore structures like a hopper dredger are classified. The classification society develops rules and guidance notes that form a standard to assure safe design and compliance with regulations. A ship sails under a flag state. The flag state determines laws and regulations to which the ship design and crew have to comply and these regulations are incorporated in the rules and guidance notes. To account for unforeseen events a ships is insured on the condition of safe design and operations and regulations. The insurance company therefore requires the owner to have a certificate provided by the classification society that assures compliance with the rules and regulations. In the design phase, plans and calculations are reviewed to demonstrate that rules are met and in operation frequent surveys, checks and tests are performed to see if rule requirements are still fulfilled sufficiently. Periodical surveys are performed throughout the design life of the ship to verify if class requirement are fulfilled. Occasionally it could be necessary to perform surveys in case of design adjustments or damage. It is the owners responsibility to request a survey to make sure the ship meets all class requirements.

Ships that are classed are given specific classification notations which describe the scope of rules to which the ships complies. Classification notations contain a class symbol, construction marks, service notations, navigation notations and optionally operating area and additional class notations. The service notation of a hopper dredger is specified as a ship specially equipped for dredging activities and carrying spoils or dredged material. The optional operating area notation for dredgers are [2]:

- Dredging within 8 miles form shore
- Dredging within 15 miles form shore or within 20 miles form port
- Dredging over 15 miles form shore

For a hopper dredger to maintain its class notations periodic surveys such as annual and class renewal surveys are performed. Class renewal surveys are done every three of five years depending on the class notation. The classification of the ship will be extended for a new period until the next class renewal survey. Annual and class renewal surveys contain visual examination and external examination of attachments and piping checks on the condition of the dredging machinery space and equipment. For class renewal additional visual examination is required of bottom doors. Occasional surveys are performed in case of the following situations [2]:

- Update of classification documents
- Damage
- Repair or renewal
- Port state control inspections
- Alternation or conversion
- Quality system audits
- Postponement or surveys or recommendations

Damages such as indents, bended material, holes, corrosion and cracks are usually the type of damages that are observed. The damages and repairs, in case these have already been done, are reported in survey reports. Any damage that, in opinion of the surveyor, will affect the ship's structural, watertight or weathertight integrity, is to be repaired [2]. This could be an immediate repair, or it could be required that the vessel is send to a suitable location for repair. In case of a repair, or temporary repair, the reparation method will be assessed and it could be required that repairs are required to be monitored or redone.

Damages found in hopper dredgers are reported in survey reports which are available to the author of this thesis. To get an indication of the locations, types and frequency of the damages, survey reports on BV classed hopper dredgers are examined in the next section.

## 1.3. Damage reports

A large amount of hopper dredgers is operating with Bureau Veritas classification. It is inevitable that these ships will suffer some kind of damage during their operating lifetime. These damages come to light during the scheduled or requested surveys which are required for the operating company to maintain classification of the ship. These damages are, in most cases, documented in the ship files of Bureau Veritas.

An analysis is done on the survey reports to find the damage cases that indicate fatigue damage. The reports only provide information about the found damage and do not classify the damage as fatigue. This means that visual inspection and damage descriptions are used to determine if fatigue is the cause of damage. Some examples of cracks that are found on hopper dredgers can be seen in **figure 1.3a**, **1.3b** and **1.3c**. A damage case is considered fatigue damage if a crack is found. Fatigue cracks are a result of specimens subjected to cyclic loading and therefore cracks are a first indication that a damage could be fatigue [71]. Cracks can be caused by a variety of failure mechanisms therefore the damage cases that describe a crack are analysed to make sure the damage is not caused by a collision or is formed due to buckling of a plate.

### 1.3.1. Fleet analysis

According to J Schijve [71] a first question in failure analysis is whether a failure is symptomatic or incidental. To see if this is the case for the damages found in hopper dredgers the survey reports of 125 Bureau Veritas classified hopper dredger have been analysed. The survey reports mention cracks in 16% of the hopper dredgers. This is a significant amount of fatigue failures keeping in mind that all dredgers are designed for a fatigue life time of at least 20 years [8]. The damage is categorized according to the location where it was found. This is illustrated in **figure 1.4b**. It can be seen that most of the damages are found in the bottom opening, coaming and void tank areas.

(a) (b) (c)

Figure 1.3: **(a)** Crack in welded detail hopper corner area, **(b)** Crack in base material hopper corner area, **(b)** Crack in weld coaming area

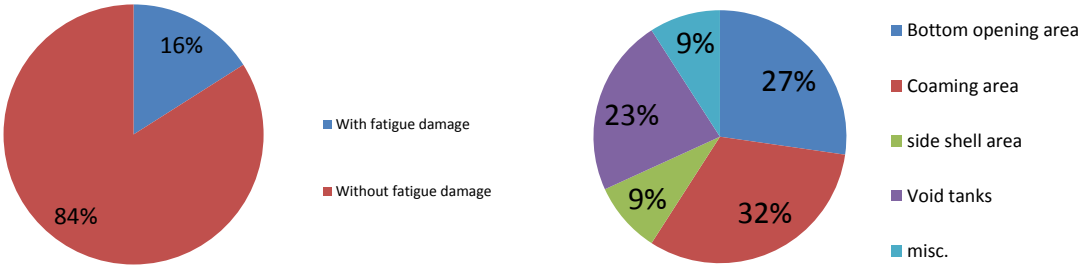


(a) (b)

Figure 1.4: **(a)** Proportion damaged hopper dredgers, **(b)** Proportion damaged areas

In **figure 1.5** the gross tonnage against the rule length of the ships is illustrated. These parameters are used to see the relation between the size of the ship associated with the damages. Fatigue damage is found in relatively large hopper dredgers and quite some hopper dredgers with a rule length $L < 170m$ m are affected by fatigue. 81% of the fatigue damaged hopper dredgers has a length of $L < 170m$. This number has to be nuanced because 90% of the classed hopper dredgers have a length smaller than the length limit for fatigue analysis. According to BV rules fatigue assessment is required for ships with $L > 170m$ and fatigue resistance for ships with a smaller length is incorporated in the global strength assessment and k-factor for material which is an adjustment for higher yield strength. 14% of ships with $L < 170m$ have shown cracks where 40% of the ships with $L > 170m$ have reported crack damages.

### Operational time

The design life time of hopper dredgers is 20 to 25 years. All cracks, except for one, that where found are detected within the design lifetime of the ships. Even 60% of the cracks are found within ten years after the date of build. The average time to failure is about eight years with some damages in the end of the design life and some already after one year. An important factor in fatigue damage is the amount of repetitions of the loading. Therefore the time until failure is seen as an important parameter in the search for the reasons for fatigue failure in hopper dredgers. The time until failure is given in a block diagram in **figure 1.6**. The time until the cracks are found is widely distributed, meaning there does not seem to be a pattern in the time until Structural details of a hopper dredger show signs of cracks. Information about the operating locations of the hopper dredgers in the fleet is unknown and could affect the time until failure significantly. This could be an

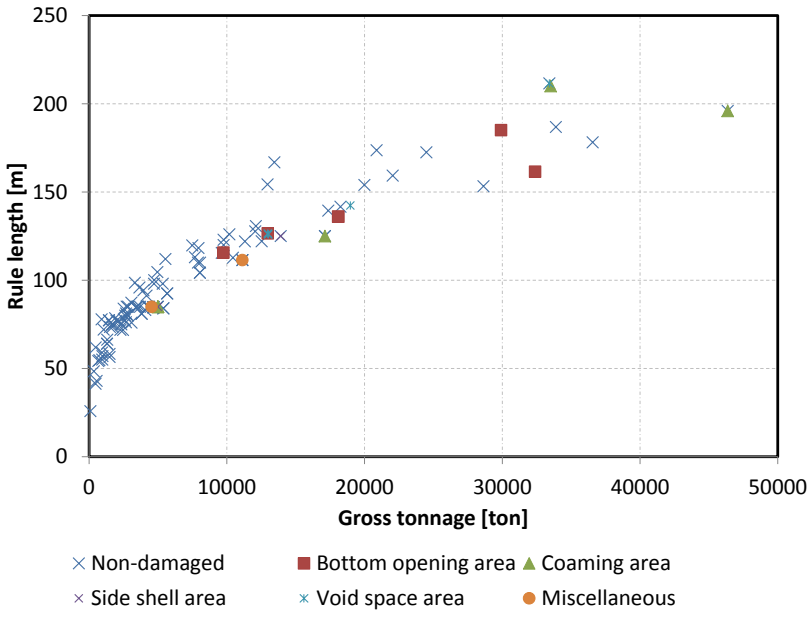


n

Figure 1.5: Damaged hopper dredgers; gross tonnage against rule length

explanation for the wide scatter in time until failure.

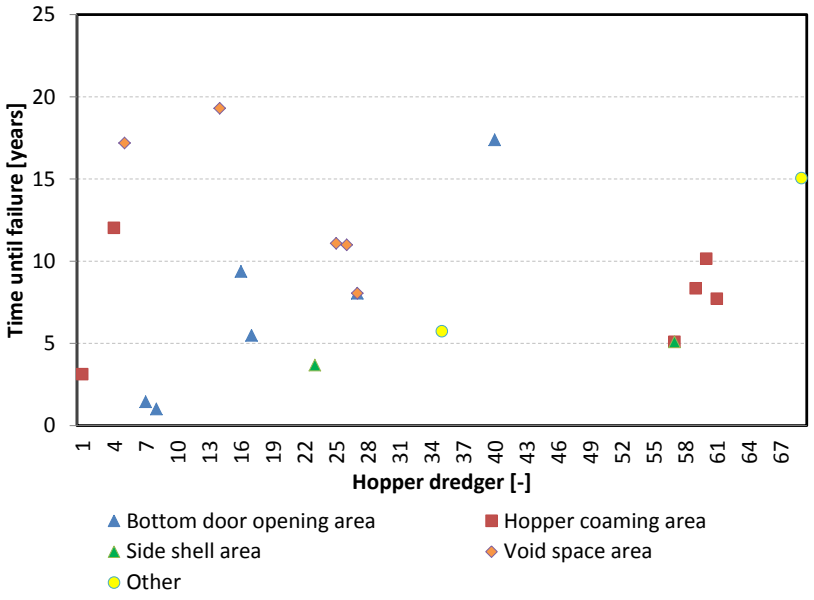


Figure 1.6: Time until damages is detected

### 1.3.2. Damaged details analysis

The damages that are found are independent on the overall dimensions. The fact that most damages are seen in relatively large dredgers is the main similarity the fatigue damaged hopper dredgers have. With this in mind it is interesting to zoom in on the locations where the damages are found. Most of the damages are found in the corners of the bottom openings and at the expansions joints in the coaming. Both locations have cracks in welded connections as well in cut plate edges. In general the damages in the bottom opening corners are found in three locations. The welded connection of the insert plate with the bottom plating, the cut plate edge of the insert plate itself and the welded connection of the transverse box with the longitudinal

bulkhead of the hopper. The cracks in the coaming area are seen in the welded connection of the crossbeam and the coaming. At this location a expansion joint is located in the coaming. Cracks are also seen in the cut plate edge of the expansion joint itself.

### 1.3.3. Conclusion of damage report analysis

The damage analysis can be summarized by first looking at the global parameters of the entire fleet. Damages are found in ships with relatively large lengths in a range from 84 up to 196 meters. Although the portion of damaged ships with $L > 170m$ is higher, a significant amount of cracks is found in ships with length below this length. There was no direct correlation found between the global dimension and the damaged ships. Also the design configuration does not seem to determine the change of fatigue damages. The cracked details in the damaged areas are identified. Because fatigue is a local problem it is expected that these details need further analysis to find the reason for the damage. The crack damages seem independent of the specific designs and fatigue in the dredgers is a global problem.

## 1.4. Problem definition

### 1.4.1. Research question

The previous section has led to a conclusion that the fatigue damage is caused by a global phenomenon. It is suspected that this is caused by the loading and unloading cycle mentioned in section 1.1.3. In FPSO's it already seen that the large stress range due to loading and offloading has a significant contribution in the fatigue life. This is because the loading and unloading cycle is considered different to that of oil tankers. FPSO's load and unload cycle can be up to once a day which is significantly more often than oil tankers and bulk carriers which load/unload ones every week. Low cycle fatigue is believed to have a significant contribution to FPSO fatigue damage and the loading/unloading cycle is the single most significant load case causing low cycle fatigue [60]. The dredging cycle of a hopper dredger occurs in the same order of frequency and up to six times a day. It is therefore suspected that this cycle has also a significant contribution to the fatigue life.

It is already noticed by G. de Jong that the dredging cycle should be taken into account in the fatigue analysis of hopper dredgers [24]. He states that the fatigue damage of the dredging cycle cannot be seen independent to damage induced by wave loading and would lead to a underestimation of the total fatigue damage. Currently BV rules do not require this cycle to be included in fatigue calculation and only the change in load condition between ballast and full load is taken into account. Fatigue damage is calculated with design S-N curves based on high cycle fatigue data. The loading and unloading cycle of a hopper dredger has however a low frequency compared to the high frequency cycles of the wave loading and raises the suspicion of low-cycle fatigue. This type of fatigue is associated with high stresses in each cycle and a low amount of cycles until failure.
This all leads to the research question of this thesis:

***What is the influence of the dredging cycle on the fatigue life of hopper dredger structural details?***

This thesis will focus on fatigue due to the dredging cycle and what its role is in the entire fatigue damage of a hopper dredger. Part of this is to identify the critical locations in a hopper dredger and to formulate a method to determine the structural response in these details. This response will be analysed and a suitable fatigue assessment method is presented on the basis of the analysis. A hopper dredger will be assessed on fatigue life according the proposed fatigue assessment method and the influence of the dredging cycle will then be up for discussion.

### 1.4.2. Sub-questions

A hopper dredger is a complex structure and it is expected that the fatigue life is affected by a wide variety of variables which should be taken into account in the assessment. These could be design specific aspects but also parameters determine by the working environment of this vessel. So the first sub-question is:

***What are the main parameters affecting the fatigue life of structural details in the hull structure of a hopper dredger?***

The type of fatigue mechanism is an important factor in determination of the contribution of the dredging

cycle. Low-cycle loading goes often hand in hand with high stresses that cause plastic deformation. This changes the local material properties and the process of fatigue crack initiation and leads to the second sub-question:

***Could the dredging cycle be seen as a low-cycle fatigue phenomenon?***

The amount of damage of the dredging cycle itself could have large contribution due to the large stress range that is associated with this cycle. If low-cycle fatigue is the case this also comes with additional plasticity phenomena which have a large effect on the fatigue resistance of the structural details. The third question is therefore:

***To what extent does the still water cycle contributes to the fatigue damage of high stressed structural details in hopper dredgers?***

The dredging cycle is not the only loading that is experienced by the hopper dredger. High cycle wave loading is seen as the main source of fatigue damage in ship structures. To determine the fatigue life of a hopper dredger the combination of these two cycles is required to take into account. The question is how to combine these two sorts of fatigue in terms of accumulated damage.

### 1.4.3. Research goal

The focus of this research is on the understanding of crack initiation behaviour in hopper dredger hull designs. The goal is to identify the main fatigue influencing parameters and to propose a simplified fatigue assessment protocol which provides low threshold guidance to determine the fatigue life of hopper dredger specific details. Although fatigue analysis is done on hopper dredgers and ships in general, knowledge on the effect of the dredging cycle and hopper dredger specific details is still a unexplored area. So the protocol is constructed to strive for better understanding and more accurate assessment of these subjects.

## 1.5. Thesis structure

In **chapter 1** the problem of fatigue in hopper dredgers is elaborated and a study is performed on survey reports to get an idea of the magnitude of the problem. Based on the problem research question are formulated to point out the direction of this thesis.

**Chapter 2** provides technical background and current knowledge knowledge in the areas of fatigue assessment and hopper dredger designs. Gathered information is used to formulate the research methodology used in this thesis.

In **chapter 3** an existing hopper dredger is chosen for structural analysis throughout this thesis. The structural behaviour of this dredger is considered to be applicable to all dredgers in principle. Hopper dredger have more or less the same load profile since they have the common purpose of dredging soil, storage and discharge. First the load profile of the dredger is formulated by starting with the dredging cycle using global ship loading documents and dredging process literature. The dredging cycle is described with multiple steps so that a maximum load range can be found and the load path could be checked on proportionality. To complete the load profile the wave loads are added with the simplified approach using BV load cases. The maximum wave load cases are identified and the probability of the stress range is adjusted so the amplitude of the wave can be added up to the dredging cycle. An indication of the structural response of the hopper dredger to the operation profile is obtained with analytical calculations and a 2D analysis using MARS 2000 software. The results are used as validation for a 3D FE analysis and to determine the loads which have to be applied on the 3D model. A bar stiffened plate model is introduced and this model is loaded with the still water pressures of the dredging cycle load steps and wave pressures of the BV load cases. The model is tuned to create a realistic loading condition at the location where the model is assessed. A coarse mesh analysis is performed to indicate high stressed areas in the bottom opening corners of the hopper and to obtain the structural response to the earlier identified loading conditions. The mesh of the high stressed areas is refined according applicable procedures and the hot spot stress is measured at the locations where high stress is seen in the fine mesh. The maximum principal stress is used to define the fatigue stress ranges.

In **chapter 4** the dredging cycle- and wave stress ranges are adjusted by fatigue influence factors to compare the stress ranges with the applicable BV SN-curves. The fatigue life and damage of the particular hopper dredger is calculated and the contribution of the dredging cycle is established. The main parameters affecting the fatigue life prediction are identified and the sensitivity of these parameters is analysed to see the effect of uncertainties in current design procedures compared to proposed alternative methods. The results of fatigue life prediction and effect of main parameters is discussed.

In **chapter 5** Hot spots prone to low-cycle fatigue are analytically assessed with use of Neuber's rule, cyclic stress-strain curve and the pseudo hot spot stress. Two methods to taken into account bi-axial plane stress are selected and compared with the uni-axial approach using Neuber's law. A proposal is made to assess the stress range in case of low cycle fatigue with cyclic plasticity and its applicability for hopper dredger fatigue assessment is discussed.

All aspects of this thesis are discussed in **chapter 6** and conclusions are drawn from its findings. Recommendations are given on the subjects in this thesis and suggestions for further research is presented.

# 2

# Technical background

*In this chapter the current knowledge regarding fatigue in hopper dredgers is elaborated and a method to address the research question is proposed. The literature consists of internal knowledge by Bureau Veritas and external knowledge in the form of scientific papers, books and material for educational purposes. First literature concerning research about hopper dredgers is presented. Hereafter different components of the hopper dredger and fatigue analysis in itself are further discussed to get an overview of the variety of aspects to the fatigue analysis of a ship such as the hopper dredger*

## 2.1. Research regarding hopper dredgers

In the late seventies and the early eighties a resurgence of hopper dredger construction is seen. This has lead to new interest in improving the design to make the dredging process more efficient and to decrease the cost of operation. In 1980 a paper is presented by E. Fortino on three new modern state-of-the-art hopper dredgers that are commissioned by the U.S. Army Corps of Engineers [33]. It discusses new design features that are still seen in today's hopper dredgers. These design features and additional features are also discussed by J.P. Martin and L.J. Mauriello [58].

It has become clear that relatively little research is available regarding the specific topic of fatigue in hopper dredgers. The subject is only found to be addressed in a paper by de Jong (2010) [24]. From an economic point of view the main subject in literature regarding hopper dredgers is about the sedimentation of the hopper. Research on the loading of the hopper is done by Miedema [62] and educational material is provided in the course dredging processes of the TU Delft [61]. These documents provide information that is useful to construct the loading process of the hopper.

The subject of the matter can be divided into multiple topics. The hopper dredger is a ship and therefore the calculation standards for ships is deemed acceptable to assess the structural integrity of the hopper dredger. The knowledge about fatigue assessment is in itself a topic that is continuously in development and the phenomenon is independent of the structure of concern. Considering this the rest of this literature review the two topics are reviewed independently due to the lack of literature that covers both hopper dredger and fatigue assessment. The structural response to the loading of the hopper dredger is analysed and applicable methods are used to acquire suitable input for an assessment approach

## 2.2. Operational profile of a hopper dredger

Fatigue is a result of static and dynamic loads to which, for example, a hopper dredger is exposed to. The frequency and magnitude of these loads is a result of the working conditions of the hopper. It is therefore necessary to determine the operational profile of the dredger to identify the main parameters of influence. The operational profile of the hopper dredger is described by the operational time during the service life, the load cycle of the hopper and the wave loading during navigation or dredging operations. The profile forms the basis of the fatigue loads on the structural details in the ship structure. Fatigue loads could be divided into two types of loads, primary and secondary loads [57]. Long term primary fatigue loads are:

- Global hull girder bending loads
- Local water oscillating loads
- Cargo loading and unloading (low cycle effects)
- Still water bending (mean level) effects

Secondary fatigue loads are:

- Slam effects
- Springing loads
- Thermal loads
- Propeller and machinery vibrations

The primary fatigue loads contribute the most to the long term fatigue damage and secondary fatigue loads are often neglected in design. Taking the aim of this thesis into account, It is chosen that the focus will be on the primary loads and the secondary loads are deemed negligible. It is assumed that the dredging cycle only effects the primary loading of the ship.

### 2.2.1. Operational time

In fatigue calculations the time in which a hopper dredger is sailing is 85% of its lifetime according Bureau veritas rules [8]. The other 15% of the time the dredger is in harbour or dry dock for repairs or inspections. During navigation the dredgers is considered to be in ballast condition and this is 20% of the sailing time. The rest of the time the dredger is 50% operational in ballast condition and 50% operational in fully loaded condition. This leads to the assumption that the hopper dredger is 60% of its operational time in ballast condition in navigating area and 40% in fully loaded condition in operating area. Note that this is a conservative assumption due to the assumption that dynamic loads at least equal that of the dynamic loads in the operating area. The distribution of the operating conditions is shown in **figure 2.1a**.

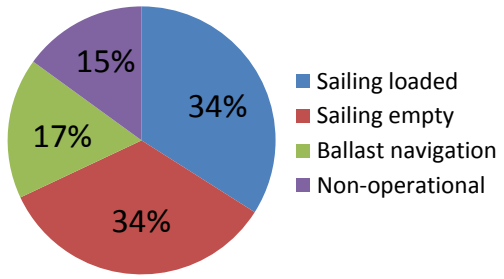


(a)

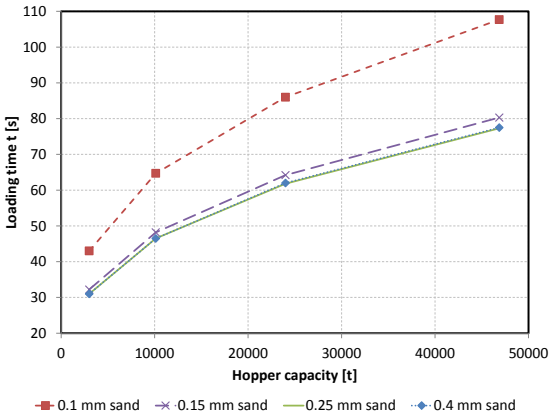


(b)

Figure 2.1: **(a)** Operational conditions Hopper dredger design life, **(b)** Loading time hopper as function of hopper capacity for multiple sand particle sizes [62]

Miedema has done sensitivity analysis of the scaling of hopper dredgers focussed on the the efficiency of hopper loading. It is found that scaling of a hopper has little effect on overflow losses if correct scale parameters are applied. In figure 2.1b the loading times that are found are presented as function of hopper size. Larger dredgers require more time to fully load the hopper and means that the dredging cycle frequency depends on te size of the hopper. This is an interesting observation considering the fact that hopper dredgers below and length of $L < 170$ do not require fatigue calculation for classification but will experience more dredging cycles compared to larger dredgers.

### 2.2.2. Load cycle

The loads are determined by the operating sea state, wave directions, loading and unloading conditions and speed of the ship. The hull of the hopper is exposed to multiple loads from multiple sources. External loads are applied by still water hydrostatic and wave hydrodynamic pressures and internal loads originate from the stored cargo in the hopper, which varies in density during loading of the hopper. The internal loads depend on the cargo density in the hopper and the level up to which the hopper is filled. The specific density of a fully loaded hopper could be up to $2.2t/m^3$.

The loading and unloading of the hopper results in a still water load cycle. A fully loaded hopper is associated with a maximum sagging still water bending moment and if the hopper is empty a maximum hogging moment present. These still water bending moments are vertical bending moments around the transverse axis of the ship and are a result of distributed shear force along the longitudinal axis of the ship. The shear force is a resultant of the difference between the upward hydrostatic pressure and the internal pressure of the spoil inside the cargo hold. According to Euler-Bernoulli simple beam theory the maximum sagging and hogging moments are seen at the location on the longitudinal axis where the resultant of the shear force is zero. So it could be concluded that the bending moment in the hopper dredger is largely affected by its loading state. In some cases the hogging bending moment is reduced by filling the hopper with water while sailing 'empty' [61]. In fully loaded condition a maximum sagging moment is usually found at midship location of the ship. Studies on the load cycle of a hopper for fatigue only the fully loaded and empty hopper conditions are of significance with the following loading conditions [24]:

- Dredger loaded to dredger load line considering cargo in liquid state.
- Dredger loaded to dredger load line considering cargo in solid state.
- Dredger sailing with empty hopper.

The cycle occurs several times a day and therefore this still water stress cycle cannot be considered static, of very low frequency or of negligible magnitude and is to be included in the fatigue strength assessment [78]. In this case static means that the loading is not considered cyclic. The dredger is normally fully loaded and entirely empty considering economical dependency. Therefore this loading/unloading cycle results in a nearly constant amplitude stress range [24]. Four loading conditions are applicable for dredgers [78]:

- Ballast in navigation area.
- Fully laden on international draught in navigation area.
- Fully laden on dredging draught within operating area.
- Ballast draught within operating area.

Classed hopper dredgers have a certain dredging notation which specifies the dredging marks of a fully loaded hopper. This mark is specified by a certain maximum draught associated with a maximum distance from shore. So the dredging mark is for example expressed by dredging mark I and dredging mark II. The classification society species a maximum allowable significant wave height for each dredging mark and a maximum operating distance form shore. The maximum significant wave height a hopper dredger will experience in its life time is relatively low due to the small free board which is up 3.5 meter. Note that this is only during dredging operations. When a dredger is sailing in transit it is allowed to sail at greater significant wave heights. The significant wave height associated with the load condition are given in **figure 2.2** and the wave loading is further explained in section 2.2.3.

### 2.2.3. Wave loading

Environmental loads are the dominating loads in the design life of marine structures [13] and wave and current loads are considered to be the most significant. The wave loading is divided into the global and local loading of the ship and methods to include wave loading in the fatigue assessment. The fatigue assessment approaches will be further elaborated in section 2.3.1.

The loading and unloading cycle of the hopper results in static loads on the hopper. The waters in which a hopper dredger is operational are not completely still due to the fact that a sea state working environment is the main operating environment of the ship. Therefore quasi static or dynamic wave loads have to be taken

| Operating area | $n_D$ | Associated $H_S$, in m | | |
|---|---|---|---|---|
| | | L ≤ 110 m | 110 m < L ≤ 150 m | 150 m < L ≤ 180 m |
| **dredging within 8 miles from shore** | 1/3 | $H_S < 1,5$ | $H_S < 2,0$ | $H_S < 2,0$ |
| **dredging within 15 miles from shore or within 20 miles from port** | 2/3 | $1,5 \le H_S < 2,5$ | $2,0 \le H_S < 3,0$ | $2,0 \le H_S < 3,5$ |
| **dredging over 15 miles from shore** | 1 | $H_S \ge 2,5$ | $H_S \ge 3,0$ | $H_S \ge 3,5$ |

**Note 1:**
$H_S$ : Maximum significant wave height, in m, for operating area in dredging situation, according to the operating area notation assigned to the ship (see Pt A, Ch 1, Sec 2, [4.6.3]).

Figure 2.2: Allowable significant wave height for Bureau Veritas classed dredgers [9]

into account in the strength and fatigue calculations of the structure. Two types of waves are considered for design; head waves, waves that travel in the same direction of the ship, and oblique waves, waves that travel in a different direction than the course of the ship. Head waves cause for additional vertical shear force and bending moment in the ship and therefore increase the hogging and sagging moments of the still water loading. Oblique waves also increase the vertical force and bending moment and result in additional horizontal shear force, horizontal bending moment and a torsional moment along the length of the ship. Hopper dredgers have large deck openings to fill the hoppers and bottom openings for discharge. Ships with these kind of large openings have lower torsional rigidity than ships with a closed cross section. Torsional loading of these type of hull designs could lead to high shear stresses in the hull. and in addition, the rotational twisting of the cross section causes warping which leads to additional stress in longitudinal direction. Warping is displacement, caused by torsional loading of a structure, parallel to the axis of torsional rotation. If a structure has free warping boundary conditions these displacements are allowed. In ships with cargo holds, like the hopper dredger, the discontinuities at the end of the cargo hold restrain the warping displacements and are the cause of warping stresses in the cross sections of the hull in the cargo hold. These stresses have an significant contribution to the hull loading for ships with large deck openings [68]. Cross beams are used in the design to increase the torsional rigidity of the hull. These are beams that span the deck opening, at deck height, from port side to star board. The cross beams do however results in stresses in the cross beams which could be linked with the fatigue damage that is found in the coaming area of some hoppers. At the moment Bureau Veritas [8] calculates warping stress with direct calculation using three dimensional finite element and thin walled structural model [8]. There is not a rule based method so calculation is required to be according finite element results.

Not only the global loading is affected by wave induced loads. The local external and internal pressures are also affected. The external sea pressure is increased and decreased due to wave travelling along the side shell of the hull. The internal pressures are changed due to accelerations of the cargo. Ship motions induced by the waves cause accelerations which increase and decrease the internal pressures in the hull. The internal pressure change due to the waves strongly depends on the state of the cargo. Liquid type of cargo is more prone to wave induces accelerations than solid type cargo which is considered to be in a solid state if the specific density inside the hopper has reached $1400 \frac{t}{m^3}$.

The structural analysis of the wave loads is much correlated with the type of fatigue assessment approach that is used. The type of approach determines the level of detail of the fatigue analysis. The wave loading could be based on multiple extreme wave conditions that are combined with a extreme value distribution like a Weibull distribution. A certain probability of the extreme values is used as a reference for the structural analysis of fatigue sensitive details. Note that these two types of approach do not say anything about the operational environment of the hopper dredger and take into account all types of wave loads seen in the world. For a more detailed approach multiple wave energy distributions are combined into a long term wave distribution based on the operational profile of the ship. The short term distributions are based on the known working environments of the ship throughout its lifetime. The speed of the ship has some effect on the structural response of the ship to wave loading. This was seen by C. Soares and T. Moan [72]. The ships speed determines the Froude number of load condition. Increasing Froude number form 0 to 0.26 increases the response by 30% on average.

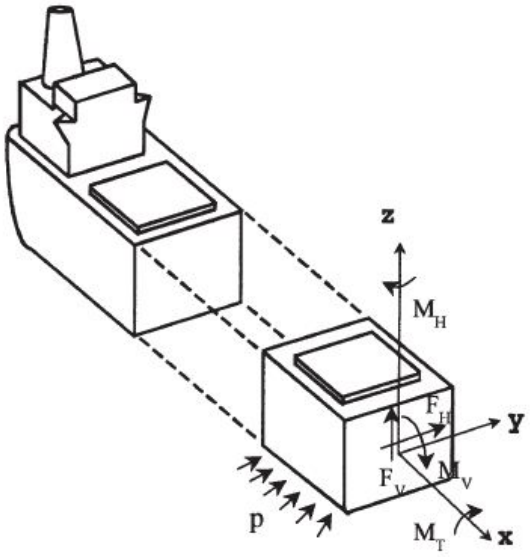


Figure 2.3: All load components on the hull structure of a ship [68]

### 2.2.4. Effect of the draghead

A third potential source of loading is the effect of the draghead on the ships motions of the hopper dredger. The motions of the drag head depend on the seabed condition, sea state and the draught of the ship. Zhanglan et al. researched the influence of the draghead of the draghead on the ship motions of a hopper dredger [87]. The analysis was performed on a $5500m^3$ hopper dredger operating at a wave height less then two meters. It was concluded that the effect of the draghead motions was insignificant relative to the ships motions due to the fact that the ships acts as a giant mass compared to the drag head and the an installed wave compensator.

## 2.3. Fatigue

Fatigue crack development starts on a microscopic level at which repeated local plastic deformations are caused by cyclic loading. Slip band, which are illustrated in **figure 2.4**, are formed on shear planes and induce crack nucleation in the material. After a significant amount of slip bands is formed a crack starts to growth from the slip bands along the plane that experiences maximum shear. A crack is initiated and a small crack appears which ends the crack initiation phase. The length of the small crack at which the crack propagation phase starts is not a distinct value and ranges between 0.1 and 1 mm [52]. Higher strength steels are less ductile and cracks originate more often from defects in the material structure and propagates normal to the tensile stress [28].

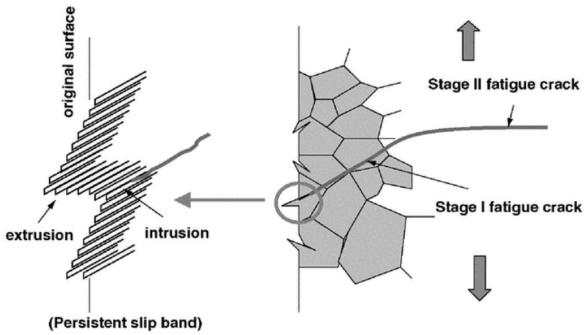


Figure 2.4: Slip band development on a tensile loaded plate edge [50]

Fatigue has been a subject of concern for engineers for over 150 years [28]. The term fatigue was first used in the early 1800s and was further discussed and studied throughout the rest of the 19th century. One of the first researchers to develop design strategies to avoid fatigue was August Wohler in the 1950s. The need for these

strategies arose from axle failures in the railway industry. He saw that fatigue was affected by cyclic loading as well by the mean stress of that loading. Design curves for fatigue nowadays are named after Wohler and these are discussed in 2.4. Fatigue analysis methods and design strategies have been further developed over the past 150 years and could be categorized in thee major approaches. The stress based approach, which is the most common used approach, a strain based approach and a fracture mechanics approach. The scope of this project lays within the crack initiation phase and therefore the stress- and strain based approaches will be further elaborated and the fracture mechanics will be ignored.

### 2.3.1. Assessment approach

In this section general fatigue assessment approaches for fatigue assessment of ships like the hopper dredger are presented. According to Y. Bai three methodologies for the estimation of accumulated fatigue damages are applicable [13]:

- Simplified fatigue assessment
- Spectral fatigue analysis
- Time-domain fatigue analysis

First a simplified procedure using a equivalent design wave is presented. Further in detail is a spectral analysis procedure where the environment is described by series of short term spectra. At last a direct time domain procedure is discussed. This is the most accurate description of the ships loading which uses generated time series of wave elevation.

The simplified method is the most common and fastest way to calculate the fatigue lifetime of a structural detail. This method uses a approximated long term distribution of stress ranges such as a Rayleigh or a Weibull distribution. This last type of distribution is commonly used in the assessment of marine structures and is used in Buerau Veritas rules and therefore the Weibull distribution is used in simplified fatigue assessment in this thesis. The Weibull distribution is depending on two parameters based on wave climate and structural response. These are a shape parameter and a scale parameter. The shape parameter has an significant effect on the fatigue analysis [18] and can only be reliably determined by spectral analysis of measurements. For this type of approach is recommended by the IACS to use fatigue loads in the region of $10^{-3}$ up to $10^{-5}$ probability of exceedance. Wave loads for simplified fatigue assessment according to Buerau Veritas rules are based on a $10^{-5}$ probability. The simplified fatigue assessment method has the advantage that a closed-form expression for fatigue damage can be derived in a relatively short time period [13]. Also, when loading and unloading sequences of a hopper dredger are not precisely known the, the deterministic fatigue damage calculation is the most suitable [11]. This low cycle cumulative damage calculation is calibrated against spectral fatigue analysis results. It will however results in more conservative results [17] because of the uncertainty of the Weibull shape parameter. The two parameter Weibull probability density function is given by equation 2.1.

$$f(S) = \frac{\gamma}{\delta}\left(\frac{S}{\delta}\right)^{\gamma-1} e^{-\left(\frac{S}{\delta}\right)^{\gamma}} \tag{2.1}$$

In equation 2.1 is S the stress range, $\gamma$ the shape parameter and $\delta$ the scale factor also known as the characteristic value of the Weibull distribution. The characteristic value is determined by a extreme stress range associated with a certain probability and is given by equation 2.2.

$$\delta = \frac{S_R}{(lnN_R)^{\left(\frac{1}{\gamma}\right)}} \tag{2.2}$$

The smaller the probability of exceeding of the extreme stress range the more influence the shape parameter $\gamma$ has. In the Bureau Veritas guidelines this $\gamma$ value is considered to be equal to one. This value depends on the type of ship, sailing route and location of the structural detail that is analysed on fatigue. Classification societies ABS and DNV provide methods to determine the shape parameter with use of a spectral analysis.

The harmonised CSR of the IACS [7] shows that the probability of the wave loading has influence on the effect of the shape parameter. A wave probability of $10^{-2}$ shows the most constant fatigue damage values for different shape parameters.

Because the simplified approach fatigue damage is very sensitive to the Weibull distribution parameters, the spectral fatigue analysis is more often used nowadays. The spectral analysis determines short term fatigue damages based on short term stress distributions in the frequency domain. The distributions are usually defined as Rayleigh distributions as in equation 2.3.

$$P(S) = \frac{S}{4m_0} exp\left(\frac{-S^2}{8m_0}\right) \tag{2.3}$$

The sum of these short term damages determines the fatigue lifetime of a certain structural detail. The method requires 3D structural modelling to determine transfer functions between the wave loading range and short term stress ranges which represent the response of the structure. To account for the loading/unloading cycle the spectral analysis uses the amplitude of the still water low frequency cycle together with wave loads based on probability of exceedance during an short term. The calculated fatigue damage has much more accuracy due to the more detailed approach of spectral analysis. This does however lead to a time consuming phase of determining the spectra and transfer functions of a ship. Another disadvantage is the fact that a spectral fatigue analysis is based on a certain sea state ate a specific location. A hopper dredgers is deployable at shores and ports with varying sea conditions all around the world. A spectral fatigue analysis will therefore not cover the entire operational life time of the ship. C. Soares and T. Moan [72] assessed model uncertainties of the long term wave induced loading of different types of ships. They used short term narrow banded Rayleigh distributions to fit the long-term two parameter Weibull distribution used in the simplified method. A significant relation between the shape factor and the ships length and a trend was seen that the shape factor increases with ship length.

An even more accurate procedure is the time domain analysis which accounts for the uncertainties in the spectral analysis method but does not necessarily require more determination time [64]. The stress time series resulting from the time domain analysis are analysed using the rainflow counting method [59] to determine the amount of cycles resulting in damage accumulation values. Eurocode 3 recommends rainflow cycle counting for long stress histories [29]. Because the time domain approach is time consuming and impractical the rainflow counting method can also be performed in the frequency domain based on the spectral analysis. A method to determine fatigue damage based on this principle is given by Huang [41]. It takes into account load combinations of low and high frequencies which can be Gaussian of non-Gaussian.

### 2.3.2. High- and low-cycle fatigue

Fatigue is divided by the number of cycles to failure and the divide is made between $10^3$ and $10^5$. The most common value to divide low- and high cycle fatigue is $10^4$. If the number of cycle is below this threshold the fatigue is called low-cycle fatigue and above it is high-cycle fatigue. This difference is made because low-cycle fatigue is a strain controlled phenomenon, due to plasticity effects, where high cycle fatigue is assessed according to the amount of stress. The low- and high-cycle regions are illustrated in **figure 2.5** and are further elaborated in the next sections.

## 2.4. High cycle fatigue

In ship structures like the hopper dredger the high cycle fatigue originates from the wave loading. High cycle fatigue is a better known phenomenon than low cycles fatigue. Loading is found within the elastic stress range of the material and results in less complexity due to the absence of non-linear plastic behaviour. If SN-curves associated with the FAT-classes of the structural details are applicable they are well suitable to assess fatigue life in the high cycle fatigue range. the FAT-class is defined by IIW recommendations and represent the fatigue strength at $2 \cdot 10^6$ cycles to failure. The high cycle fatigue region is illustrated in **figure 2.5**. This stress based fatigue assessment requires a stress range which is assessed in agreement with a specific SN-curve that is used. The stress range is made up of the stress ranges of the individual stress components. The stress range could then be described by the maximum principal stress range which is a significant fatigue parameter for the fatigue analysis of fatigue crack growth [52]. This stress range is in the direction in which the stress range

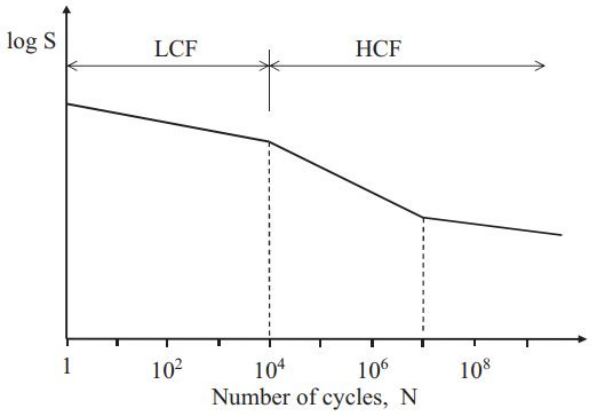


Figure 2.5: Low- and high-cycle fatigue regions of the stress-life curve [52]

between two load conditions is at its maximum. A few common concepts to interpret the stress which is used to compute a stress range are the nominal stress, the hot spot stress and the notch stress. The stresses are illustrated in **figure 2.6** and are further elaborated in sections 2.4.1, 2.4.2 and 2.4.3.

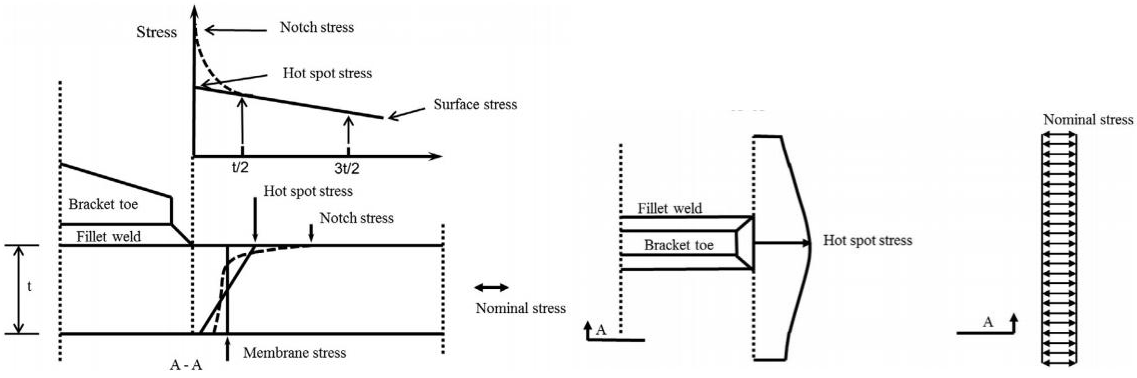


Figure 2.6: Stress types [52]

## 2.4.1. Nominal stress concept

The nominal stress approach is the most simplified method to assess fatigue life of structural details. It is considered a global approach where the stress range originated from the stresses that is present in the critical cross section of a considered structural detail. The nominal stress takes into account stresses caused by macro-geometric shape parameters of a joint but excludes stresses due to the presence of a weld [70] [39]. The nominal stress in an analysed structural detail is therefore compared with its appurtenant S-N curve. These S-N curves can be found for FAT classed structural details. Structural detail identification and FAT-class description are given by Hobbacher and Eurocode 3 [39] [84]. An unlimited amount of FAT classes can be defined because of endless structural detail designs possibilities but the number is limited to about 80 classes [25]. The downside of the nominal stress concept is the dependency to the specified FAT classes. In reality the structural details do not perfectly match the FAT class description and the determination of the nominal stress becomes a complex problem witch is relatively time consuming.

## 2.4.2. Structural hot spot stress concept

Bureau veritas specifies multiple structural hot spot stress approaches for types of structural details [8] [11]. The hot spot stress approach uses the structural or geometric stress at a hot spot. The structural stress includes all stress affecting parameters of a structural detail excluding the local weld profile [39]. This results

into a certain geometric stress concentration factor which is used to determine the hotspot stress range as function of the nominal stress range. The hot spot stress approach reduces the amount of S-N curves significantly in comparison to the nominal stress approach. The geometric stress are already accounted for in the stress magnitude of the hot spot stress. Hobbacher [39] defines several S-N curves for multiple types of welded structural details. Fricke and Kahl [35] performed a comparison study of different structural stress approaches. Methods described by the IIW, Dong, Xiao and Yamada are compared to fatigue tests of three small scale specimen. It shows that the approaches result in calculated fatigue lifetimes not to far from each other. The results are all quite conservative except for one calculated fatigue life by the approach of Xiao and Yamada. The reason for the rather conservative result is explained by the fact that the approaches neglect the effect off residual stress which will be further explained in section 2.7.2.

### 2.4.3. Effective notch stress/strain concept

There are some limitations to the hotspot stress approach. The approach does not explicitly accounts for plate thickness effects and notch stresses. The effective notch stress approach accounts for stress concentration effects as well as strength reduction at the notch and plate thickness effects due to non-linear through thickness stress distribution. Because both effects are considered in the stress range of the structural detail only a single S-N curve is required. Note that this approach only applies for welded details because of the presence of notches for this type of discontinuities. The approach is restricted to assessment of naturally formed as-welded weld toes and weld roots. Bureau Veritas [8] elementary stress range used for fatigue calculation according the rules for steel ships is the notch stress range. The stress range originates from the hot spot stress range and is multiplied by three factors taking into account weld pre described configurations and structural misalignment.

### 2.4.4. SN-curves

The SN-curves, also known as the whöler curves, are a way of describing the fatigue resistance of a structural detail on a logarithmic scale. An example of the curve can be seen in **figure 2.7**. The curve expresses the number of cycles until failure versus the operational stress range of the structural detail based on experimental fatigue data. Two types of curves are used in Bureau Veritas rules, a single slope curve for specimens in corrosive environment and a two-sloped SN-curve for specimens in a marine air environment specimens with cathodic protection. The transition point between the first and the second slope represents the fatigue limit. In double sloped SN-curve stress ranges below the fatigue limit are considered to be non-damaging. This is for variable amplitude fatigue loading situations not true according to Haibach [**?** ]. Periodic damaging cycles above the fatigue limit initiate fatigue cracks and the cycles below the fatigue limit could propagate these cracks and are therefore considered damaging as well. Haibach proposed that the SN-curve has to be linear extrapolated for stress below the fatigue limit. The slope of this extrapolation depends on the first slope of the SN-curve. The two-sloped SN-curve given in the Bureau Veritas guideline can be seen in **figure 4.7**.

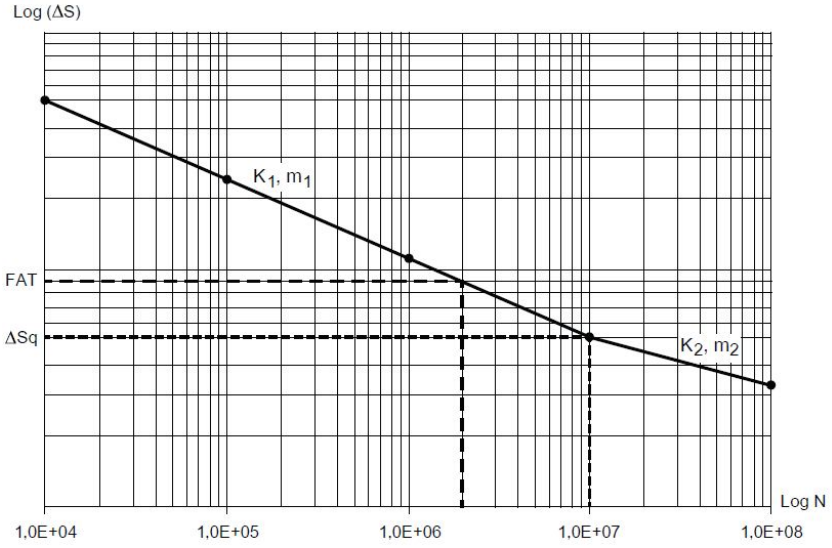


Figure 2.7: Two-sloped SN curves used in Bureau Veritas guideline for fatigue assessment [11]

SN-curves with a characteristic application purpose are based on fatigue failure data of test specimens tested with representative conditions. Specimens are loaded with a certain stress range, mean stress, joint eccentricity, and stress ratio. The number of cycles until failure of the specimen determines the location of the data point in the SN-plot area. All the data points of number of cycles to failure at a certain stress range level are assumed to be normally distributed on a log-log scale [52] [79] and is illustrated in **figure 2.8**. The normal distributions at every stress range level is assumed to have the same standard deviation which is used to compute the design SN-curve. First the mean SN-curve is determined with regression analysis and the design SN-curve is found by subtracting two times the standard deviation of the mean SN-curve. The design SN-curve has then a probability of survival of 97.7% and is expressed with equation 2.4

$$log_{10}(N) = log_{10}(K) - m \cdot log_{10}(\Delta\sigma) - 2 \cdot \sigma_{stdv} \tag{2.4}$$

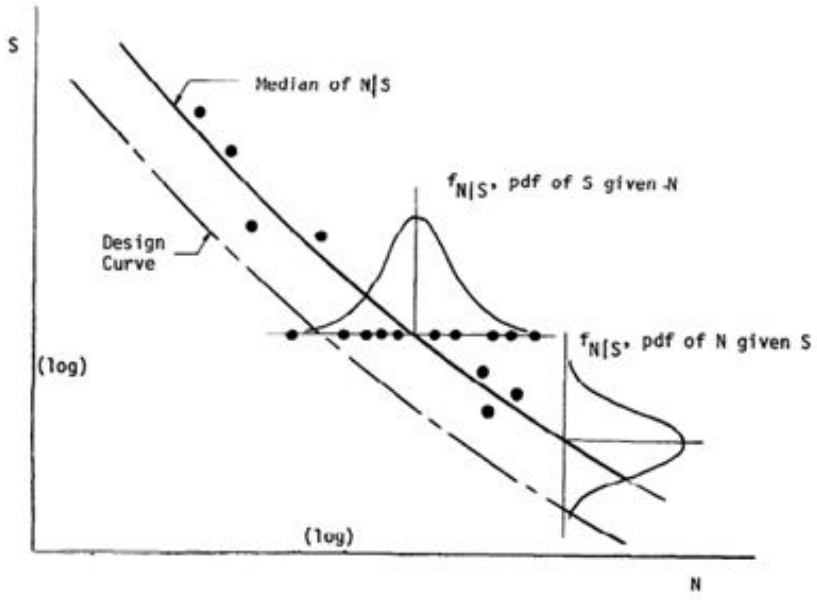


Figure 2.8: Normally distributed SN-data on a log-log scale

### 2.4.5. Fatigue damage accumulation

The cycles until failure result form design SN-curves and are used to determine the total fatigue damage of the structural detail at a certain point in time. If the loading has a constant amplitude the fatigue damage is simply the amount of cycles op to that point divided by the number of cycles associated with the stress range of the constant amplitude loading. Wave loading that affects a hopper dredger could not be seen as constant amplitude loading due to the fact that not all waves are the same. In case of this variable amplitude loading the fatigue damage associated with each occurring stress range could be summed up to determine the total fatigue damage assuming a linear cumulative damage summation. The linear cumulative damage rule is also called the Palmgren-Miner rule and was developed in the 1920s to predict the life of ball bearings [28]. the rule is expressed by:

$$D = \frac{N_1}{N_{f1}} + \frac{N_2}{N_{f2}} + \frac{N_3}{N_{f3}} + ... = \sum_{i=1}^{k} \frac{N_i}{N_{fi}} \tag{2.5}$$

In which $N_i$ represents the number of cycles up to the point of fatigue damage calculation and $N_{fi}$ the number of cycles to failure according the applicable design SN-curve. Failure due to fatigue is considered when damage parameter $D \geq 1$.

The level of fatigue damage is in reality not a linear process and especially not if variable stress amplitudes are present. Models for non-linear accumulation require often unknown material properties and detailed knowledge of load cycles within the design life of the structure. These uncertainties justify the use of Miner's

rule if a simplified approach is used for fatigue assessment. It is a rather rough estimate of fatigue damage but results in acceptable crack initiation predictions [48].

## 2.5. Low-cycle fatigue

Cyclic stress in the case of low cycle fatigue are found in the plastic range of the material and are therefore often strain based [14]. The cycles to failure of a specimen that suffers low-cycle fatigue are seen on the region between 0 and 10000 cycles to failure which is illustrated in **figure 2.5**. Low-cycle fatigue is seen in structures with loading/unloading operations that cause for relatively large fluctuating stresses in structural details and is a more critical factor for ship structures compared to offshore structure. As explained before a typical example is an FPSO, where loading/unloading happens around 1000 times in 20 years [44].

Giulio Ballio and Carlo A. Castiglioni [14] show that an approach to assess low cycle fatigue based on the assumptions that, for a given structural detail, the relationship between the number of cycles to failure and the cyclic amplitudes expressed in displacements have the same meaning for low and high cycle fatigue. This holds for high cycle amplitudes in the elastic range and low cycles in the plastic range. A second assumption is that damage accumulation is linear and Miner's rule [63] is applicable for both high and low cycle fatigue. The cyclic amplitudes could be assessed with multiple procedures and fatigue life curves. During low cycle fatigue load cycles these cyclic amplitudes are often seen in the plastic region of the material. Because of this the low-cycle fatigue assessment approach is often strain based. Multiple procedures are proposed which use either linear elastic or non-linear plastic analysis and the fatigue lives are calculated with stress or strain life curves.

### 2.5.1. Strain based approach

In the late 1950s and early 1960s the need for fatigue analysis of structural details with a relatively short fatigue life resulted in the development of a strain based fatigue assessment approach [28]. Instead of stress versus life curves (SN-curves) this approach uses strain versus life. The strain-life curve is composed of a low cycle fatigue region where plastic strain curve is considered and a high cycle fatigue region where a elastic strain curve is considered. The low cycle region is described independently by Coffin and Manson plastic strain life curve [56] [22] and the high cycle region is described by a modified Basquin equation [15] which is the original and commonly used equation for the well known SN-curves. The Basquin equation is modified by Socie et al. [74]. Independent damages of high and low cycle fatigue cannot be simply added. An approach to combine these damages is made by Kim et al. [47] and is based on a modified Coffin-Manson curve and Miner's rule. A downside to the use of this rule is that it ignores the stresses below the fatigue limit and the load interaction effect under variable loading and does not capture loading sequence effects. To account for these effects Karunananda et al. [45] proposes a fatigue damage model to combine high and low cycle fatigue damage for bridges. The proposed model uses a modified strain-life curve (**figure 2.9**) to estimate the fatigue life of a structural detail and calculates the combined damage with use of a damage indicator. The methods is only validated for uni-axial stress states and is recommended to extend to multi-axial stress states. The steps in the method by Karunananda et al. are given in **figure 2.9**. The strain equation of the low and high cycle regions are respectively given in equations 2.6 and 2.7.

$$\epsilon = \frac{\sigma'_f}{E}(2N)^b + \epsilon'_f (2N)^c \tag{2.6}$$

$$\epsilon = \epsilon_e \left(\frac{N+N_u}{N+N_e}\right)^{b'} \tag{2.7}$$

Here are $\sigma'_f$ and $b$ the fatigue strength coefficient and exponent respectively and $\epsilon'_f$ and $c$ the fatigue ductility coefficient and exponent. Fatigue test are required to obtain the fatigue material properties of a specimen. These tests are often impractical and require time and high costs and therefore many methods are proposed to estimate these properties. Several method to estimate the properties with the use of hardness have been evaluated by K. Lee and J. Song [49]. It is concluded that the direct hardness method by Roessle and Fatemi estimates the material properties in all cases very well and in some cases even excellent. Roessle and Fetemi's method uses Brinell hardness properties to express the fatigue material properties and they also concluded that the Brinell harness is highly correlated with the ultimate tensile properties of the material. The fatigue

strength coefficient, fatigue ductility coefficient, fatigue strength exponent and fatigue ductility exponent are respectively:

$$\sigma'_f = 4.25HB + 225 \tag{2.8}$$

$$\epsilon'_f = \frac{0.32(HB)^2 - 487HB + 191000}{E} \tag{2.9}$$

$$b = -0.09 \tag{2.10}$$

$$c = -0.56 \tag{2.11}$$

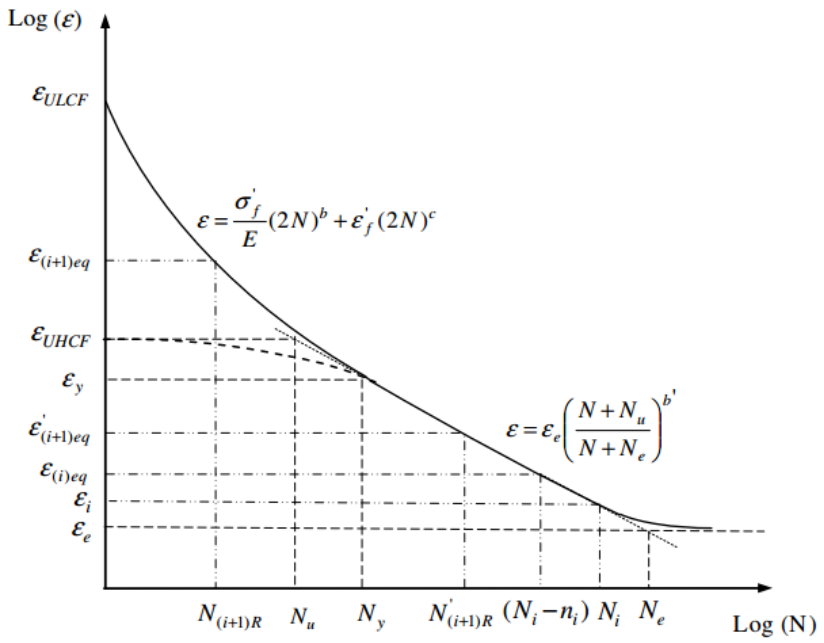


Figure 2.9: Strain-life curve proposed byKarunananda et al.

## 2.6. Yield and flow criteria

The local stresses and strains are a sum of elastic and plastic components expressed in equation 2.12. The relationship between elastic stress and strain is described by Hook's law presented in equation 2.13 [28]. If applied stress state exceeds a certain yield criterion such as proposed by Von Mises, Hook's law is no longer valid. When the material is continuously loaded beyond this yield point a flow rule which describes the incremental behaviour after yielding. The rule determines the next plastic at any point after yielding.

$$\epsilon = \epsilon_{le} + \epsilon_{pl} \tag{2.12}$$

$$\begin{cases} \epsilon_{x,le} = \frac{1}{E}[\sigma_{x,le} - \nu(\sigma_{y,le} + \sigma_{z,le})] \\ \epsilon_{y,le} = \frac{1}{E}[\sigma_{y,le} - \nu(\sigma_{x,le} + \sigma_{z,le})] \\ \epsilon_{z,le} = \frac{1}{E}[\sigma_{z,le} - \nu(\sigma_{x,le} + \sigma_{y,le})] \\ \gamma_{xy,le} = \frac{\tau_{xy}}{G} \\ \gamma_{yz,le} = \frac{\tau_{yz}}{G} \\ \gamma_{zx,le} = \frac{\tau_{zx}}{G} \end{cases} \tag{2.13}$$

The Von Mises effective stress and plastic strain in case of a multi axial stress state is then given by equations 2.14 and 2.15.

$$\sigma_{eff,VM} = \frac{1}{\sqrt{2}}\sqrt{(\sigma_{1,le}-\sigma_{2,le})^2+(\sigma_{2,le}-\sigma_{3,le})^2+(\sigma_{3,le}-\sigma_{1,le})^2} \tag{2.14}$$

$$\epsilon_{eff,VM} = \frac{\sqrt{2}}{3}\sqrt{(\epsilon_{1,pl}-\sigma_{2,pl})^2+(\sigma_{2,pl}-\sigma_{3,pl})^2+(\sigma_{3,pl}-\sigma_{1,pl})^2} \tag{2.15}$$

### 2.6.1. Cyclic stress strain curve

Low cycle fatigue is a strain controlled phenomenon and fatigue is assessed by the strain range at the hot spot in stead of a stress range. The relation between stress and strain is different for fatigue compared with ultimate strength assessment. A monotonic stress strain curve results in too optimistic strain values for amplitudes below 0.6% strain. A cyclic stress strain curve is needed to accurately describe the stress strain relation in case of fatigue assessment due to hardening of the material when it is subjected to cyclic loading. This curve is different form the known monotonic stress strain curve which is used for static yield checks of structures. The difference is seen at the point where the curve deflects from the elastic curve and the behaviour between plastic strain and stress after this point is exceeded compared with the monotonic curve. Higher strength steel such as AH-36 ship building steel, which is typically used in hopper dredgers, have initially a high dislocation density in the material. When the material is cyclic loaded the dislocations are re-arranged and it is softened so the required loading for plastic deformation is decreased [42]. The result of the softening could be seen in **figure 2.10** where the cyclic stress-strain curve shows plastic deformation below the Monotonic curve. The curves in the graph represent stress-strain curves of a higher strength steel similar to AH-36 ship building steel.

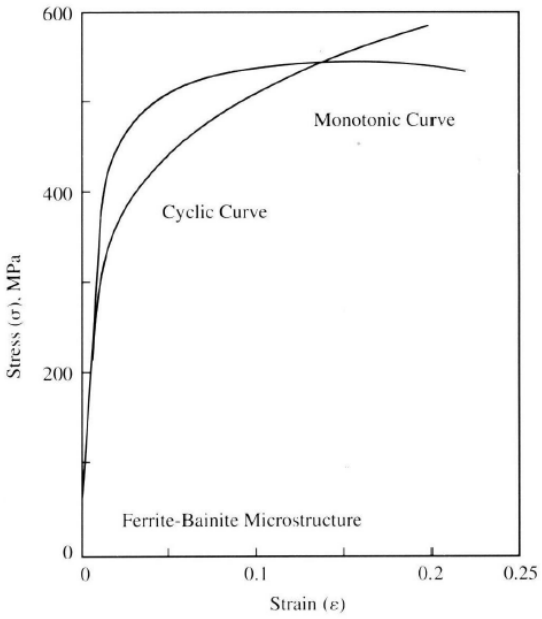


Figure 2.10: Monotonic- and cyclic stress strain curve of a ferrite-bainite higher strength steel [42]

### 2.6.2. Neuber's rule correction

To determine the strain during plastic deformation non-linear numerical methods are required [28]. These are costly and time consuming analysis, which could be necessary in some cases, and in some cases be avoided with use of Neuber's rule. This method uses the linear-elastic analysis and estimates the equivalent elasto-plastic stresses and strains. Neuber's rule states that the product of the true stress and strain of the Ramberg-Osgood curve is equal to the squared linear-elastic stress divided by the Youngs modulus. The relation is expressed by equation 2.16.

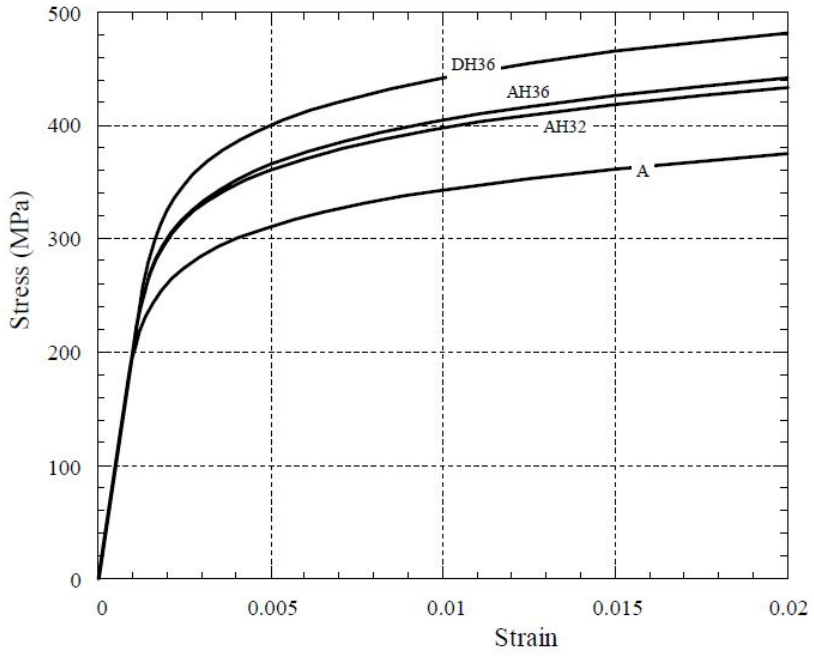


Figure 2.11: Cyclic stress strain curves for multiple ship building steels [83]

$$\sigma\epsilon = \frac{K_t^2 \sigma_n^2}{E} \tag{2.16}$$

With this relation the true strain in the notched is found and this strain is used to compute a pseudo stress in the linear-elastic domain. If plasticity occurs the true strain will be of larger magnitude than the elastic strain found with linear elastic numerical analysis and as a result the pseudo stress will be of larger magnitude as well. The pseudo stress could then be compared with high cycle stress-life SN-curves which are common practice. **Figure 2.12** illustrates the described procedure in case the notch stress is used for fatigue analysis. Note that any type of stress could be used with the requirement that the associated SN-curve is used. A generalized form of Neuber's rule was presented by Hoffmann and Seeger to account for multi-axial stresses at the notch surface. This type of stress could also be accounted for in the cyclic stress strain curve according to Dowling [28]. The cyclic stress-strain curve according to Dowling depends on the ratio between the first and second principal stress at a notch. Botch these methods are based on the notch stress and do not include the prediction of fatigue life.

### 2.6.3. Pseudo-elastic stress

Strain-life curve properties are difficult to the determine and limited to the notch stress approach. To avoid the use of such curves the local strains could be used to compute a pseudo-elastic stress. According to Wang et al. 83 the hotspot stress could be used in combination with a linear elastic hot spot stress SN-curve to determine the fatigue life taking into account plasticity effects. Combined TWI test data based on Neuber's rule and DSME data led to a design curve which has a slope of $m = 2.43$. He compared this curve with a D-curve which has a slope of $m = 3$ and it shows that the D-curve is conservative below $10^{-4}$.

The application of the pseudo stress range has been used by classification societies such as DNV and ABS. DNV fatigue guideline [80] uses a plasticity correction factors to make use of design S-N curves instead of strain-life curves. It combines hotspot stress ranges of high cycle fatigue due to waves and low cycle fatigue due to loading and unloading. The wave stress range is based on a wave with a probability of exceedance of $10^{-8}$. An effective pseudo stress range is composed to determine fatigue damage and is found with the combined stress range and a non-linearity correction factor containing the plasticity correction factor. This factor is based on corrected stress with Neuber's rule in case of a plane stress state. If plane strain behaviour

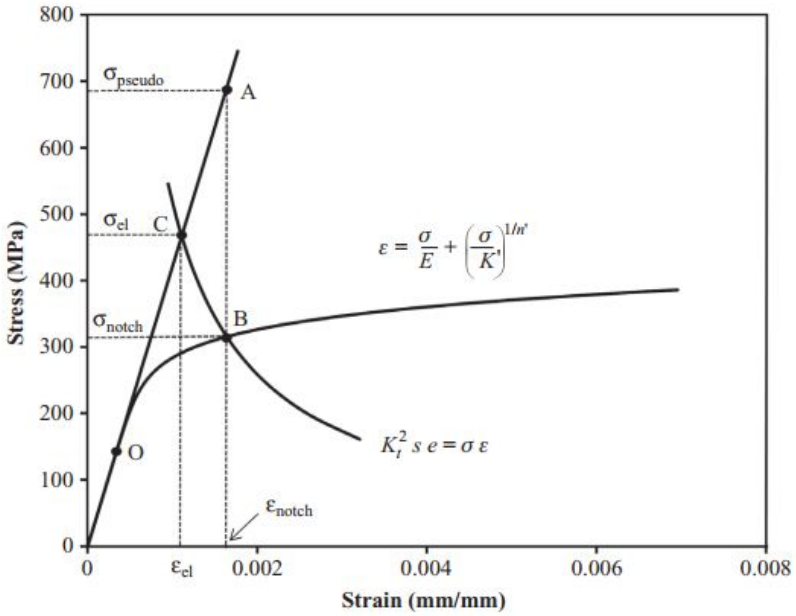


Figure 2.12: Illustarion of the procedure of using Neuber's rule [52]

is seen the Glinka rule [65], based on strain energy density, may be used according to the guideline. With the plasticity corrections factor method a linear elastic solution found with finite element analysis can be used for this non-linear plastic phenomenon. If the part of low cycle fatigue damage is above 0.25 it is considered significant.

### 2.6.4. Strain hardening

When the amplitude is above yield there will be local plastic deformation of the material which expands the yield surface at the location. The expansion of the yield surface causes strain hardening of the material and depends on the type of hardening. If plasticity effects occur in the cyclic loading of a structural detail either kinematic or isotropic hardening has to be taken into account. The hardening rule has effect on the unloading part of the cycle and determines the minimum strain of an individual cycle. The Bauschinger effect describes the material behaviour when a specimen is unloaded and residual stresses on a microscopic scale remain in the material. As a result yielding in the unloaded part of the cycle will occur at a reduced stress which depends on the type of hardening rule that is assumed. If kinematic hardening is assumed this effect occurs at a reversed stress of two times the yield stress and when assuming isotropic hardening the effect is seen at a reversed stress of two times the maximum stress amplitude which usually means that the Bauschinger effect is seen when a kinematic hardening rule is assumed [32].

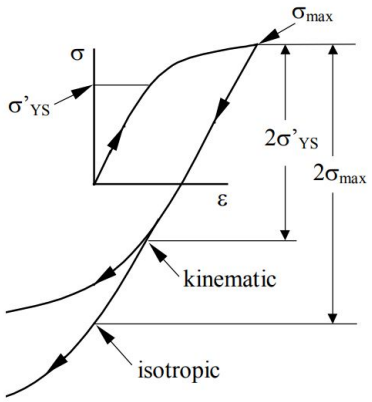


Figure 2.13: Effect of hardening rule on unloading part of load cycle[32]

If a cyclic hysteresis loop is computed this could be done assuming Masing type behaviour. This simplifies the formulation of the unloading part of the cycle. The minimum stress is found by using a reversed cyclic stress-strain curve magnified by a factor two. This is similar to the isotropic hardening rule.

## 2.7. Fatigue influence factors

Fatigue tests are mostly done on uni-axial loaded test specimens with nearly perfect conditions and surface smoothness. In structures like a hopper dredger the structural details are prone to a wide variety of variables that influence the structural behaviour and affect the fatigue life of the details. In this section a variety of variables is described which are most applicable for details of a hopper dredger.

### 2.7.1. Multi-axial fatigue

Generally, SN-curves are based on uni-axial test data and therefore a multi-axial fatigue assessment approaches is applicable in case of a multi-axial stress state. Multi-axial fatigue theories are divided into three main approaches. One is the extend of the static yield criteria to fatigue which is based on stress where the Yield criteria of Tresca an Von Mises are often used. A second approach is the use of energy as a correlation parameter to assess multi-axial fatigue. Another type of approach is the critical plane approach which is based on either maximum shear or normal strain depending on the type of material. This is illustrated in **figure 2.18**. Bäckström [12] used multiple methods to assess fatigue in multi-axial loading conditions. These methods are used to do a re-analysis of experimental results based on nominal and hot spot stresses. Three damage parameters where used; principal stress range, maximum shear stress range, and a modified critical plane approach. A schematic critical plane is illustrated in **figure 2.14** The critical plane method was the most successful in resolving the test data to a single S-N curve but it is concluded that the method needs further improvement due to large scatter of the results. The used critical plane method was based on a modified Findley model proposed by Marquis et al. This approach was first proposed by Brown and Miller [20]. They define the critical plane as the plane experiencing the maximum shear strain amplitude. Analysis was done in the low-cyle fatige region of the state of strain in a plane which is considered to have maximum shear strain. Because the parameters in the approach of Brown and Miller are in terms of strain they do not account for out-of-phase loading. This non-proportional loading increases the fatigue damage significantly. Therefore a modification is proposed, by Fatemi and Socie [31], to predict fatigue life under in and out of phase loading. Non-proportional loading will be further explained in this section.

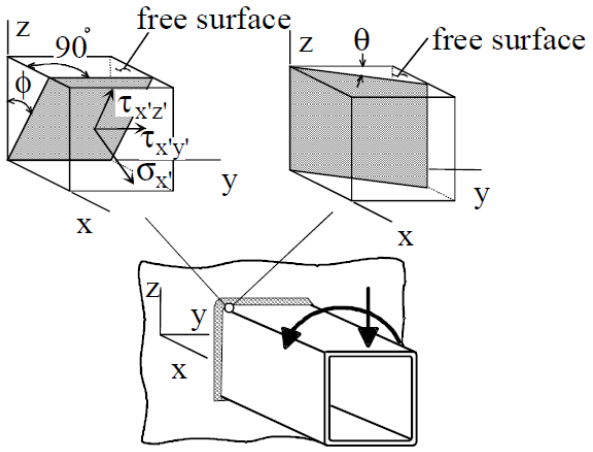


Figure 2.14: Critical plane orientation at weld toe given by [12]

The stress in a structural detail could be expressed in terms of principal stress that is calculated with use of Mohr's circle. Using these this type of stress a two dimensional stress state in a plate can be described by the bi-axiallity ratio that is expressed with equation 2.17.

$$a = \frac{\sigma_2}{\sigma_1} \tag{2.17}$$

Where $\sigma_1$ and $\sigma_2$ are the first and second principal stress. A structural detail in a uni-axial stress state has a biaxiallity ration equal to zero because the first principal stress is in direction of the loading. If $\sigma_2 \neq 0$ the biaxiality ratio is not equal to zero and a multi-axial stress state is present.

Bureau Veritas guideline proposes the use of a maximum principal stress range based on hot spot stress finite element analysis to account for multi-axial stress. This type of stress is often specified in design codes and recommendations but it has some limitations and in some cases it is assessed according different methods. One of the inconstancies between multiple design rules and recommendations is regarding the direction of the principal stress relative to the normal direction to the weld. Bureau Veritas defined two sectors, see **figure 2.15**, in which the principal stress is assessed. The sector in with the principal stress range is found is determined by the direction of the stress range. Principal stresses found in sector one have a directional angle between 0° and 45° and a SN-curve that is associated with this sector should be used. This sector is seen as perpendicular where sector two is seen as parallel to the weld seam. Sector two has an associated SN-curve for loading parallel to the weld seam.

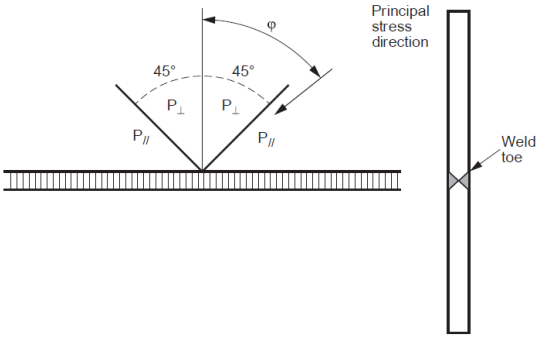


Figure 2.15: Principal stress dierectional sectors according BV [11]

The principal stress range is also used in Eurocode 3 [29] where it is limited to be applicable for proportional loading which is discussed in section 2.7.1. The principal stress range defined by Bureau Veritas guideline uses principal stresses with the same directional angle where Eurocode 3 defines the range as the greatest difference between principal stresses within 45 degrees apart.

Proportionality
Proportionality describes the relation between shear and normal stresses during the load cycles of a structural detail. Cyclic loading could be proportional or non-proportional. If the principal stress does not significantly changes direction during the load cycle the loading is considered proportional and the shear and normal stress are in-phase which is illustrated in **figure 2.16**. If the direction during the load cycle does change the loading is considered non-proportional and the shear and normal stress could be between 0 deg and 90 deg which could be seen in **figure 2.17**.
Non-proportional loading results in cyclic strain hardening of the fatigue sensitive location. The level of hardening depends on the shape, sequence and amplitude of the load path, which can be seen in the right side in **figures 2.16** and 2.17, and on the local micro structure of the material [30]. The local hardening of the material is often seen as the cause for shorter fatigue life for specimen under non-proportional loading.
A comparative study has been carried out by Lieshout et al. [77]. It is a comparison between codes, approaches proposed in literature and a method based on Path-Dependent-Maximum-Range multiaxial cycle counting. It is concluded that non-proportional multiaxial loading (out-of-phase loading) has a significant negative effect on fatigue lifetime estimates.

## 2.7.2. Mean stress and residual stress relaxation

The two loading conditions of the hopper dredger cause for a variable non-zero mean stress during operation which has effect on the fatigue life. Increasing the tensile mean stress will decrease the load range for a given number of cycles in the fatigue life time [46]. Because of this mean stress effects have to be taken

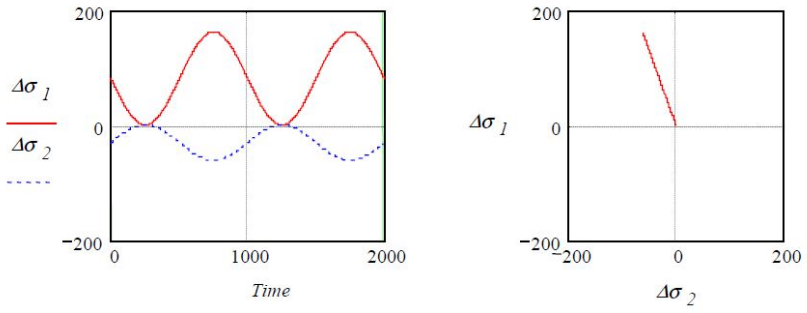


Figure 2.16: Proportional loading [12]

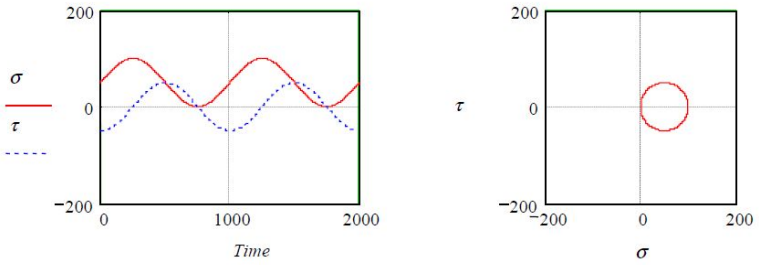


Figure 2.17: Non-proportional loading[12]

into account. The effect is examined by Wehner and Fatemi [84]. They found that mean stress effect only occurs when the mean stress does not relax to zero. In other words; it depends on the strain amplitude of loading. Small strain amplitudes show more mean stress effect on fatigue lifetime which can be seen in **figure 2.19**. This indicates that mean stress has more effect in the high cycle fatigue region and less in th low cycle region. Low-cycle fatigue goes hand in hand with large strains which cause local plasticity which results in residual stress relaxation at the hot spot. Wehner and Fatemi also found that mean stress effect has a positive influence in case of a negative load ratio. For positive load ratios the mean stress affect has a negative influence. Equivalent stress ranges, accounting for mean strain effect, can be determined with multiple methods like Soderberg, modified Goodman, Gerber, Morrow, Smith-Watson-Topper (SWT), Smith and walker in the elastic strain region. The damage due to plastic mean strain in low cycle fatigue is given by Kikukawa et al. [54]. In general, the mean plastic strain has no effect on low cycle fatigue. Also, the plastic strain in high cycle fatigue is very small and is therefore neglected. The portion plastic strain in low cycle fatigue is larger than for high-cycle fatigue which explains why the mean stress or strain has less effect in the low-cycle region. The residual stress in the hot spot is decreased due to the plastic deformation and therefore the mean stress will decrease as well if the amplitude of the loading is unchanged. In the strain-life approach of Karunananda et al. [45] the mean strain effect is accounted for with the modified Goodman relation.
It is well known that the mean stress has effect on the fatigue life of specimens which are repeatedly loaded with a certain stress range. The SN-curve for as welded joints used for fatigue damage calculation in the previous section has included the thermal residual stress due to welding. Fatigue of welded joints is often considered to be independent of the mean stress of the loading due to the high residual stresses that occur at the weld toe after welding. In case of variable amplitude loading the mean stress is considered to have effect in some extent. It is often questioned if the assumption, that the mean stress has little effect due to the high tensile residual stress, is too conservative according to Mcdonald [53]. Especially when the loading is partially compressive. This is based on the uncertainty of the residual stress in the joint throughout its design life. Stress relief of the residual stress could cause for the mean stress to be more significant but unfortunately this parameter is seldom known at the joints in a welded structure. Little is known about the residual stress in joints and predicting initial and present residual stress is hard due to the dependency to a wide variety of thermal, geometric and load history parameters. Relief of the residual stress could be done by post weld treatment techniques and cyclic loading itself. The contribution of the stress ranges to the fatigue damage could decrease as a result of this relaxation. The load conditions of a floating structure could have more effect on residual stress relaxation than structures only loaded by wave loading [52]. Floating structures like


Figure 2.18: Multi-axial fatigue assessment procedure **??**

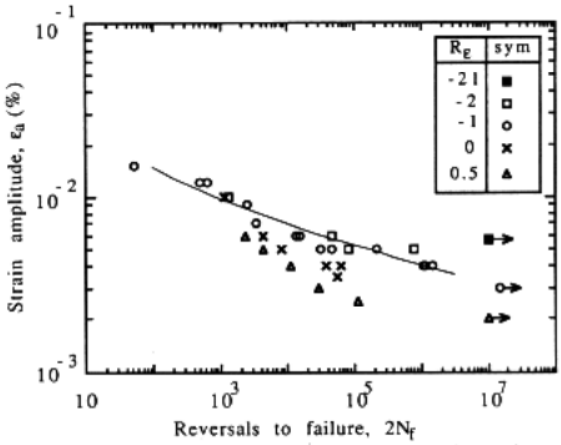


**Fig. 5 Strain amplitude versus reversals to failure for all strain ratios employed**

Figure 2.19: Effect of load ratio on fatigue strength **??**

a hopper dredger have initial load conditions such as empty or loaded conditions which could results in high stresses. According to Lotsberg the requirement for documentation of full relaxation of residual stress has to comply with equation 2.18. It states that the maximum hot spot stress measured in a year times the a weld notch factor of 1.5 has to exceed the yield stress of the base material.

$$\sigma_{max,year} \cdot K_w \geq \sigma_{yield} \tag{2.18}$$

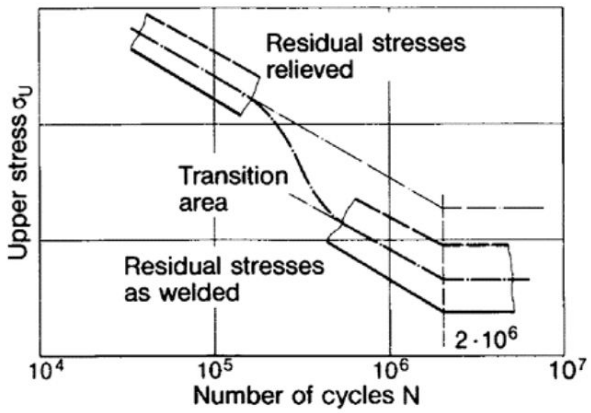


Figure 2.20: Change of fatigue resistance due to residual stress effects [69]

In 1987 Glinka [36] showed with a theoretical analysis and experiments that residual stresses are insignificant when low cycle fatigue is of concern. Radaj [69] showed the effect of low-cycle fatigue an a SN-curve of a welded joint and shows that fatigue strength is increased when tensile residual stress is relaxed in de low- and medium cycle range which could be seen in **figure 2.20**. A literature review was done by the 2013 ship structure committee [85] on the residual stress relaxation and mean stress effects in welded joints and base material details in ship structures. They concluded that due to high residual stress the stress ratio has little effect and that the compressive part of the cycle does not enhance the fatigue strength if the stress ratio is above -1. However there are indications that the mean stress has effect in case of variable amplitude loading. It was concluded that large amplitude static ship loadings could reduce the initial residual stress to great extend due elastic-plastic behaviour of the material. Most of the relaxation occurs on the first tensile amplitude of the loading and is significant if the initial hot spot stress is above 60% of the yield stress. If the first half cycle equals the yield stress the residual stress is on average decreased by 60%. A new model is proposed which is rather conservative on the prediction of the mean stress effect. According to I. Lotsberg [52] a sufficient tensile stress amplitude could shake down the residual stress, partially to a lower stress level, or full shake down to zero residual stress which could be seen in **figure 2.21**. Due to the the reduction of the residual stress the compressive part of the cycle is less damaging and some stress range reduction factors are introduced to enhance the fatigue strength.
The large stress amplitude of the dredging cycle could result in significant relaxation of the thermal induced residual stress due to the large stress amplitude of the cycle. It is interesting to see what the effect is of taking the mean stress effect into account assuming stress relaxation due to the large stress amplitude of the dredging cycle. This would give an impression of the beneficial effect of the compressive part of the dredging cycle. The mean stress effect is usually taken into account with use of a equivalent completely reversed cyclic amplitude which is compared with a SN-curve based on a load ratio of $R = -1$. Hobbacher recommends a fatigue enhancement factor to adjust the SN-curve to a curve with zero mean stress when the residual stress is known [39]. The SN-curve could also be adjusted with use of mean stress theories such as the walker mean stress theory [82]. The residual stress is often unknown and is an uncertain parameter so the effect of mean stress is determined assuming fully relaxed residual stress to a zero stress value. This gives an indication of mean stress effect in case it is taken into account and it shows the effect of residual stress relaxation. This assumption is supported by a study performed by Zhang and Moan on the effect of mean stress in fatigue of welded joints in FPSO's [86]. A improved mean stress factor is presented based on four mean stress corrections including the IIW correction and the hot spot stress concept. A equation is provided so the residual stress can be calculated when the hot spots stress exceeds the yield stress and results in shakedown of the

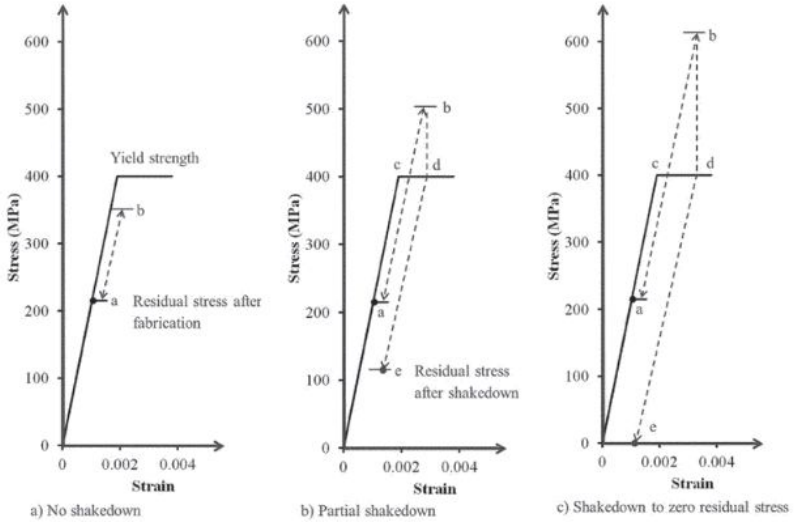


Figure 2.21: Shakedown effect due to stress that exceeds the material yield stress [52]

residual stress. The procedure is validated with test and finite element models loaded with a high stress pre-load before cyclic loading. The equation for the adjustment of the residual stress is given by 4.19. The mean stress factor formulated in this improved procedure condenses cyclic loads with multiple stress ratios to a equivalent stress ratio of $R = 0$ which equivalent stress range could be assessed with use of a FAT90 SN-curve. It has to be noted that this method is only validated for small scale uni-axially loaded specimens.

According to the IIW [39] a SN-curve should be shifted to account for a load ratio of $R = 0.5$ and therefore the BV SN-curve is based on such a load ratio to account for the presence of residual stresses [55]. When residual stress is demonstrably reduced, enhancement factors on the SN-curve FAT class are recommended and are given for welded and non-welded details. It has to be noted that fatigue classes of complex welded structures are not recommended to be enhanced. Also, a simplified method is given which states that 60% of the compressive part of the cycle is effective for non-welded and stress relieved structures.

### 2.7.3. Geometry

In 1981 Gurney [37] presented the significance of increasing plate thickness of welded plates on the fatigue strength. He suggested a correction on the stress range given by equation 2.19.

$$\Delta\sigma = \Delta\sigma_0 \left( \frac{t_0}{t} \right)^{1/4} \tag{2.19}$$

Here are $\Delta\sigma_0$ and $t_0$ the stress range and the reference thickness respectively. The reference thickness is the thickness on which fatigue tests used for the applicable SN-curve are based. Based on the knowledge that if the size of a specimen is increased, while maintaining all other parameters, the fatigue strength will decrease a study was done in 1985 on the influence of weld geometry of welded joints [16]. The study is focussed on the effect of the welded plate thickness and it was seen that the fatigue strength could decrease by 40% if the plate thickness is increased from 12.5 up to 80 mm. It is concluded that the proposed correction by Gurney [37] is applicable up to a plate thickness of 80 mm of the load-carrying plate and that the size effect is purely caused by welded joint geometry. Berge states that the thickness effect is caused by the following parameters:

- Stress concentration at the weld toe.
- Stress gradient in plate of toe crack.
- Number of cycles of crack growth in the steep stress gradient area relative to the total number of cycles to failure.

The stress gradient at the weld has significant effect on the influence of the thickness effect and this is why bending loads on a plate increase this effect due to the larger through thickness stress gradient. Bending

loaded welded joint usually have a longer fatigue life relative to membrane loaded joints and therefore the increasing thickness effect could lead to conservative conclusions if the joint is only loaded with this type of loading.

The size effect has been recommended by the IIW [39] in a similar form as it was presented by Gurney. This procedure has also been adopted by classification societies such as BV for welded joints, bolted joints and base material. The correction factor for plate thickness according IIW and BV is presented by equation 2.20

$$f_{thickness} = \left(\frac{t_{eff}}{t_{ref}}\right)^{n} \tag{2.20}$$

Here is $t_{eff}$ the thickness of the attached plate including the weld leg lengths and $t_{ref}$ and $n$ are the reference thickness and thickness exponent which are based on the type of joint and the SN-curve used to assess the fatigue strength. Note that the thickness exponent proposed by Gurney was 0.25 and is now adjusted according to the joint type.

An third geometric entity that has effect on fatigue strength of a joint is misalignment

### 2.7.4. Corrosion

The working environment and type of cargo loading form a corrosive environment which has a negative effect on the fatigue life of structural details. The main mechanism behind this is effect that a corrosive environment has on the surface condition of steel plates in a structure like a dredging ship. The soil particles cause for local notches, indents and abrasion and the chemical composition of the environment could cause for corrosion pitting. All these types of surface roughness increasing defects result in stress concentrations which will amplify the initiation of cracks. Radaj [69] divides material diminution of welded joint into corrosion and wear of the material. examples of corrosion are:

- Contact corrosion between two unevenly electro-positive materials.
- Pitting of surface.
- Stress corrosion due to permanently present stress such as residual and static stress.

Corrosion in weld welds is enhanced by plastic deformation which is therefore linked to low cycle fatigue. the type of environment plays a large role in the amount of corrosion on steel structures. The corrosion phenomenon occurs combined with wear mechanisms such as:

- Deformation of steel plates.
- Erosion wear due to friction forces of sand particles.
- Repeated removal of surface oxide layer.

In marine structures corrosion is included in the design by corrosion additions to plate dimensions and weld geometry. Corrosion additions are given in common structural rules for bulk carriers [7] and are accounted for in structural strength calculation of ship designs. Additional to the geometry reduction corrosion is implemented in the fatigue resistance curve which is often single sloped and reduced by 30% to account for corrosion effects.

## 2.8. Finite element analysis

A hopper dredger is a complex design which results in complex stress field in the structure. The plating arrangement and complex discontinuities such as bottom- and deck openings all have an effect on each others structural behaviour which makes it difficult to analytically calculate the stress in a detail suitable for fatigue analysis. The ship structure committee of 2002 did a study on the design of openings in primary ship structures [1] in which is said that finite element methods are required for ships with such a complex geometry.

According to ABS [4], fatigue assessment is performed on high stressed geometrical discontinuities in a finite element model. In ships this is usually at midship section because this drawing is available in early design

stages. The stress that is found in the FE model depends on the mesh and it should be taken into account that this stress is a virtual stress that could exceed the yield strength. If a shell elements are used for the analysis the stress at the discontinuity goes into the direction of infinity with decreasing mesh size. The high and unrealistic stresses are filtered with use of the hot spot stress concept. Stress is measured away from the hot spot and is linearly extrapolated to the hot spot and thereby the non linear stress gradient is eliminated.

The focus of this thesis is on the bottom opening corner details around the midship area of the cargo hold. C. Soares [73] assessed fatigue damage of a tanker with use of a spectral analysis and used a modelling technique to reduce the size of the model to a cargo hold model at amid ships. It is a plate and beam element model with boundary conditions at the fore and aft parts of the model. Loading is determined with use of a 3D panel method and is applied at an auxiliary so called "umbrella structure" according Bernoulli's hypothesis. The modelling technique is illustrated in **figure 2.22**

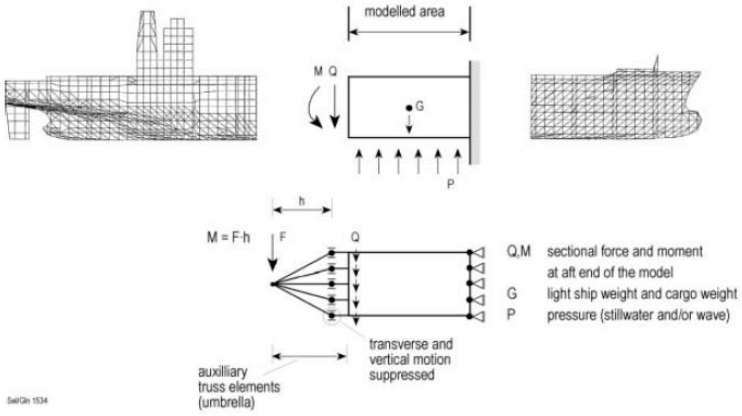


Figure 2.22: Boundary conditions cargo hold model C. Soares [73]

# 3

# Load profile and structural response

*Fatigue analysis is based in the loading and working conditions of a structural member. In this chapter the loading and the structural response to this loading is described. A hopper dredger is introduced for fatigue analysis and is representative for modern hopper dredger designs. According to the ship specifications a dredging cycle is described and hull girder and pressure loads are calculated. Stresses in fatigue sensitive details are obtained with use of a finite element numerical method and the main fatigue input parameters are established.*

## 3.1. Analysed hopper dredger

A representative recent design of a hopper dredger is chosen to use for fatigue analysis. The hopper dredger is a complex structure and therefore numerical methods are applied to account for the geometric structural complexity. In this thesis solutions are obtained with use of the finite element method. A cargo hold model will be used, which is not the entire ship, but will require significant modelling time. BV has software, called Veristar Hull, which applies the rules on a finite element model such as a shell model of a cargo hold. A ship could have a Veristar Hull notation which means that a finite element model is available throughout it's classification. In case of design changes or checks on the ships structural integrity this model could be called up on. This notation is not obligated for classification of hopper dredgers and therefore not all vessels have a such a FE model available. This is one of the main reasons the analysed design in this thesis is chosen.

Not only the avoidance of geometric modelling, also the vessel specifications give reason for the choice of this vessel. The hopper dredger has a length smaller than 170 m which is interesting because BV rules only require fatigue analysis for ships with $L > `170m$ and the majority of the fatigue damages was found in ships below this length. It should be noted that this is interesting to take into account but does not effect the general principle of the dredging cycle fatigue assessment. The contribution of the dredging cycle is assumed independent of the ship model and should be applicable for all hopper dredgers. Cracks have not been seen, or are expected, in this hopper dredger design and therefore the analysis in this thesis is not focussed on solving specific damage cases. The model is purely used to see what the contribution of the dredging cycle is compared to the wave loading and to get an indication of the stress magnitudes to determine if low cycle fatigue assessment is applicable. The specifications of the ship are given in **table 3.1**.


Figure 3.1: 3D render of a typical hopper dredger

Table 3.1: Ship specifications hopper dredger used for analysis

| Variable | Value | Unit |
|---|---|---|
| Rule length | 140 | m |
| Hopper capacity | 15000 | $m^3$ |
| Depth | 14.00 | m |
| Breath | 30.00 | m |
| Blockage factor | 0.88 | - |
| Draught (Summer mark) | 8.00 | m |
| Draught (Dredging mark I) | 9.00 | m |
| Draught(Dredging mark II) | 10.00 | m |
| Ship speed | 16.00 | Knots |

## 3.2. Operational profile

In this section the static and quasi static loads on the analysed hopper dredger are determined. First the dredging cycle is established which lead to the still water bending, shear and pressure loads. Wave loading is determined according BV load cases which are applicable for a deterministic method.

### 3.2.1. Dredging cycle

The loading profile of a hopper dredger consists of quasi static wave loads and static still water loads. These still water loads fluctuate due to loading and unloading of the hopper dredger during dredging operations. This cycle is performed four to six times a day. Due to loading and unloading the ship reaches maximum sagging and maximum hogging in one cycle respectively. Miedema [61] divided the dredging cycle in eight phases which describe the process of filling the hopper up to which the hopper is be considered fully loaded. The phases can be summarized by the following steps and are illustrated in **figure 3.2**:

- **Phase 1:** Fully loaded hopper.
- **Phase 2:** Sailing to Dumping area.
- **Phase 3:** Dumping load.
- **Phase 4:** Pump remaining water out.

- **Phase 5:** Fill hopper with mixture to overflow level.
- **Phase 6:** Loading with minimum overflow losses.
- **Phase 7:** Maximum draught reached (CTS). Overflow level is adjusted.
- **Phase 8:** Hopper is fully loaded. Overflow losses increase rapidly.

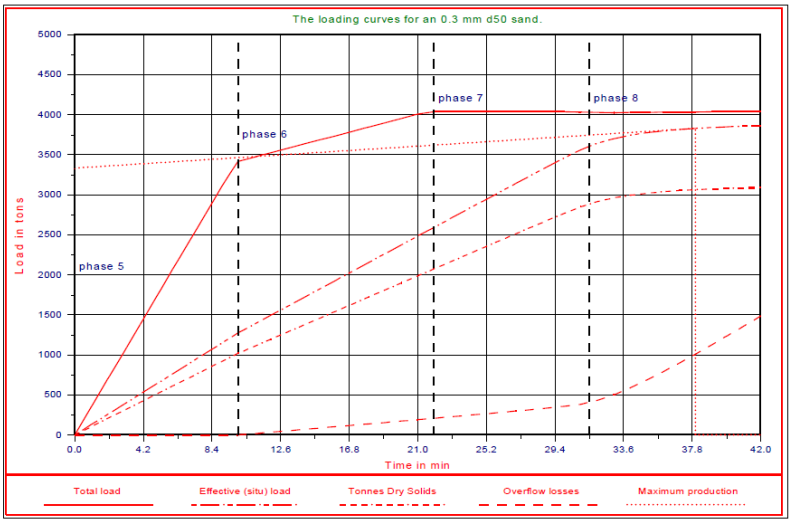


Figure 3.2: Hopper loading cycle [61]

To describe the dredging cycle multiple variables are identified. Not only the weir level in the hopper increases due to filling the hopper. During the cycle also the draught increases because the displacement of water has to equal the weight increase when the hopper is filled. The increase of weight is due to filling the hopper and settling of particles which increases the specific density of the cargo inside the hopper. The increase of these three variables result in a still water bending moment along the length of the ship and the maximum moment is usually found at midship section if the hull is seen as a simple beam. The draught, specific density and still water bending moments for each step in the dredging cycle are extracted from an preliminary still water bending moment document which is available for the analysed dredger. A few assumptions are made to complete the description of the dredging cycle:

- When dredging operation starts the hopper is filled up to overflow level with mixture. The density of the mixture depends on the specific dredger, the operational conditions and the soil that is being dredged. In a sensitivity analysis of scaling TSHD's performed by Miedema [62] a mixture density of $1.3 t/m^3$ is used as a common value to represent the mixture density. This value is used as a starting specific density in the hopper. At this point any settling of particles that influence the local density in the hopper are neglected out of simplicity. Later the influence of the local pressure on the structural response will be examined in section 3.5.6.
- When the density increases due to settlement of the particles it is considered fully loaded when a specific density of $2 t/m^3$ is reached [9]. In terms of loading of the midship section it is therefore interesting to increase the specific density more. In case the local pressure does have a significant contribution in the loading of the structural details this will effect the magnitude of the stress as well. If more soil is settled in the hopper the local pressures change and therefore it is expected that a certain maximum value should be identified with associated load condition.
- Another assumption is that the increase of draught, weir level and still water bending moment is linear between the point where the hopper is empty and where the mixture reaches the overflow level. This is

done because only the 'empty' and 'hopper filled with mixture' loading conditions are provided in the still water bending moment document. The variables are considered linear because they change due to a volumetric increase of the hopper which is considered to be a linear process. If the weir level increases linear with time then the draught and still water bending moment will increase linear. Note that this is only valid when the specific density does not changes when the hopper is filled up to overflow level. The assumption is made that particles are not settling during this part of the dredging cycle to avoid non-linear parameters and simplify the calculation of the loading variables.

Fatigue assessment is usually done in the design phase and actual dredging information is not applicable. However, still water bending moment and hopper tables are constructed in this phase and could used to formulate a dredging cycle. The dredging cycle phases are translated into hopper loading steps in terms of design data from preliminary still water bending moment diagrams and hopper loading tables which are available to the author. Full description of the dredging cycle requires the following data for each step from an empty- to a fully loaded hopper with maximum specific density:

- Specific density $t/m^3$
- Mixture density $t/m^3$
- Draught empty $mm$
- Weir level $mm$
- Still water bending moment $Nmm$

It is expected that the stress in the hopper dredger specific details is multi-axial and according to the previous chapter 2 a check should be done to see identify if the loading of the hopper dredger is proportional. This analysis requires the definition of the load path which realized by definition of the dredging cycle in terms of hopper dredger global and local loading containing the previously discussed data. It is proposed to design the dredging cycle using five steps in the rise of the weir level in phase 5 and five steps in increasing the specific density until the hopper dredger is considered to be at maximum loading. **Table 3.2** shows the loading steps from empty hopper to a fully loaded hopper with a specific density of $2.0t/m^3$ to use for still water analysis of the hopper and this is illustrated in **figure 3.3**. More detailed specifications of the analysed hopper dredger dredging cycle can be found in appendix A **table A.1**.

Table 3.2: Load steps dredging cycle

| | Max. weir level | Max. draught | Max. specific density |
|---|---|---|---|
| Step 1 | 0% | 0% | 65% |
| Step 2 | 25% | 25% | 65% |
| Step 3 | 50% | 50% | 65% |
| Step 4 | 75% | 75% | 65% |
| Step 5 | 100% | 100% | 65% |
| Step 6 | 100% | 100% | 70% |
| Step 7 | 100% | 100% | 75% |
| Step 8 | 98% | 100% | 80% |
| Step 9 | 93% | 100% | 85% |
| Step 10 | 84% | 100% | 90% |
| Step 11 | 81% | 100% | 95% |
| Step 12 | 77% | 100% | 100% |

### 3.2.2. Still water load components

The considered still water load components are static internal and external pressures which lead to shear force and bending moment distributions along the length of the ship. The external sea pressure is given by equation 3.1 where $T_i$ is the draught of the associated load case i and load condition j.

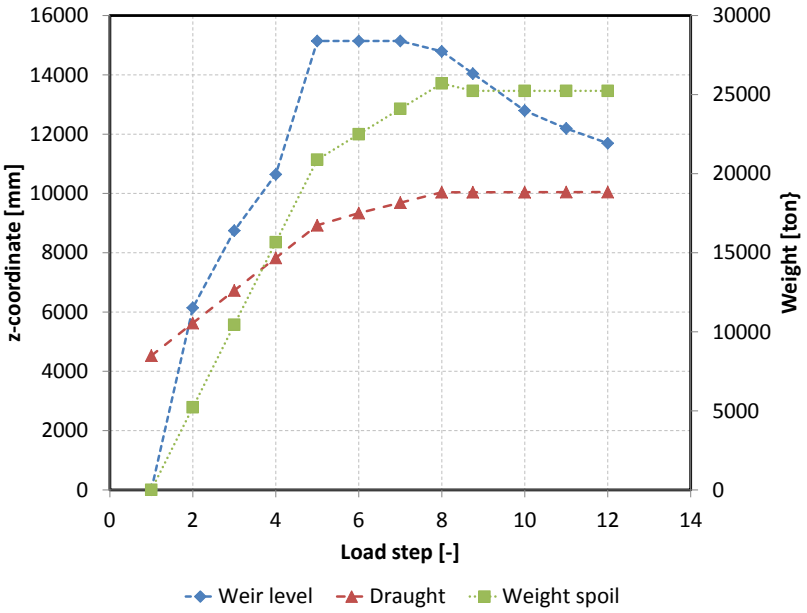


Figure 3.3: dredging cycle; ballast to fully loaded

$$P_{sea} = \rho_{seawater} g(T_{i,j} - z) \tag{3.1}$$

The internal pressure is not simply seen as a liquid. Due to the type of cargo and angle of the considered hopper plating the specific density varies. As explained earlier the cargo behaves as a 'solid' when a specific density of $1.4 t/m^3$ is reached. When the 'solid' state is reached the pressure on the plating changes relative to the angular slope of the plate. The internal pressure is given with equation 3.2 according to Bureau Veritas Rules.

$$P_{cargo} = \rho_{sd} g(d_i - z) \tag{3.2}$$

Where $d_i$ is the spoil is the spoil height associated with the loading condition. The adjusted specific density is given by equation 3.3 in which $\rho_{cargo}$ is the specific density of the spoil inside the hopper and $\alpha$ is the angle between the horizontal axis and the surface to which the pressure is applied. The sea- and cargo pressures for a fully loaded hopper are illustrated with use of MARS software in **figure 3.4**.

$$\rho_{sd} = \begin{cases} \rho_{cargo}, & \text{if } \rho_{cargo} < 1.4 \\ \rho_{cargo} + (1.4 - \rho_{cargo}) sin^2 \alpha, & \text{if } \rho_{cargo} \geq 1.4 \end{cases} \tag{3.3}$$

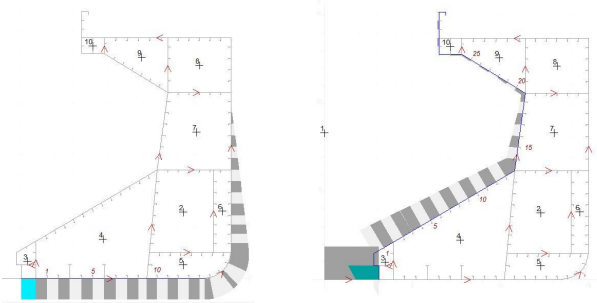

Figure 3.4: Sea- and cargo distribution fully loaded hopper

A still water bending moment document is available in which the bending moment and shear forces for multiple load conditions are specified. As explained before the load conditions of the minimum and maximum response of the dredging cycle are hogging and sagging respectively. The considered empty hopper load condition is one with a fully empty hopper and 10% storage. The fully loaded condition is specified in section 3.5.3. The shear force and bending moment distribution of both conditions are plotted in **figures 3.5a** and **3.5b** respectively. Deformations in the midship cross section give an indication of the structural behaviour of the hopper dredger and are presented in **figures 3.8a** and **3.8b**

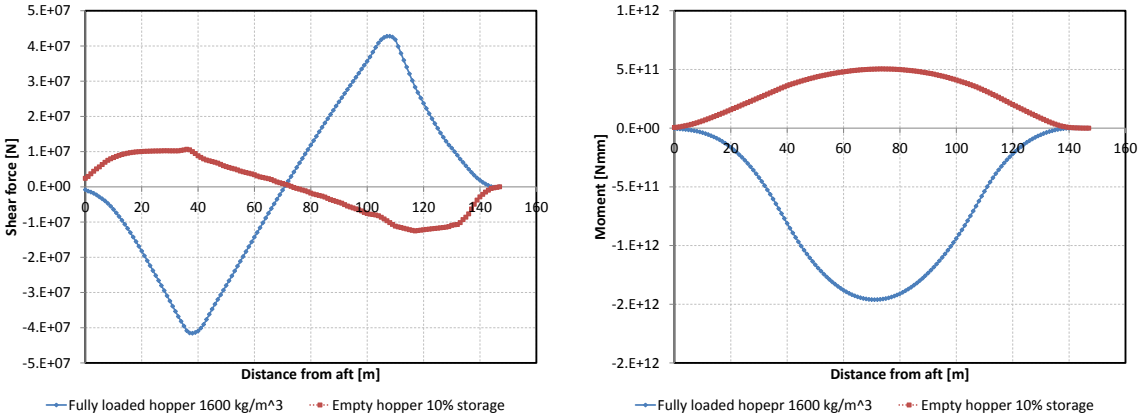


(a) (b)

Figure 3.5: **(a)** Shear force distribution hogging and sagging condition, **(b)** Vertical still water bending moment distribution hogging and sagging condition

The bending moment causes for longitudinal loading of the ships cross sections and the shear force loads the ship in vertical direction. Pressures on the fore and aft bulkhead of the hopper cargo hold result in additional longitudinal loading of the sections but this is relatively complex to determine due to the complex shape of the fore and aft part of the ship compared to the side shell of the ship. It is the expectation of the author that the longitudinal force, resulting from pressure difference between the external and internal pressures in longitudinal direction at the for and aft side of the ship, is negligibly small compared to the vertical bending moment and could therefore be neglected. This assumption is checked in section 3.3.5 where the FE model is loaded by internal pressures which are not compensated by external pressures on the fore and aft in any way. The resulting longitudinal force in x-direction due to the internal pressure is compared to the load of the bending moment.

It is assumed that the cross section of the cargo hold is symmetrical enough so that the shear stress distribution in transverse direction is negligibly small, compared to the vertical shear force, and is therefore not taken into account in the still water analysis. This does however only applies for the total cross section. The transverse shear force in half a cross section is expected to have a influence on the loading of the hull structural details. Therefore the resulting force and moment due to the pressures internally and externally are calculated for half a hull cross section. The resulting force and moment are borne by the transverse boxes in the bottom of the hopper and the cross beams at deck height. The damage reports show that fatigue is seen at the locations where longitudinal and transverse structural components meet. The hypothesis is that at these locations, due to the loading on the structural details in both longitudinal and transverse direction, the stress will be multi-axial which has an effect on the the fatigue assessment of the details.

To check the magnitude of the load, forces and moments on half a cross section including half a transverse box are calculated. the resulting transverse force and moment are determined at the neutral line of the transverse box te get an idea of the loads that are borne in the transverse boxes. Each box in the hull is loaded by the pressure that is applied on the length between the the centres of the boxes which is illustrated in **figure 3.6**. The resulting force and moment are calculated by a summation of the forces in y- and z direction and the moments in x-direction according equations 3.4, 3.5 and 3.6. The calculated force and moments are compared with the FE model is section 3.3.5

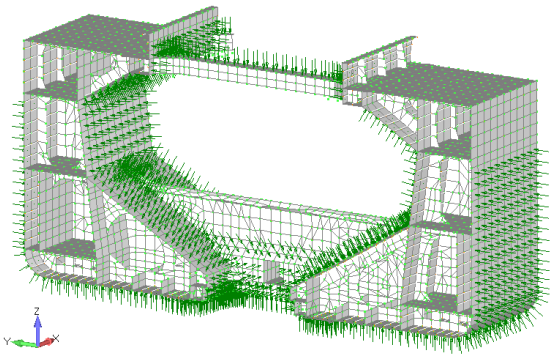

Figure 3.6: Iso view of section used for analytical analysis

$$F_y = \sum_{i=1}^{n} P_{cargo,i} \cdot A_i \cdot cos(\alpha_{y,i}) \tag{3.4}$$

$$F_z = \sum_{i=1}^{n} P_{cargo,i} \cdot A_i \cdot cos(\alpha_{y,i}) \tag{3.5}$$

$$M_x = F_y \cdot r_y + F_z \cdot r_z \tag{3.6}$$

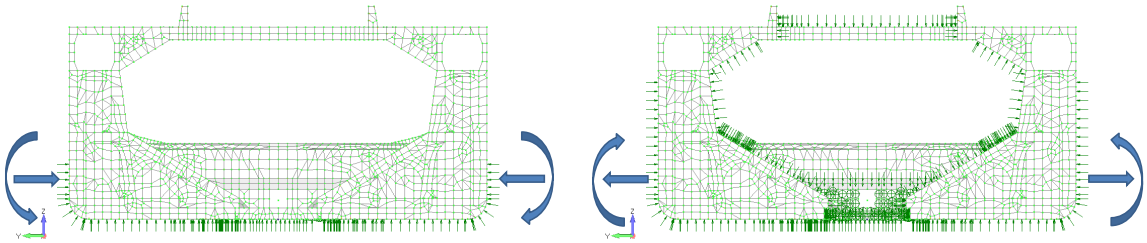

(a) (b)

Figure 3.7: **(a)** Direction of resulting force and moment on half cross section in hogging, **(b)** Direction of resulting force and moment on half cross section in sagging

### 3.2.3. Wave load components

In this section the second most significant source of fatigue loading is discussed; the wave loads. In chapter 2 the type of waves, the wave height and assessment approaches to address the waves have been discussed. The structural response of the hopper dredger due to wave loading is calculated with use of rule waves which are applicable with the simplified method for fatigue assessment. The wave loading is based on a probability of $10^{-5}$ which is equal to a wave that could occur ones every two weeks. Two types of wave loads are taken into account; global and local loads which are similar to the dredging cycle loads in the previous section. In addition to the internal local loads also inertia of the cargo due to quasi static loads is taken into account.

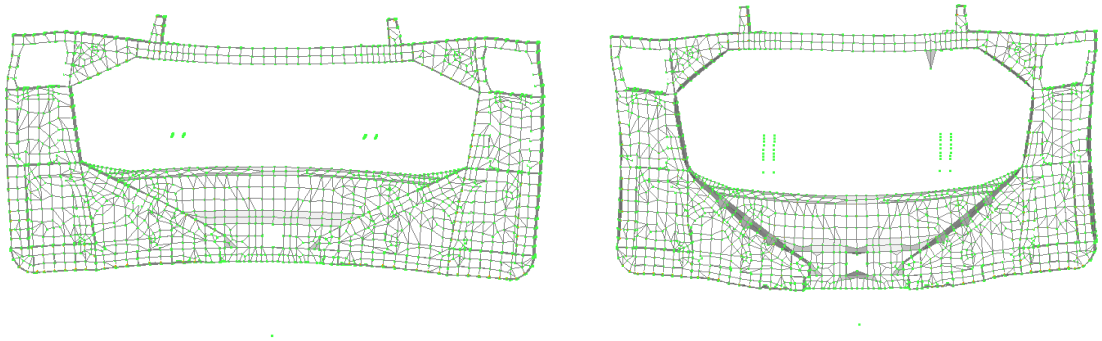

(a) (b)

Figure 3.8: **(a)** Deformed midship cross section in empty hopper condition, **(b)** Deformed midship cross section in fully loaded hopper condition

Bureau Veritas rules specify four load cases that are described by global hull girder loads, wave pressures and inertial spoil pressures. The load cases cover the extreme loads, based on a $10^{-5}$ probability, the ship will experience during its lifetime and are integrated in the rule based simplified approach to calculate the fatigue damage due to the wave loading. The following load cases are specified:

- **Load case a:** Upright ship condition taking into account static wave pressures due to head waves.
- **Load case b:** Upright ship condition taking into account inertial cargo pressures due to head waves.
- **Load case c:** Inclined ship condition taking into account static and dynamic wave and cargo pressures due to oblique waves including torsion.
- **Load case d:** Inclined ship condition taking into account static and dynamic wave and cargo pressures due to oblique waves.

The min- and max- of each load case form the stress range and are each other's conjugates except for the vertical still water bending moment bending moments which determine the load condition of the hopper. The wave load cases are illustrated in **figures 3.9** and **3.10**.

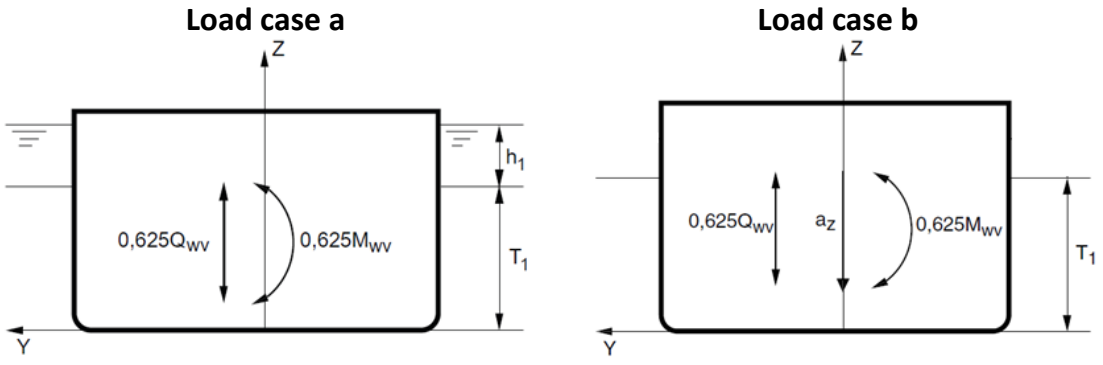


Figure 3.9: BV load cases a and b

In **figure 2.2** of chapter 2 it was shown that the allowable significant wave height depends on the load condition of the hopper dredger. According to the service notation of the assessed hopper dredger a fully loaded

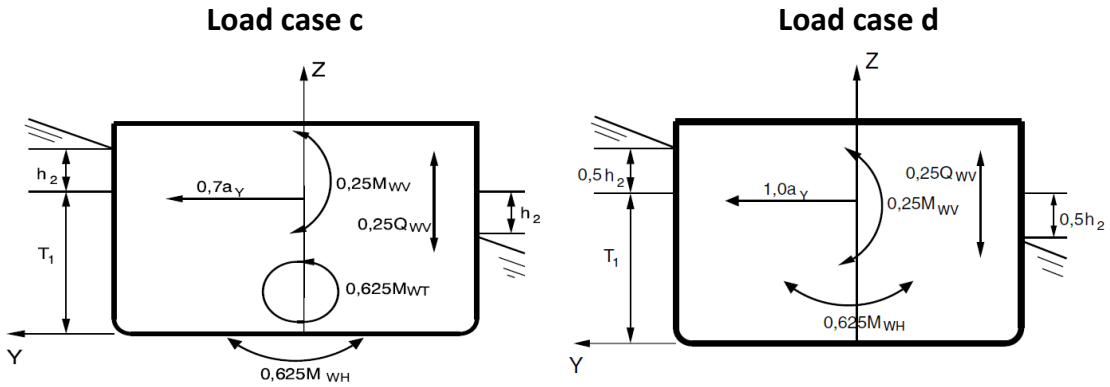


Figure 3.10: BV load cases c and d

dredger is dredging within eight miles from shore and has a dredging navigation condition coefficient of a third of the unrestricted navigation coefficient which means that much smaller wave heights are allowed. The wave loading of the dredging condition is calculated for an empty and a fully loaded hopper and the navigation condition is modelled with a hopper filled with ballast water and loaded up to summer load line according to [24]. During unrestricted navigation ballast water is pumped in the hopper to increase the stability of the ship and a higher wave height is allowed. The stress ranges in the structural details due to the wave loading are given in section 3.5.4 and are calculated for the three types of load conditions with associated navigation coefficients. The hull girder loads and local pressures used for each load case are summed up in **table 3.3**. These combinations of local pressures and hull girder loads will be used for further analysis of the hopper dredger details at midship. Note that at midship location the vertical and horizontal shear force is not taken into account due to the assumption that the still water and hull girder loads are governing factors in the determination of the structural response and the shear force is zero at maximum bending moment.

Table 3.3: Summary of BV global hull girder- and local pressure loads

| Load | Load case | | | | | | | |
|---|---|---|---|---|---|---|---|---|
| | a-min | a-max | b-min | b-max | c-min | c-max | d-min | d-max |
| Vertical wave bending moment | 1 | -1 | 1 | -1 | 0.4 | 0.4 | 0.4 | 0.4 |
| Horizontal wave bending moment | 0 | 0 | 0 | 0 | 1 | 1 | 1 | 1 |
| Torsional moment | 0 | 0 | 0 | 0 | 1 | -1 | 0 | 0 |
| Vertical wave shear force | 0 | 0 | 0 | 0 | 0 | 0 | 0 | 0 |
| Wave pressure | 1 | 1 | 0 | 0 | 0.7 | -0.7 | 1 | -1 |
| Inertial pressure | 0 | 0 | 1 | 1 | 1 | 1 | 0.5 | -0.5 |

Where the still water bending moments of the previous chapter could be obtained with use of detailed calculated bending moment document the wave bending moments are not provided in such a way. The bending moments induced by the wave loading at any given hull transverse section are given by Bureau Veritas rules [8] and could be seen in **figure 2.3** of the previous chapter. The hull girder loads resulting from the design waves are:

- Vertical wave bending moments (y-axis)
- Horizontal wave bending moments (z-axis)
- Torsional wave bending moment (x-axis)

The torsional moments on a ship cross section is the sum of the St. Vernant- and warping moments which result in St. Vernant- and warping shear stress. In addition to this the warping moment induces normal stress due to the fact that warping displacement in x-direction are restricted by the fore and aft of the hopper

dredger. Wave load cases c takes into account torsional loads on the hull structure which requires the definition of a shear centre. However, due to the complex cross sectional geometric properties it is quite labour intensive to determine the exact shear centre. It is initially assumed that the hopper dredger cross section is a thin walled U-profile. According to Paik et al. the vertical location of the shear centre in a thin walled U-profile cross section is provided based on equation 3.7[68].

$$e = -\frac{1}{I_z}\int y\omega(s)t\,ds \tag{3.7}$$

Initially a shear centre based on a simplified cross section of a bulk carrier will be used. This leads to equation 3.8 based on the geometric variables which are shown in **figure 3.11**. The shear centre e is the described by the vertical distance below the base line of the hull on the vertical neutral axis.

$$e = \frac{3B^2D^2t_s + 2D\cdot c\cdot(3B^2 - 4c^2t_d)}{B^3t_d + 6B^2Dt_s + 2c(3(B-c)^2 + c^2)t_d} \tag{3.8}$$

cdcd

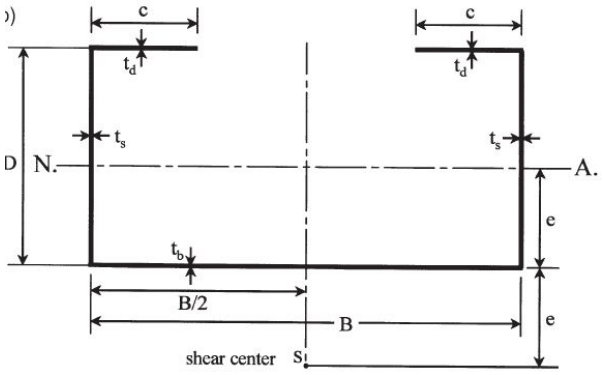


Figure 3.11: Simplified bulk carrier cross section [68]

The dimensions $t_d$, $t_s$ and $t_b$ are the deck, side shell and bottom plate thickness respectively.

A combination of waves that hit the ship and motions of the ship result in external wave pressures and internal inertial pressures. The external wave pressures are based on a reference wave heights $z_{1,2}$ along the length of the ship which is constant between 0.3L and 0.7L[8]. Hydrostatic pressure is then found with 3.9.

$$P_{wave} = \rho g z_{1,2} \tag{3.9}$$

The pressure distribution along the bottom and side shell of the hull are illustrated in **figures 3.12a** and **3.12b**.

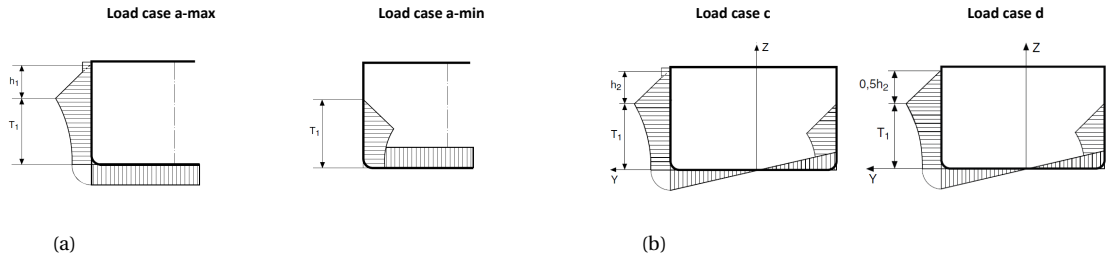


(a) (b)

Figure 3.12: **(a)** Pressures on hull due to waves for load cases a-min and a-max, **(b)** Pressures on hull due to waves for load cases c and d

The total pressure distributions due to still water and waves is plotted in **figures 3.13a**, **3.13b** and **3.13c**. Wave pressures in fully loaded condition have much less effect on the total pressure compared to an empty hopper which indicates that stress ranges in the latter condition could be larger. The model is loaded with pressure

loads using data surfaces that linearly distribute the pressure form $z = 0$ to the height of the water level. The calculated pressures are nearly linear and therefore this method is deemed accurate.

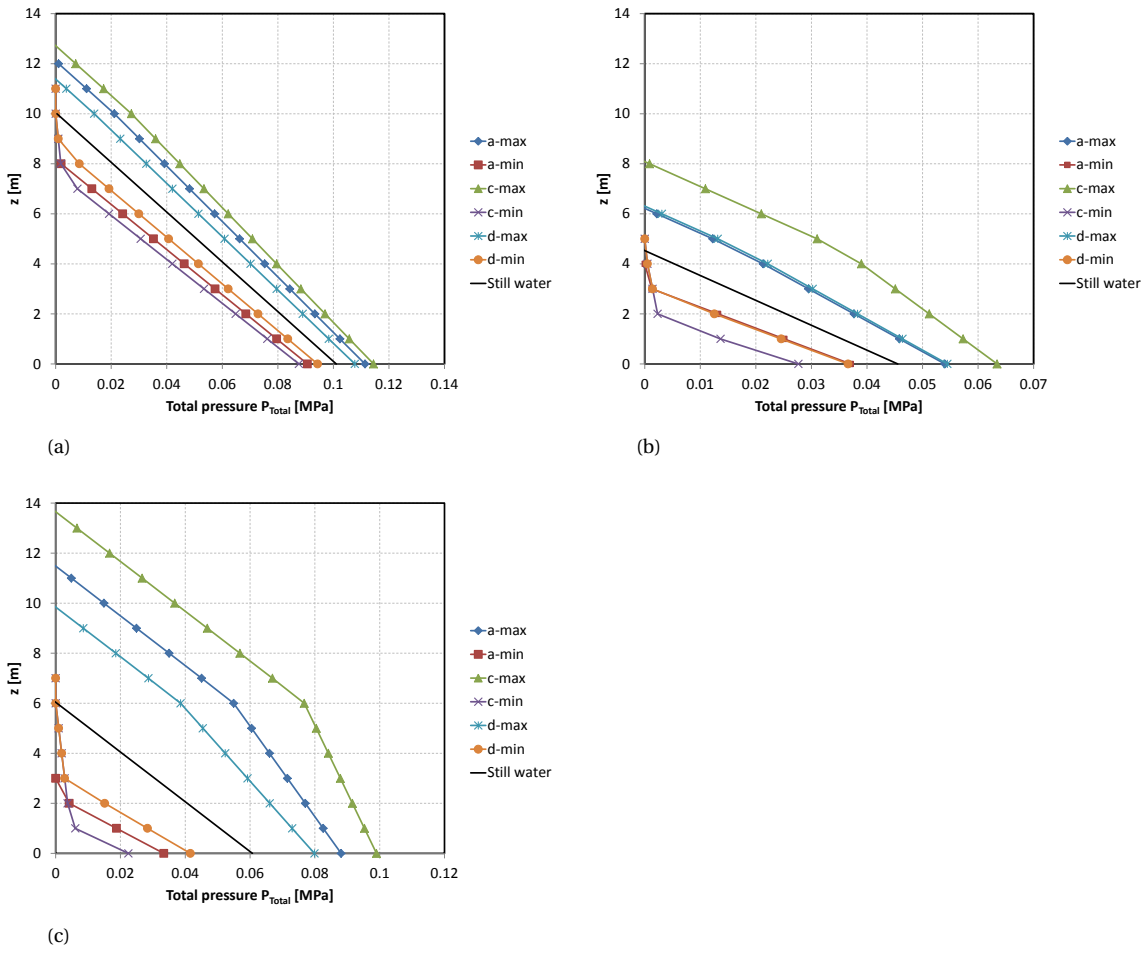


Figure 3.13: **(a)** Direction of resulting force and moment on half cross section in hogging, **(b)** Direction of resulting force and moment on half cross section in sagging, **(c)** Direction of resulting force and moment on half cross section in hogging

Calculated accelerations take into account all ship translations; surge, sway and heave and rotations roll, pitch and yaw. The acceleration in the centre of gravity of the cargo are used to compute the inertial pressures on the hopper plating. All acceleration are checked with MARS software. As explained in section3.3.3 of chapter 3 the pressure depends on the specific density, weir level and the inclination of the plate relative to the horizontal plating. With use of equations 3.2 and 3.3 the inertial pressures are expressed with equation 3.10. Note that $a_{z1}$ and $a_{z2}$ are not the same and are specifically calculated for each ship condition [8], upright or inclined.

$$P_{inertial} = \begin{cases} \rho_{sd}\sqrt{a_{x1}^2 + a_{z1}^2}\, d_i & \text{for upright ship condition} \\ \rho_{sd}\sqrt{a_{y2}^2 + a_{z2}^2}\, d_i & \text{for inclined ship condition} \end{cases} \tag{3.10}$$

## 3.3. FE model

A finite element model is used to identify and compare high stress areas with the damages found. The complexity of the hopper dredger hull structure requires a finite element analysis to capture all geometrically concentrated stress components for hot spot stress analysis. A 3D model of the analysed hopper is available to the author for analysis.

### 3.3.1. Cargo hold model

The FE model is a cargo hold plate model and contains the hull structure around the cargo area of the hopper dredger. The scope of this project is limited to this part of the hopper hull structure. This is also expected to be the part of the ship that experiences the largest loads and load differences. There are some limitations to the cargo hold model that should be taken into account. The cargo hold FE model cannot accurately simulate the torsional stress distributions because the boundary conditions depend on the structural design of the missing fore and aft part of the ship. Proper boundary conditions need to be determined to make a good representation of the actual loading of the cargo hold as close as possible.

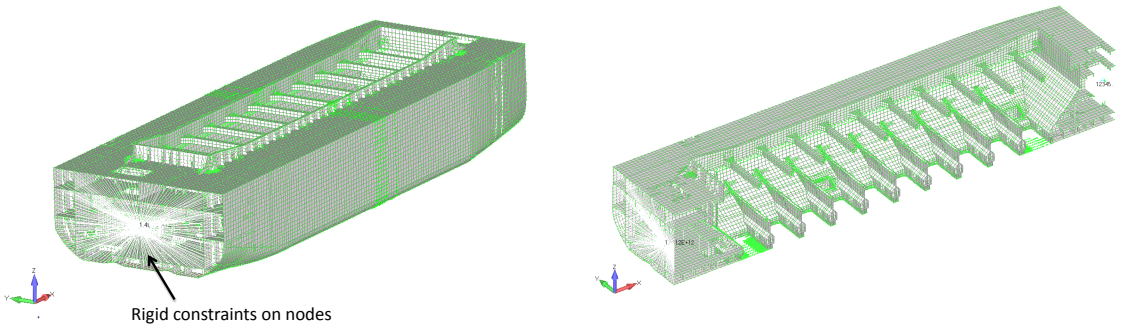


(a) (b)

Figure 3.14: **(a)** Cargo hold model FE model, **(b)** Longitudinal cross section cargo hold model FE model

### 3.3.2. Model properties

#### Finite element analysis software

A initial two dimensional analysis is performed with use of MARS2000 version 2.9h. The three dimensional FE analysis of the cargo hold model is performed with use of FEMAP v11.3.2 and solved with NX Nastran 5.

#### Coordinate system

The model is build in a basic rectangular coordinate system which finds its origin at the aft perpendicular on the centreline at the base. The axis orientation is as follows and can be seen in **figure 3.14a**:

- **X-axis:** along length of the ship from aft to fore.
- **Y-axis:** along the width of the ship from centreline to portside.
- **Z-axis:** along the height of the ship from base to deck.

#### Element types

The model is build out of plate, bar and rigid elements. Two types of plate elements are used. Three-noded triangle and four-noded quadrilateral elements. Al primary and secondary plating is build with these elements. The stiffeners are modelled with bar elements to take into account the stiffness. At both ends of the cargo model, where the fore and aft are attached, a node is placed and is connected to all nodes of the cross section with rigid body element RBE2 as can be seen in **figure 3.14a**. This is done so that the nodes of the section at the free end are still in plane after deformation. This gives a realistic representation of the connection with the aft side. As a result of using plate elements the stresses in the elements are all in a plane stress state and multi-axial loading is composed of two stress direction at maximum. Plate elements also induce the assumption that significant bending effects do not occur. The rigid body elements restrict warping displacement that is induced by torsional loads.

#### Mesh

Coarse mesh analysis is performed according BV rules for a coarse meshed three dimensional finite element model [8]:

- Webs and primary members are modelled with at least three elements in height.
- The plating is meshed with at least two elements between two primary members.
- The aspect ratio of elements is three at maximum.

And for fine mesh:

- High stresses areas are meshed with elements of at least 50x50 mm.
- Refined area is extended over at least ten elements.
- A low gradient of mesh size is applied away from the concerned area.
- Triangular shaped elements are avoided. All elements in the high stressed are are of the quad type.

#### Material

the ship hull is constructed with high strength steel AH-36 of which the material properties are given in **table 3.4**. Weld materials are not included due to the use of shell elements.

Table 3.4: Material properties AH-36 steel

| Variable | | Value | Unit |
|---|---|---|---|
| Youngs Modulus | E | 206000.00 | MPa |
| Shear Modulus | G | 79230.77 | MPa |
| Poisson's Ratio | $\nu$ | 0.30 | - |
| Yield Strength | $\sigma_y$ | 355.00 | MPa |
| Mass Density | $\rho_s$ | 7.80 | $t/m^3$ |

### 3.3.3. Corrosion addition

During the ships lifetime the thickness changes due to corrosion. A simplified approach to take corrosion addition into account is provided by IACS common structural rules [7]. The approach assumes a thickness reduction from zero thickness initially, to thickness reduction equal to the corrosion addition at the end of the design life. The thickness of the plates will have effect on the fatigue life of the structural details because less material will increase the amount of stress. If thickness would be considered as a variable value the analysis would become time consuming and rather impractical and will induce additional uncertainties. It is therefore chosen that the thickness of the plates and bars equals half the net thickness, which complies with the common structural rules for bulk carriers, and represents an average thickness during the lifetime of the ship. Model thickness which account for corrosion is expressed with equation 3.11.

$$t_{cor} = \frac{t_{gross} - t_{net}}{2} \tag{3.11}$$

#### Pressure loads

The sea pressure is applied on the bottom and side shell plating of the FE model and is linear in z-direction and constant in x-direction. The loading of the FE model is done with elemental pressures normal to the face of the elements and for each load condition j and load case i a data surface is specified to linear distribute the pressure from the bottom to the water surface. The internal cargo pressures are applied in a similar manner. Elemental pressures are defined by data surfaces which are specified for each load condition j, load cased i and depends on specific density that is used to determine the pressure according equations 3.2 and 3.3.

### Bottom doors

The bottom doors do not contribute to the longitudinal strength because otherwise the doors would be impractical for use and are therefore not included in the model. loads on the doors are directly applied on nodes in the bottom openings to simulate the presence of the doors. The main load on the doors is the pressure difference between the pressure from above, due to the mixture inside the hopper cargo hold, and the sea pressure on the bottom of the door. The pressure difference is seen as a force on the hull structure at the hinges and the supporting shaft of the bottom door opening mechanism. The mechanism is not modelled in the FE model for simplicity reasons and it is chosen to apply the forces directly on the web frame to which the support mechanism is attached. It is assumed that this will not have effect on the stress in the structural details of concern because the web frame is the load carrying support in this part of the structure. The location of the applied force is not located at any of the structural details of concern and supports the assumption of applying the forces on the web frame.

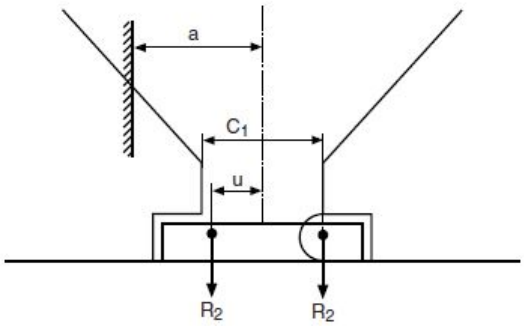


Figure 3.15: Schematic illustration hopper well type 2 [9]

$$F_{R,1} = gAP_{cargo}(\frac{c_1}{c_1 + 2u}) \tag{3.12}$$

$$F_{R,2} = gAP_r(\frac{2u}{c_1 + 2u}) \tag{3.13}$$

The applied forces are calculated with use of rules for steel ships by Bureau Veritas [9] where multiple types of bottom door configuration are specified. Type two is considered to be the most suitable for the Hopper dredger design. A schematic illustration of this type is given in **figure 3.15**. The reaction forces due to the pressure difference over the bottom door is calculated with use of equations 3.12 and 3.13. For simplicity reasons it is assumed that the reaction force on each side of the bottom door is evenly distributed over four nodes located at the hinges and the supports at one side and on four nodes on the web frames on the other side. The locations of the loads are indicated in **figures 3.16a** and **3.16b**

## 3.3.4. Boundary conditions

Boundary condition are applied to simulate to take into account the absence of the fore and aft of the ship. Six degrees of freedom are taken into account; translation in x-,y- and z-direction and rotations in x-,y-,and z-direction. Initially the shear forces and bending moments in the model are not of the same magnitude due to the absence of the fore and aft. In a modelling point of view it is difficult to have the accurate bending moment at all x-coordinates along the length of the model. It requires that at each location the bending moment has to be measured and tuned to account for the behaviour of the fore and aft. The focus of the analysis is on the area amidships and is called the tuning point. According to a sensitivity analysis of a ships structural detail performed by Chiraca et al. [21], the highest occurrence of cracks is found amidships. It is assumed that the inaccuracy of the bending moments away from the tuning point does not affect the behaviour of the structural details located at this point. The vertical bending moment is not steeply sloped as is illustrated in **figures 3.18a** and **3.18b**.

Model tuning is done assuming the cargo hold is a simple beam. According Euler-Bernoulli beam theory the shear force has to be zero at the location of maximum moment which is at the location of interest. The

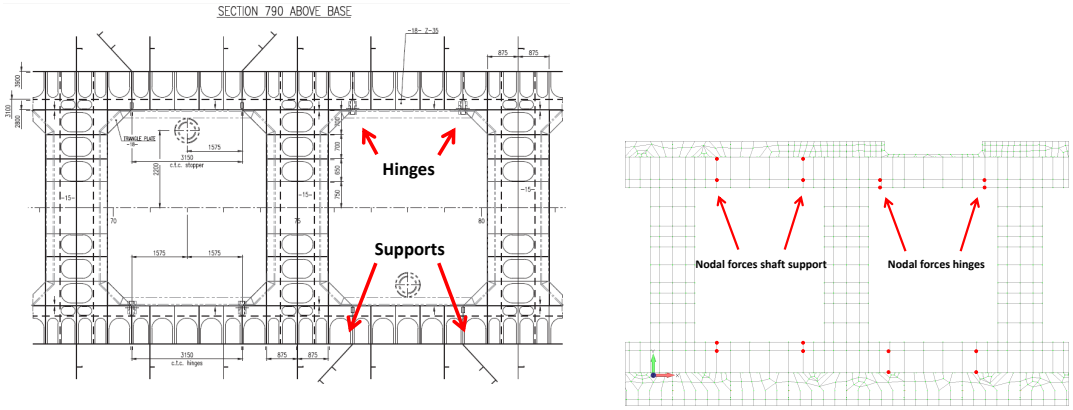


(a) (b)

Figure 3.16: **(a)** Bottom view bottom door opening drawing, **(b)** Bottom view load introduction points bottom door

following steps lead to a reasonable accurate model that is tuned for analysis and accuracies are presented in appendix A. A schematic representation of the cargo hold including tuning force and moment is given in **figure 3.17**.

- **Step 1:** Modelling of a freebody at the tuning point to capture the nodal forces and moments.
- **Step 2:** Establishment of global shear force and bending moment by nodal result summation.
- **Step 3:** Application of tuning forces and moments at free end of the model.
- **Step 4:** Determination of shear force accuracy.
- **Step 5:** Application of bending moments at free end.
- **Step 5:** Determination of bending moment accuracy.

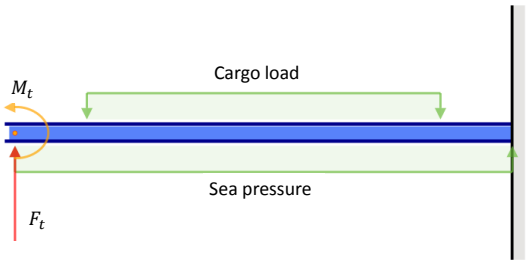


Figure 3.17: Beam representation of the cargo hold model

### 3.3.5. Model validation

The FE model is validated to assure an accurate representation of the structural response compared to the analytical response. Due to the complexity of the structure the model is validated by calculation of the global loads. Local loads due to geometrical discontinuities are assumed to be accurately calculated by finite elements results. **Figures 3.18a** and **3.18b** shows the moments, obtained from the still water document, and the moments measured in the tuned model. The figures show the bending moments along the length for the

empty and fully loaded condition. The model is tuned at 71 meters where the maximum moment for the fully loaded condition is found. The bending moment in sagging is significantly larger than the moment in hogging and is considered to have the most contribution to the stress range for that reason it is chosen to tune the model at the location where the maximum sagging moment occurs.

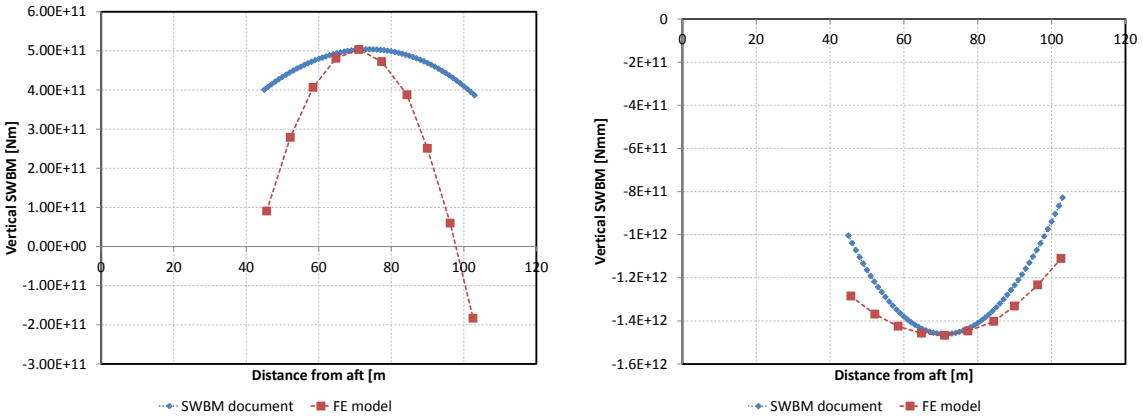


(a) (b)

Figure 3.18: **(a)** Vertical still water bending moment maximum hogging condition, **(b)** Vertical still water bending moment maximum sagging condition

The moment lines that are plotted in the figure above show that only at the tuning point the moment is equal to the actual moment. An error can be seen away from the tuning point which is a result of the shear force distribution along the length of the model. The shear force lines for both conditions are plotted in **figures 3.19a** and **3.19b**. The exponent of the shear force of the FE model in hogging condition is significantly higher than the actual shear force exponent. This difference is assumed to be due to the absence of distributed mass along the length of the model. The superstructures on the deck of the ship cause a mass distribution along the length of the ship and affect the gradient of the shear force line.

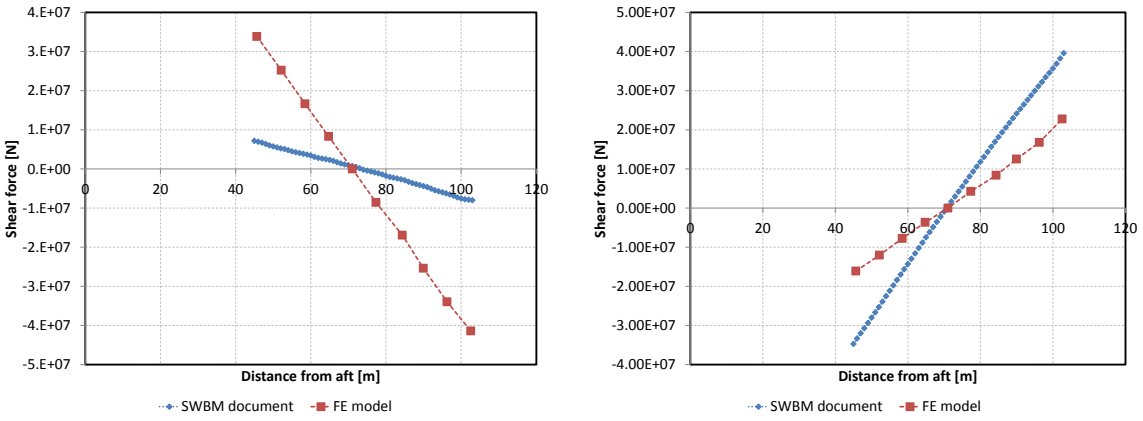


(a) (b)

Figure 3.19: **(a)** Shear force hogging condition, **(b)** Shear force sagging condition

## Stress

Simple beam theory is used to calculated the stress at the tuning point with use of the cross sectional properties obtained by Mars software. Since longitudinal forces are not considered solely the bending moment is used in determination of the normal stress as by equation 3.14.

$$\sigma_{x_l e} = \frac{M_x}{Z} \tag{3.14}$$

The stress at the openings (coaming and bottom openings) is higher due to geometrical stress concentrations and is therefore the stress further away from the openings is considered nominal and used for comparison. The results are given in **table 3.5**. Stress measured in the model is comparable with analytical calculation and the model is therefore considered sufficiently accurate at the tuning point. Stress is determined with a globally loaded model to exclude the effect of tertiary loads due to local plate pressures.

Table 3.5: Normal stress values in x-direction deck and bottom

| | Analytical | FE model | error |
|---|---|---|---|
| $\sigma_x$ Bottom [MPa] | 136.16 | 139.32 | 2.27% |
| $\sigma_x$ Deck [MPa] | -154.77 | -154.90 | 0.08% |

The assumption that model calibration for forces in longitudinal direction could be neglected is checked. The normal stress induced by the longitudinal force is calculated with equation 3.15 assuming that the entire cross section is effective. It is concluded that the normal stress has little effect on the total stress and could be considered insignificant.

$$\sigma_{x,le} = \frac{F_x}{A} \tag{3.15}$$

Table 3.6: Normal stress due to resulting longitudinal force

| | Normal stress bottom | Longitudinal force normal stress | portion |
|---|---|---|---|
| $\sigma_x$ Empty hopper [MPa] | 47.27 | -0.22 | 0.47% |
| $\sigma_x$ Fully loaded hopper [MPa] | 139.32 | 8.43 | 6.05% |

Validation of secondary local pressure loads is done by comparison of the resulting force and moment in the neutral axis of the transverse box which where determined analytically in section 3.2.2. The force in y-direction and moment in x-direction of calculated values and FE model results are presented in **table 3.7**. Both calculations give similar values and the FE model is therefore considered accurate in terms of transverse pressure difference.

Table 3.7: Comparison of force and moment in transverse box analytically and FE model result

| | | Analytical | FE model | Errror |
|---|---|---|---|---|
| Tension force [N] | $F_y$ | 5.34E+06 | 5.66E+06 | -5.98% |
| Moment [Nmm] | $M_y$ | 1.83E+10 | 1.77E+10 | 3.31% |

## 3.4. Coarse mesh analysis

The structural response in the area of the tuning point is validated and a coarse mesh analysis is performed to identify fatigue critical details for fine mesh analysis.

### 3.4.1. Area of analysis

The loading of the hopper results in high stressed areas in the hull structure which require a more detailed analysis due to the fact that fatigue is a local phenomenon. This is initially done with a coarse mesh that meets BV requirements. It is already concluded that most damages are found in the area of the bottom door openings and the splash coaming amidships. It is chosen that the coaming area is outside the scope of this project and further analysis is done on the structural details in de bottom door opening corners based on the expected higher stresses in the bottom plating compared to the deck due to the smaller hogging moment.

### 3.4.2. Still water analysis

Initially the model is loaded with still water loads according the load conditions specified in the dredging cycle. Paths along the width of the bottom are used to get en indication of the structural behaviour in the

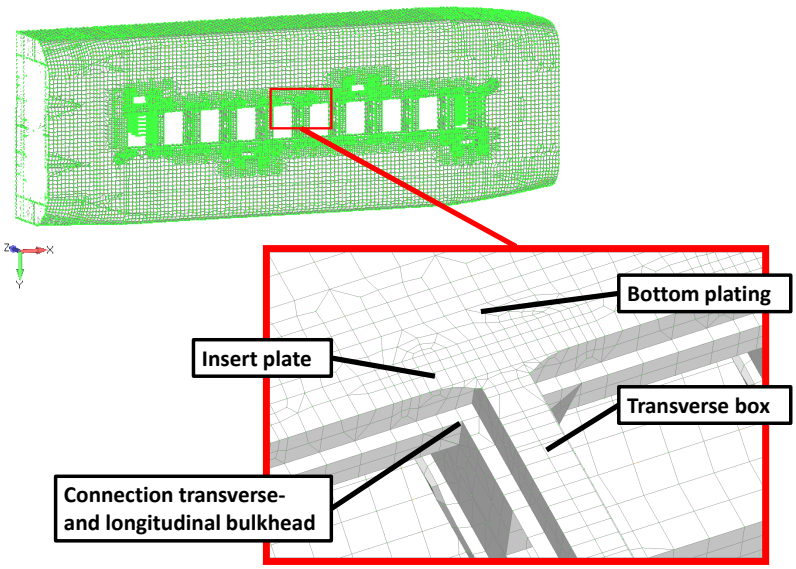


Figure 3.20: Illustration of studied area at bottom opening corner amid ships

midship cross section through the transverse structure separating the discharge openings. **Figures 3.21a** and **3.21b** show the normal stresses in the bottom for an empty and fully loaded hopper. This confirms the expected structural behaviour from the analytical analysis in section 3. Neglecting the fact that ellipses of the insert plates in the opening corners captures some stress induced by longitudinal forces it is concluded that the transverse box does not to contribute to the longitudinal strength.

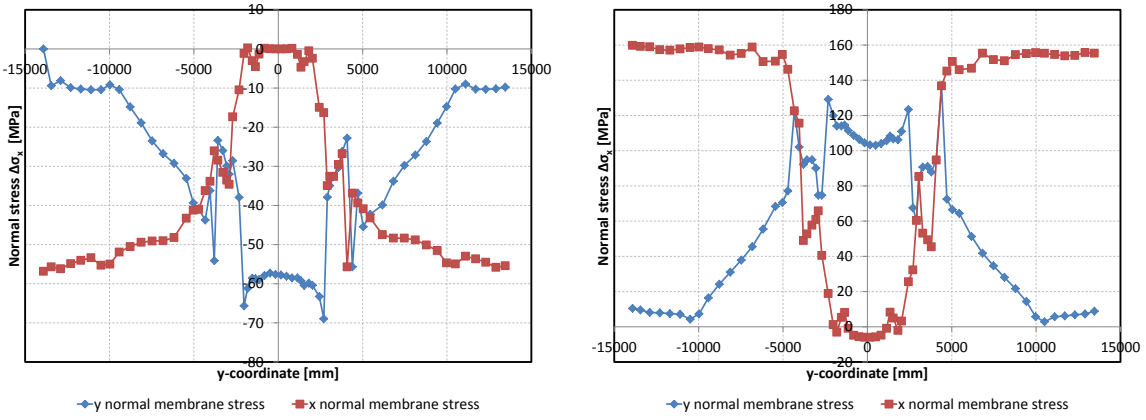


(a) (b)

Figure 3.21: **(a)** X and Y normal stress empty hopper along width at midship, **(b)** X and Y normal stress fully loaded hopper along width at midship

The fact the the ratio between the x- and the y normal stress change entering the transverse box means that the direction of the principal stress deviates. This validates the assumption that the stress in the bottom corners is in a multi-axial stress state. The results of this analysis raises two questions which are further assessed in the fine mesh analysis. To establish the maximum stress range, the load step at which the dredging cycle reaches the maximum stress should be determined. It would also be interesting to know the effect that the local pressure has on the total stress range. If the dredging cycle is dominant in fatigue analysis and the stress range is determined mainly by hull girder loads, a initial fatigue check could be done in an early design stage without requirements of pressure loading calculations.

## 3.5. Fine mesh analysis

High stress structural details in the bottom opening corners are selected from the coarse mesh analysis and are:

- Corner longitudinal hopper bulkhead plating 790 mm above base.
- Corner transverse bulkhead plating 790 mm above base.
- Insert plate ellipse at base.

Fine mesh is made of the structural details according applicable mesh requirements associated with the selected hot spot stress calculation procedures. These require mesh size dimensions equal to the plate thickness. Mesh convergence is confirmed in all hot spots by increasing mesh. The selected procedures describe modelling and post processing methods which are applicable with specific design SN-curves to which the hot spot stress is calibrated.

Table 3.8: Element properties of fine mesh; *plate thickness with half corrosion addition

| | Cruciform joint | Insert plate ellipse | |
|---|---|---|---|
| Element type | Shell | Beam | |
| Nodes | 4 | 2 | |
| Shape | Quad | Line | |
| Plate thickness * | 13.75 | 28.75 | mm |
| Element dimensions | 13x13 | 25x1x28.75 | mm |

The height of the beams are as that of the thickness of the insert plate width half the corrosion addition. The width of the beam is very small so the beams do not contribute to the stiffness of the insert plate.

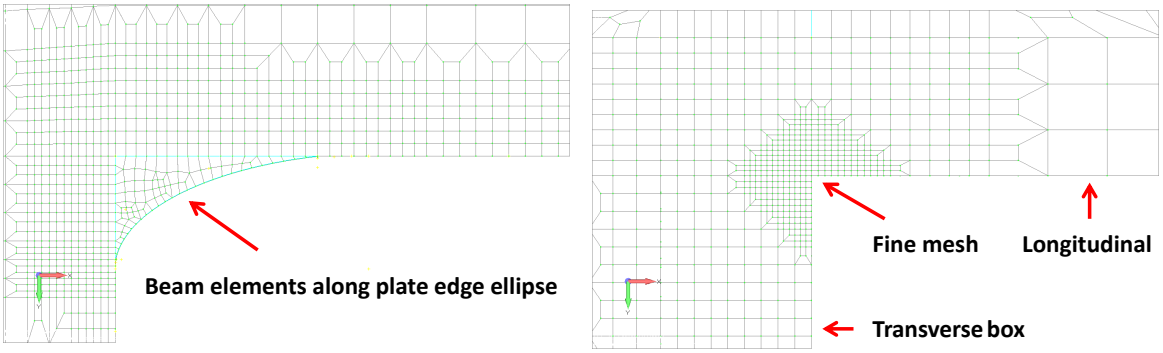


(a) (b)

Figure 3.22: **(a)** Bottom view of fine mesh of the insert plate at midship, **(b)** Fine mesh of connection transverse box and hopper longitudinal

### 3.5.1. Transverse box connection

The connection of the traverse box with the hopper longitudinal is interpreted as being a web stiffened cruciform. The conventional hot spot stress extrapolation method proposed by the IIW will lead to exaggerated hot spot stress values in a shell model according to a comparative study performed by Osawa et al. [67]. Bureau Veritas Guideline for fatigue assessment [11] provides a procedure to determine the hot spot stress in this type of welded joint. The same procedure is described in Common Structural Rules (CSR) for bulk carriers by IACS [6] and was originally proposed by I. Lotsberg [52]. Lotsberg's procedure will give slightly higher values of the hot spot stress but is deemed accurate [67] in case of a web stiffened cruciform joint. The procedure is calibrated such that the surface hot spot stress at the actual weld toe is calculated. The weld is not included in the shell model so the stress is measured at a position 3.17 shifted from shell element intersection given by equation 3.17. In the flanges this read-out point depends on the weld leg length of the weld between the longitudinal and transverse bulkhead. The properties of structural detail used for hot spot stress calculation are given in **table 3.9**.

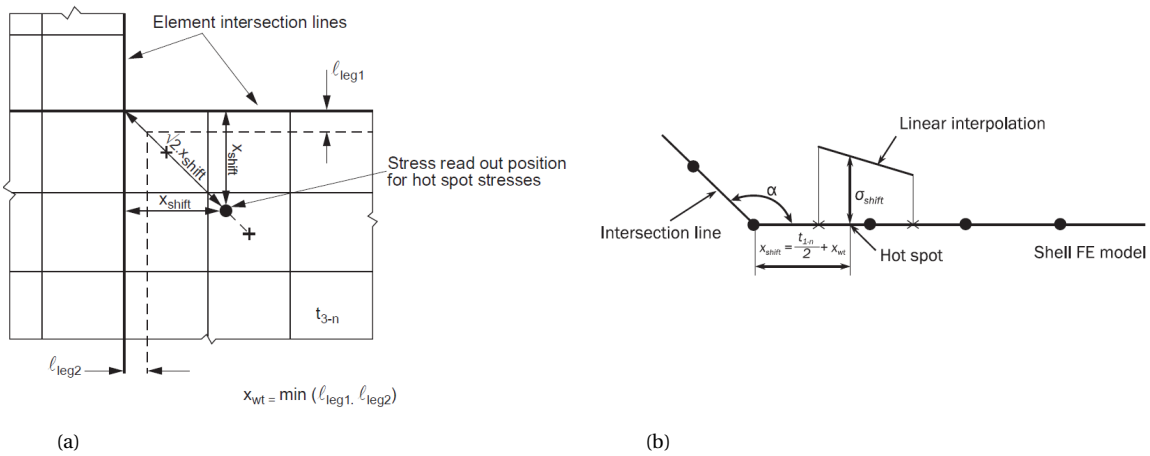


Figure 3.23: **(a)** Hot spot stress read-out position, **(b)** Hot spot stress read-out position flange

Table 3.9: Structural detail specifications longitudinal- and transverse bulkhead

| Variable | | Value | Unit |
|---|---|---|---|
| Half net plate thickness longitudinal bulkhead | $t_{0.5net}$ | 13.75 | mm |
| Half net plate thickness Transverse bulkhead | $t_{0.5net}$ | 13.75 | mm |
| Weld throat | ac | 7.75 | mm |
| Weld leg length | $x_{wl}$ | 10.85 | mm |

$$\sigma_{hs} = 1.12\sigma_{shift} \tag{3.16}$$

$$x_{shift} = \frac{t_{0.5net}}{2} + x_{wl} \tag{3.17}$$

$$\sigma_{shift,le} = f_w f_s[\sigma_{m,le}(x_{shift}) + \sigma_{b,le}(x_{shift})]\beta_{hs} \tag{3.18}$$

Here are $f_w$ and $f_s$ correction factors to take into account stress gradient along the weld line and effect of the supporting member respectively. $\sigma_{m,le}$ and $\sigma_{b,le}$ are the membrane and bending stresses of the elemental stress tensor and $\beta_{hs}$ is the hotspot stress correction factor which takes into account the effect of the angle between the transverse bulkhead and the longitudinal bulkhead.

The hot spot stress procedure to determine the hot spot stress in the web plate of the cruciform joint is slightly different to the procedure applicable for the flange. At this location two welds meet and both welds need to be accounted for in the hot spot stress measurement. The location of the hot spot stress tensor is located at an $x_{shift}$ distance from both welds dominated by the weld with the least weld leg length. The specifications of the structural detail are given in **table 3.10**. Equations 3.17 and 3.18 are used to calculate the stress tensor and is equivalent to the hot spot stress which is expressed in equation 3.19.

Table 3.10: Structural detail specifications web plate

| Variable | | Value | Unit |
|---|---|---|---|
| Half net plate thickness longitudinal bulkhead | $t_{0.5n}$ | 13.75 | mm |
| Half net plate thickness transverse bulkhead bulkhead | $t_{0.5n}$ | 13.75 | mm |
| Half net plate thickness web plate | $t_{0.5n}$ | 13.75 | mm |
| Weld throat | ac | 6.75 | mm |
| Weld leg length | $x_{wl}$ | 9.45 | mm |

$$\sigma_{hs,le} = \sigma_{shift,le} \tag{3.19}$$

The stress in the cruciform joint is multi-axial and therefore the maximum principal stress range is selected. Two principal stress ranges with each a certain angle relative to the perpendicular direction of the weld are calculated. The stress ranges of the stress components are used to compute the maximum principal stress range between two load conditions. With use of the theory of Mohr's circle the stress range components are transformed in the direction of the maximum principal stress range. This is done with the transformation matrix P and a certain principal stress directional angle $\theta$.

$$\begin{cases} \Delta\sigma_{x,le} = \sigma_{x1,le} - \sigma_{x2,le} \\ \Delta\sigma_{y,le} = \sigma_{y1,le} - \sigma_{y2,le} \\ \Delta\sigma_{xy,le} = \sigma_{xy1,le} - \sigma_{xy2,le} \end{cases} \tag{3.20}$$

Here is $\sigma_{ii}$ the hot spot stress tensor component for a certain load condition and load case. $\Delta\sigma_{le}$ is the stress difference in the direction of the each stress tensor component. The principal stress angle is then calculated with use of these stress differences using the expression:

$$\theta = 0.5 tan^{-1}[\frac{2\Delta\sigma_{xy,le}}{\Delta\sigma_{x,le} - \Delta\sigma_{y,le}}] \tag{3.21}$$

Where $\theta$ is the angle of the hot spot principal stress range relative to the perpendicular to the weld. The first and second maximum principal stress ranges are then expressed by:

$$\begin{bmatrix} \Delta\sigma_{1,le} \\ \Delta\sigma_{2,le} \end{bmatrix} = [P] \cdot \begin{bmatrix} \Delta\sigma_{x,le} \\ \Delta\sigma_{y,le} \\ \Delta\sigma_{xy,le} \end{bmatrix} \tag{3.22}$$

$$[P] = \begin{bmatrix} 0.5[1 + cos(2\theta)] & 0.5[1 - cos(2\theta)] & sin(2\theta) \\ 0.5[1 + cos(2\theta + \pi)] & 0.5[1 - cos(2\theta + \pi)] & sin(2\theta + \pi) \end{bmatrix} \tag{3.23}$$

### 3.5.2. Insert plate ellipse

Cracks in the insert plate ellipse form at the cut edge surface of the ellipse. As presented in **figure 3.24a** the stress is concentrated at the edge. The maximum stress in the cross section of the beam elements at the edge is considered to be the hot spot stress. The rotational stiffness of the beam elements in direction of the z-axis is negligibly small due to the small width of the beam. The bending moment around the strong axis and the resultant axial force in the cross section determine the hot spot stress which is calculated according equation 3.24.

$$\sigma_{le} = \frac{M_y \cdot z}{I_y} + \frac{F}{A_{beam}} \tag{3.24}$$

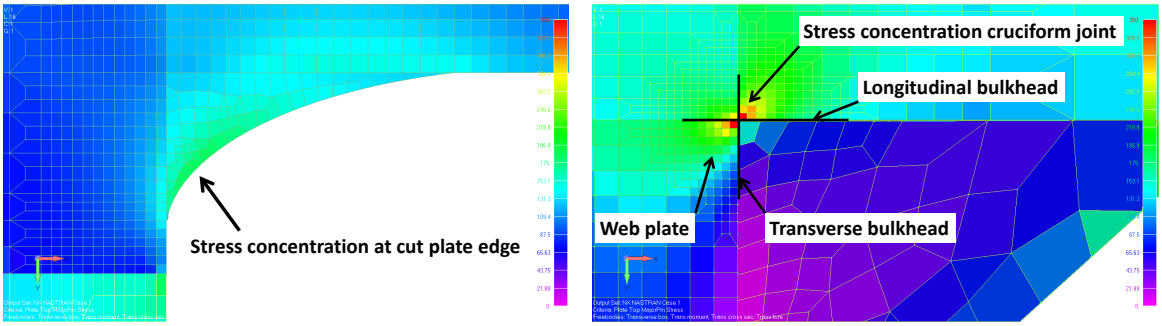


(a) (b)

Figure 3.24: **(a)** First principal stress insert plate in fully loaded condition, **(b)** First principal stress transverse box connection in fully loaded condition

### 3.5.3. Still water stress ranges

The still water stress range is described by the minimum and maximum stress that is seen in one load cycle of the hopper. The description of the dredging cycle shows that the draught and still water bending moment do not significantly change after a specific density of $1600 kg/m^3$. The weir level and specific density on the other hand do change. **Figure 3.25** shows that the stress as function of the specific density in the hopper. A maximum hotspot stress is calculated for a specific density of $1600 kg/m^3$. This leads the conclusion that the weir level in the hopper has more effect on the stress than the specific density that is present in the hopper. This is accompanied by the fact that the spoil in the hopper is considered a solid substance when a specific density of $1400 kg/m^3$. Only the surfaces in the hopper that have an angle less than 90° with the horizontal plane are affected by pressure increase due to increasing specific density.

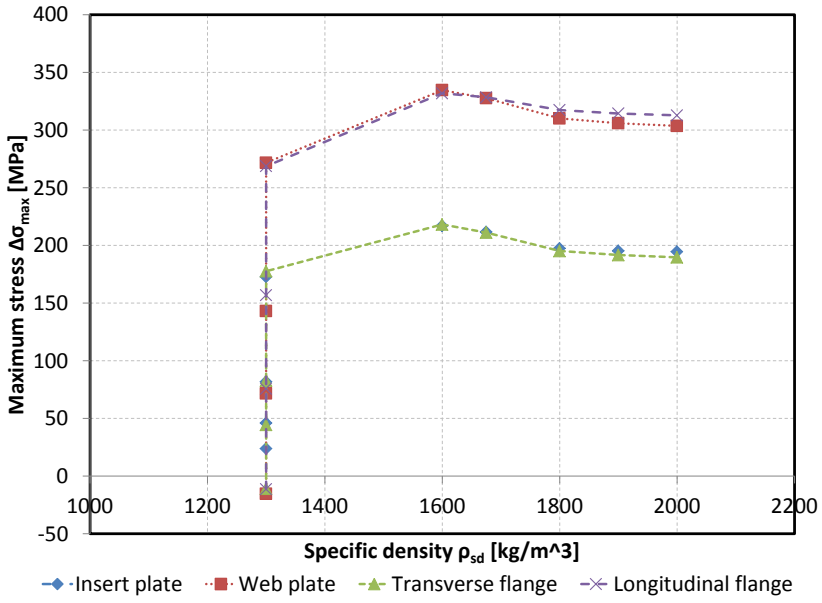


Figure 3.25: Maximum hotspot stress in analysed critical details for each load condition in dredging cycle

Table 3.11: Maximum principal stress ranges

| | Still water stress range $\Delta\sigma_{le}$ [MPa] |
|---|---|
| Longitudinal bulkhead | 439 |
| Transverse bulkhead | 316 |
| Web plate | 463 |
| Insert plate ellipse | 327 |

### 3.5.4. Wave stress ranges

The hotspot stresses are calculated with use of the procedures explained in section **??**. The wave stress ranges in the fully loaded condition are calculated for a the maximum load condition determined in section 3.5.3. The hotspot stresses are presented in tables 3.12, 3.13 and 3.14.

Table 3.12: Stress ranges empty hopper during dredging operations

| Load case | a | c | d |
|---|---|---|---|
| Longitudinal flange [MPa] | 14 | 32 | 22 |
| Transverse Flange [MPa] | 31 | 7 | 10 |
| Web plate [MPa] | 21 | 19 | 16 |
| Insert plate ellipse [MPa] | 36 | 30 | 6 |

The stress ranges in **table 3.12** show that head waves result in higher stress ranges as a result of load cases a and b. This is a trend that is also seen for the fully loaded hopper in **table 3.13** and the hopper in navigation condition according to **table 3.14**.

Table 3.13: Stress ranges fully loaded hopper during dredging operations

| Load case | a | b | c | d |
|---|---|---|---|---|
| Longitudinal flange [MPa] | 17 | 11 | 19 | 22 |
| Transverse Flange [MPa] | 38 | 128 | 4 | 8 |
| Web plate [MPa] | 25 | 86 | 15 | 15 |
| Insert plate ellipse [MPa] | 38 | 98 | 17 | 12 |

Load case a, c and d do not seem to be affected by the local pressure since the stress ranges due not significantly change between empty and fully loaded hopper. The stress ranges of these load cases are higher for the navigation condition because of higher significant wave heights. The large increase of stress range seen for load case b is explained by the presence of cargo in the hopper and the fact that load case b considers downward accelerations where the countering sea pressure does not change.

Table 3.14: Stress ranges partially filled hopper during navigation

| | a | b | c | d |
|---|---|---|---|---|
| Longitudinal flange [MPa] | 54 | 26 | 62 | 31 |
| Transverse Flange [MPa] | 104 | 82 | 30 | 28 |
| Web plate [MPa] | 107 | 69 | 35 | 35 |
| Insert plate ellipse [MPa] | 126 | 100 | 54 | 38 |

The wave stress ranges for each load condition are illustrated in **figure 3.26**. Head waves seem to be dominant for the hot spots located in the transverse box. This is different on the longitudinal side where the maximum load case is in inclined ship condition.
According to the CSR-H [7] the wave loading is the governing load component in longitudinal stiffeners located in the side shell. This could explain why the stress ranges at the hot spots in the bottom area, close to the vertical neutral axis, are this low. Wave energy dissipates in depth which means that the cycle range at the water surface is higher than the wave load change at more depth. Regarding the global wave induced

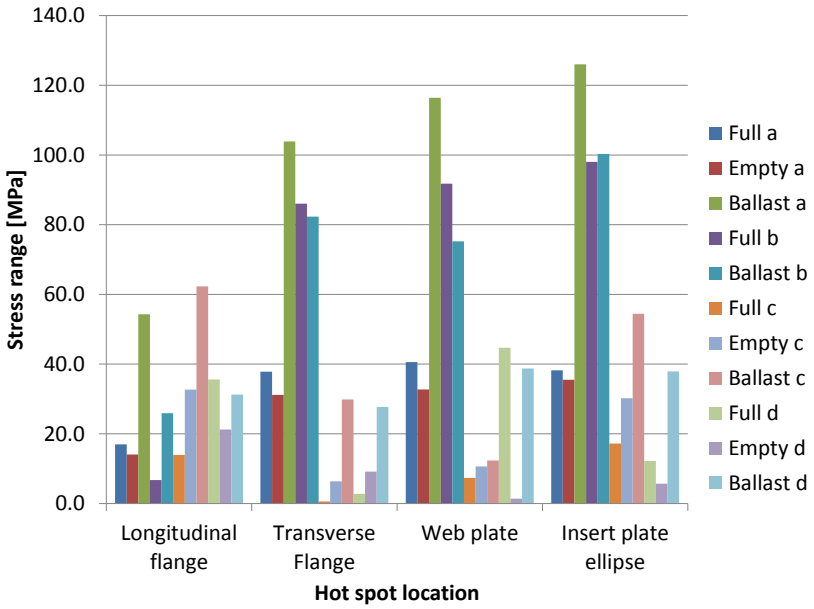


Figure 3.26: Wave stress ranges at hot spot of multiple load condition and load cases

loads; hull girder loads due to waves, such as vertical, horizontal and torsional moments, result in a higher stress further away from the neutral axis. The bottom door openings in this v-shaped hopper are located in the longitudinal centre line of the ship and will experience less effect of moments other than the vertical still water bending moment.

### 3.5.5. Dredging cycle waves

The still water load cycle is established in section 3 with identification of the maximum load conditions. According to the BV guideline the still water stress amplitude with maximum wave amplitude that could occur during hopper loading fully describes the dredging cycle. The wave loading in the previous sections is based on a probability of a wave that occurs once in about two weeks and has to be reduced to simulate a wave that occurs every day. This means that the probability of the wave has to be increased from $10^{-5}$ to a probability of $10^{-4}$. The dredging cycle stress range is illustrate in **figure 3.27** and is called the loading/unloading cycle in this figure.

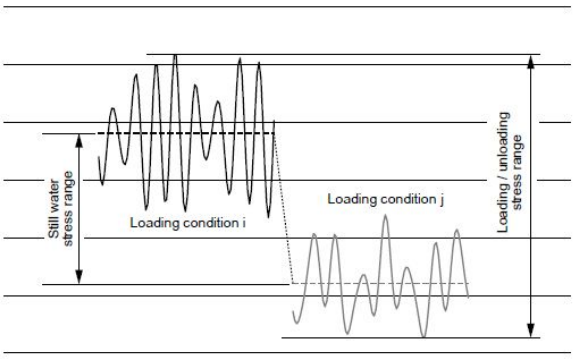


Figure 3.27: Combined still water and wave loading [11]

Reducing the waves requires for reduction of the global hull girder loads and relative ship motion parameters. Global hull girder loads specified in the load cases of Bureau Veritas are multiplied by a factor of 0.625 which represents the wave reduction of a wave with $10^{-8}$ to a wave with a probability of $10^{-5}$ and is found with use of the Weibull probability density function. A reduction factor is calculated by the derivation in the equations below. The Weibull distribution is given by equation 3.25 [4].

$$P(S \leq s) = 1 - e^{-\left(\frac{s}{\delta}\right)^{\gamma}} \tag{3.25}$$

To find the stress range associated with the probability of $10^{-4}$ a reference stress range with associated reference probability is introduced. Initial wave probability of $10^{-5}$ is the reference probability $\frac{1}{N_{ref}}$. The reference stress range $S_{ref}$ is the wave stress range from section 3.5.4. The scale parameter $\delta$ of the reference Weibull distribution is given by equation 3.26 [4].

$$\delta = \frac{S_{ref}}{ln(N_{ref})^{\frac{1}{\gamma}}} \tag{3.26}$$

$$P(S > S_{ref}) = \frac{1}{N_{ref}} \tag{3.27}$$

The probability that the stress range exceeds the reference stress range is adjusted to $10^{-4}$ and is substituted into equation 3.25 which results in equation 3.28. A shape parameter is not known for this vessel so a shape parameter $\gamma = 1$ is assumed according Bureau Veritas guideline [11] and the final expression of the reduced stress range is given in equation 3.29.

$$ln(10^{-4}) = -\left(\frac{S_{10^{-4}} \cdot ln(10^5)^{\frac{1}{\gamma}}}{S_{ref}}\right)^{\gamma} \tag{3.28}$$

$$S_{10^{-4}} = S_{ref} \cdot \left(\frac{ln(10^{-4})}{ln(10^{-5})}\right) \tag{3.29}$$

The derivation shows that the wave stress ranges should be multiplied by 0.8 to find the stress range for a wave probability of $10^{-4}$. Note that the wave stress range in direction of the maximum principal still water stress range is used so the stresses could be added up. When the reduced stress range is known the amplitude of the wave cycle is considered to be half that of the stress range since the minimum and maximum conditions of the load cases are each other's conjugates and it could be expected that the amplitudes of these conditions are nearly the same. The amplitudes are added up to the still water stress range and the dredging cycle is obtained and given in **table 3.15**.

Table 3.15: Maximum principal stress ranges for still water stress range including maximum wave amplitude

| | Stress range $\Delta\sigma_{le}$ [MPa] |
|---|---|
| Longitudinal bulkhead | 489 |
| Transverse bulkhead | 379 |
| Web plate | 514 |
| Insert plate ellipse | 381 |

### 3.5.6. Effect local pressure

It is interesting to see what the influence of the local pressure is on the structural response of the ship. This results in a better understanding of the structural behaviour of the hull of the hopper dredger. Also, in section 3.5.3 it is seen that the local pressure does have some influence in some extent. If global hull girder loads are dominating the structural response the damage in terms of fatigue due to the dredging cycle could already be estimated in a early design phase since the global loads are part of the main specification of a hopper dredger.

First the model is loaded with only the still water bending moment at the end of the non-clamped side. This results in a constant moment along the entire length of the model. Secondly pressure loads are applied and the model is tuned according to the same required global loading. **Table 3.16** shows the difference in hot spot

stress range between a model that is loaded with local and global loads and a model that is only loaded with global loading.

It is found that local pressure has a significant effect on the loading of the structural details in case these are found in the transverse box structure. This can be explained by the contribution of the transverse boxes to the longitudinal strength of the ship. If the hull is loaded with only global hull girder loads there is almost no stress seen in the transverse boxes. If transverse pressures are applied the transverse boxes catch the tension and bending loads due to the internal and external pressure difference. As a result the bottom opening corners are loaded in a second (transverse) direction in which even larger stresses are seen than due to longitudinal bending loads. In case of the insert plate the location of maximum stress range shifts along the edge of the ellipse from the longitudinal side towards the transverse side between the model that is loaded with and without local loads.

Table 3.16: FE model stress ranges compared with global loaded model

| | $\Delta\sigma_{le}$ global + local [MPa] | $\Delta\sigma_{le}$ global [MPa] | Proportion global loading |
|---|---|---|---|
| Longitudinal bulkhead | 443 | 304 | 69% |
| Transverse bulkhead | 379 | 86 | 23% |
| Web plate | 514 | 207 | 40% |
| Insert plate ellipse | 388 | 60 | 15% |

### 3.5.7. Proportionality

The potential effect of proportional loading is discussed in chapter 2. The direction of the principal stress ranges calculated in section **??** show that the stresses in the connection of the transverse box are of multiaxial nature which is especially true for the transverse box plating. The directional angle between the normal direction to the weld and the maximum principal stress range in the cruciform joint are given in **table 3.17**. An analysis of all principal stress directions during the dredging cycle is done to see if the ratio between shear and normal stress deviates. **Figure 3.28** shows the load paths of the stress in each hotspot in the connection of the transverse box. The stress in the insert plate is considered to be a plane stress state due to the fact that it is a plate and therefore thickness effects are neglected. This means that at the edge of the plate the stress direction will always be in the direction along the edge of the plate and therefore the stress in the insert plate is anyway proportional and excluded from the analysis. The load paths in the figure show a linear relation between the shear and normal stress and it is therefore concluded that the loading of the corner is proportional.

Table 3.17: Maximum principal stress range directions

| | Direction maximum principal stress $\theta$ | Axis normal direction weld |
|---|---|---|
| Longitudinal bulkhead | 6.47° | x-axis |
| Transverse bulkhead | 11.85° | y-axis |
| Web plate | 39.14° | y-axis |

The maximum principal stress range directions of the wave loading deviate relative to the still water dredging cycle loading. For fatigue analysis the fatigue damage due to wave loading is independently calculated and added with Miner's sum. In design codes [11] [79] and IIW recommendations [39] the principal stresses within a certain angular sector are considered normal to the weld if wave stress range angles do not exceed 45 degrees. This means that different directions of the wave load cases do not affect the fatigue assessment on condition of the direction being within the first sector. In addition to this, the waves are based on a deterministic approach which uses equivalent design waves that cover the extreme conditions to which the ship is exposed to. If the wave loading would be considered non-proportional the assessment of the load path would be non-realistic and require a more detailed approach of the wave loading. The stress ranges in dredging condition are relatively low and the navigation condition is a small part of the operational life so therefore it is chosen to keep this out of the assessment.

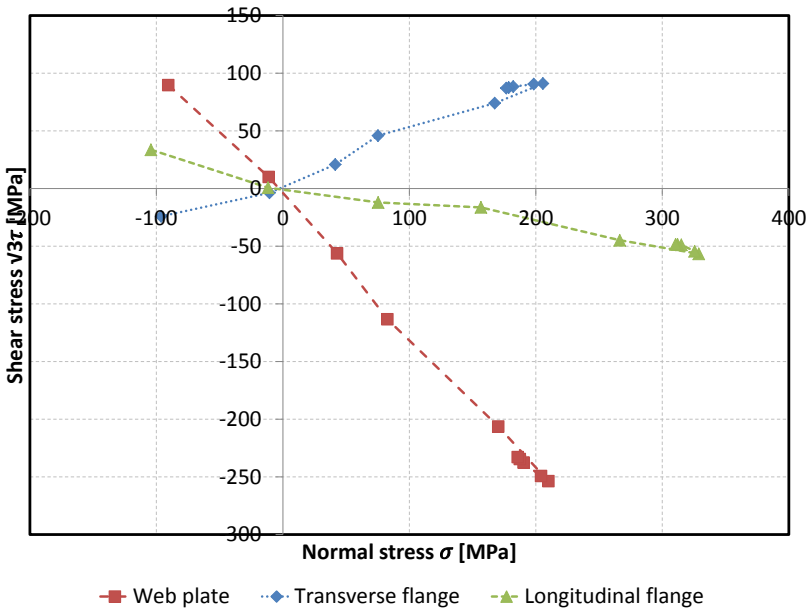


Figure 3.28: Load path of stress in connection transverse and longitudinal

## 3.6. Summary

The structural response of a representative hopper dredger to its loading and unloading cycle is analysed and the stress ranges for fatigue assessment have been determined. Still water loads are calculated using a dredging cycle based on a pre determined still water bending moment document and wave loads are computed with use of quasi static deterministic BV wave load cases. A finite element shell and bar model is used to obtain the structural response to the previously described load cases and -conditions. The model is tuned amidships to simulate the appropriate loading in the area of analysis. Structural hot spot stress ranges are established at four high stress locations in the bottom opening corner. The output of this chapter functions as input for fatigue life prediction in the next chapter. The following conclusions are drawn from the findings in this chapter:

- A maximum dredging cycle load condition is identified at a cargo specific density of $1600\,t/m^3$ which is not the maximum specific density in the considered dredging cycle. This leads to the conclusion that weir level in the hopper is a governing parameter in the dredging cycle description if a dredger has a constant tonnage system. This is accompanied by the finding that local transverse pressure difference between external and internal pressure plays a significant role in the dredging cycle. The dredging cycle stress range is much lower if only hull girder loads are considered and would greatly underestimate the stress levels in the hot spots.
- The dredging cycle causes high stresses in the analysed hot spots compared to the wave loading. Dredging cycle stress ranges between 379 and 515 MPa are found versus operational wave stress ranges in almost all cases below 100 Mpa. Wave loading contribution, in terms of dredging cycle range, does however increases the stress range on average by 15% relative to the still water cycle. It is therefore concluded that the wave contribution in the dredging cycle stress range is an important factor in fatigue assessment which could lead to serious under or over estimation of the predicted fatigue life. Sensitivity of the that determine the contribution is discussed in the next chapter.
- The directions of the principal stress ranges in the cruciform joint show a bi-axial stress with negative and positive biaxiality ratios. The load paths from empty to fully loaded show that multi-axial loading at the hot spots is proportional if the directions of the maximum principal stress ranges due to wave loading is neglected. The low stress ranges due to wave loading justify this assumption. The fact that the loading is proportional simplifies further multi-axial fatigue assessment procedures since non-proportionality requires more complex analysis of all load components and it would therefore be questionable if the use of a simplified fatigue analysis is still in place.

# 4

# Fatigue life prediction

*In this chapter the damage caused by a combination of the structural response and its frequency is assessed. This is initially done according linear-elastic fatigue assessment according Bureau Veritas rules and SN-curves. Dredging cycle induced damage is then compared with the total fatigue damage at the hotspot locations discussed in sections 3 and 3.2.3. The contribution of the dredging cycle is discussed as well as whether the fatigue is a low- or high-cycle phenomena. The effect of some of the main parameters in the current simplified fatigue assessment is presented in this chapter and the result of this analysis is discussed.*

## 4.1. Fatigue life prediction BV guideline

SN-curves are based on test data that is, in most cases, not comparable with the structural details that are assessed, at least not immediately. In this section fatigue influencing factors are discussed which are adjustments to the SN-curve to make it suitable for the detail of concern. This could be done by shifting the SN-curve, which will result in a individual SN-curve for each hot spot, or by adjusting the stress range that is compared with a general design SN-curve. All factors influencing the fatigue strength are combined in an correction factor $f_{eff}$ which is multiplied with the previous calculated stress ranges to compute an equivalent stress range $\Delta\sigma_{eff}$ given in equation 4.1. These factors cover yield stress differences, Loading mean stress and thickness effects which are explained in section 2.7 of chapter 2.

$$\Delta\sigma_{eff} = f_{eff} \cdot \Delta\sigma_{le} \tag{4.1}$$

The fatigue resistance is first determined with use of the Buereau Veritas guideline [11] which distinguishes yield stress effect for fatigue assessment of welded joints and base material. Fatigue strength of welded joints is independent of the yield strength of the material. For non-welded details with crack initiation in base material such as cut plate edges this is different. The SN-curves for cut-edge details are based on tests done on specimens with a yield stress of 235 MPa and therefore the stress range has to be adjusted to account for the difference since the material used in the hopper dredger has a yield stress of 355 MPa. The correction factor to account for the yield stress is given by equation 4.2

$$f_{yield} = \frac{1200}{965 + \sigma_{yield}} \tag{4.2}$$

Bureau Veritas guideline does not take into account mean stress for the loading and unloading cycle, however the residual stress is taken into account in the design SN-curves for welded joints and the curves are based on high stress ratios of $R = 0.5$ in case of welded joints. As explained in section 2.7.2 of chapter 2 the mean stress decreases due to high stresses. Not taking the mean stress effect into account will lead to conservative results since the dredging stress range is quite large and will relax the mean stress with greater magnitude than the wave loading. The maximum, minimum and means stress of the dredging cycle are presented in table 4.1. The mean stress correction of the BV guideline is given by equations 4.3 and 4.4 for as welded joints and hot spots located at cut plate edges respectively.

Table 4.1: Linear elastic dredging cycle stress range properties

| | $\sigma_{max,le}$ [MPa] | $\sigma_{min,le}$ [MPa] | $\sigma_{mean,le}$ [MPa] | Load ratio R [-] |
|---|---|---|---|---|
| Longitudinal flange | 363 | -127 | 118 | -0.35 |
| Transverse Flange | 264 | -114 | 75 | -0.43 |
| Web plate | 350 | -134 | 108 | -0.38 |
| Insert plate ellipse | 256 | -125 | 65 | -0.49 |

$$f_{mean,wl} = \begin{cases} Min\left[1.0; 0.9 + 0.2 \cdot \dfrac{\sigma_{mean,le}}{\Delta\sigma_{le}}\right], & \text{if } \sigma_{mean,le} \geq 0 \\ Max\left[0.3; 0.9 + 0.8 \cdot \dfrac{\sigma_{mean,le}}{\Delta\sigma_{le}}\right], & \text{if } \sigma_{mean,le} < 0 \end{cases} \tag{4.3}$$

$$f_{mean,c} = \begin{cases} Min\left[1.0; 0.8 + 0.4 \cdot \dfrac{\sigma_{mean,le}}{\Delta\sigma_{le}}\right], & \text{if } \sigma_{mean,le} \geq 0 \\ Max\left[0.3; 0.8 + \dfrac{\sigma_{mean,le}}{\Delta\sigma_{le}}\right], & \text{if } \sigma_{mean,le} < 0 \end{cases} \tag{4.4}$$

here are $\sigma_{mean,le}$ and $\Delta\sigma_{le}$ the linear-elastic mean hot spot stress and stress range respectively. If the maximum stress exceeds the yield strength the mean stress is corrected to take into account the shakedown effect. Correction of the mean stress is done with equation 4.5 and means that the mean stress is decreased with the difference between the maximum and yield stress.

$$\sigma_{mean,le} = \sigma_{yield,le} - \sigma_{max,le} + \sigma_{mean,le} \tag{4.5}$$

According to the IIW [39] thickness effects have to be taken into account if fatigue resistance of weld toes is of concern. This applies if the thickness of the plating is thicker than the reference thickness of the associated SN-curve. The stress range is corrected as a function of the effective thickness and a certain thickness exponent depending on the type of joint. The thickness reduction factor according to the IIW, which is also used in BV rules, is given by equation 4.6 [39]. Here is $t_{ref}$ the reference thickness of the applicable SN-curve, $t_{eff}$ the effective thickness of the detail including the weld leg lengths and is n the thickness exponent depending on the type of joint and load direction.

$$f_{thickness} = \left(\frac{t_{ref}}{t_{eff}}\right)^n \tag{4.6}$$

Table 4.2: Effective wave stress ranges

| | Unit | Dredging sailing loaded | | | | Dredging sailing empty | | | | Ballast navigation | | | |
|---|---|---|---|---|---|---|---|---|---|---|---|---|---|
| Load case | - | a | b | c | d | a | b | c | d | a | b | c | d |
| Longitudinal plate | [MPa] | 17 | 7 | 14 | 22 | 4 | 0 | 10 | 6 | 52 | 26 | 55 | 24 |
| Transverse plate | [MPa] | 38 | 86 | 1 | 3 | 9 | 0 | 2 | 3 | 95 | 72 | 23 | 24 |
| Web plate | [MPa] | 41 | 92 | 7 | 45 | 10 | 0 | 3 | 0 | 108 | 69 | 10 | 30 |
| Insert plate | [MPa] | 35 | 90 | 16 | 11 | 10 | 0 | 8 | 2 | 97 | 78 | 37 | 18 |

### 4.1.1. Fatigue life

Fatigue life of the analysed details in the hopper dredger is initially calculated according Bureau Veritas rules and guidelines [2] [11] assuming that the SN-curves are valid for high and low cycle fatigue. The fatigue life is determined with use of the damage that is caused due to cyclic loading and fatigue failure is considered if fatigue damage $D_{total} \geq 1$. The value of damage parameter $D_{total}$ is a cumulative summation of the damage of each individual cycle in the lifetime of the dredger which is according Miner's sum and expressed with

Table 4.3: SN-curve specifications

| | Symbol | D-curve | C-curve | Unit |
|---|---|---|---|---|
| FAT | $\Delta S$ | 63.27 | 85.86 | MPa |
| Characteristic constant | $log_{10}(K_{97.7})$ | 11.7046 | 12.1025 | - |
| Slope | m | 3 | 3 | - |
| Reference thickness | $t_ref$ | 25 | 25 | mm |

equation 2.5. The total damage at each hot spot per year is calculated and the fatigue lives are established. The contribution of the dredging cycle is discussed and the fatigue is qualified being either low- or high cycle fatigue according to the number of cycles to failure.

The number of cycles to failure of the weld toes at each hot spot are determined with the applicable Bureau Veritas SN-curves [11]. As explained in section 2.4.4 of chapter 2 the curves are based on test data which is Gaussian distributed on a log-log scale [52]. The SN-curves presented in the guideline have a probability of survival of 97.7% which is a curve shifted downwards from the mean curve with two standard deviations, see equation 4.7. Applicable design SN-curves are selected so that the number of cycles to failure and therefore the fatigue damage could be calculated. The SN-curve applicable for the hot spots in the cruciform joint is a D-curve for welded joints in a free corrosion environment. This curve corresponds with the hot spots stress measurement procedure and the use of a principal stress range due to the bi-axial plane stress state at the hot spots. It should be noted that the angle of the principal stress range relative to the normal direction of the weld is taken into account. If the angle between the normal weld direction and the principal stress range becomes to large the notch at the weld to will become less effective. The effect of the notch is included in hot spot stress based SN-curves [52] and a less effective notch would therefore result in a SN-curve with higher with higher fatigue strengths. The directions of the dredging cycle stress range are presented in table 3.17. All directions to the welds at the hot spots are within 45 degrees and the hot spot D-curve is applicable.

The fatigue life of non welded details is highly dependant on the surface finish at the location where the stress concentrates. The cargo of hopper dredger does not only lead to corrosion but also to erosion effects when discharging. The scope of this thesis doe not include a full analysis of the wear of the edges of the insert plates. However, the condition of the edge has some effect on the fatigue life since the design SN-curve depends on the edge condition of the cut plate edge. The insert plate is in the discharging passage of the hopper and will be affected by erosion and corrosion. A C-curve is selected and is associate with a plate without edge treatment such as grinding or polishing. It is assumed that any kind of edge treatment is sanded away be the passing soil. A next assumption is that the plate is considered to be machined cut so residual stress due to thermal heating is not included. The specification of both curves are presented in table **4.3** and plotted in **figure 4.1**

$$log_{10}(N) = log_{10}(K) - m \cdot log_{10}(\Delta\sigma) \tag{4.7}$$

### 4.1.2. Fatigue damage

Simplified fatigue damage calculation is based on a Weibull extreme value distribution to formate a closed form expression of the fatigue damage presented by equation 4.8. A closed form fatigue damage equation is used to calculate wave induced fatigue damage due to the fact that the probability of the design waves has to be accounted for in the damage accumulation

$$D_{i,j} = \frac{N_{wave}}{K_{97.7}} \cdot \frac{\Delta\sigma^m_{eff,i,j}}{(-ln(P_r))^{\frac{m}{\gamma}}} \cdot \mu \cdot \Gamma\left(1 + \frac{m}{\gamma}\right) \tag{4.8}$$

In which $N_{waves}$ is the amount of wave cycles in the lifetime of the dredger based on an average period according equation 4.9. $K_{97.7}$ is the SN-curve characteristic value based on a 97.7% probability of survival and m is the value of the inverse slope of that curve. $P_R$ is the probability of the wave loading which is based on a probability of $10^{-5}$. As explained in chapter 2 the Weibull shape parameter $\xi$ is based on the ship dimensions and affects the shape of the distribution and therefore the fatigue damage. The Bureau Veritas guideline

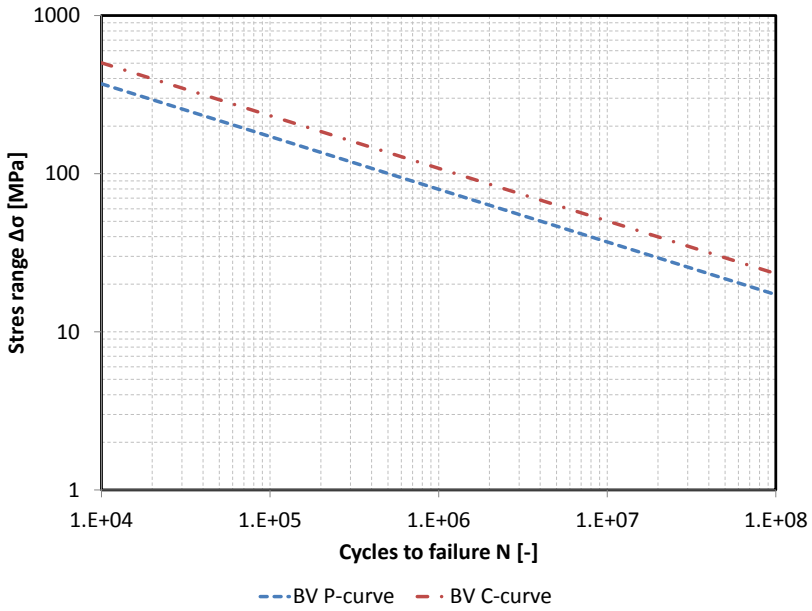


Figure 4.1: BV principal hot spot stress SN-curves taking into account the use of principal stress range and a corrosive environment

specifies a shape parameter equal to 1 where ABS mentions that the shape parameter for ships could be found between 1 and 1.3 [4] and according to [18] between 0.7 and 1.3. the effect of the assumption to use this shape parameter is discussed in section 4.3.3. If the SN-curve is double sloped the coefficient $\mu$ takes into account the change of the slope at the fatigue limit. The details analysed in this thesis are located in the corners of the bottom door openings and are prone to free corrosion due to the harsh environment of the cargo spoil. SN-curves that take into account this type of environment are single sloped and therefore the coefficient $\mu$ equals 1. The damage is calculated for each load case (wave type) and load condition (Empty, fully loaded and navigation) which are represented by subscripts i and j respectively.

$$T_{average} = 4log(L) \tag{4.9}$$

In addition to the previous the fatigue damage due to the waves does depend on the operational profile as discussed in chapter 2. The number of wave cycles experienced in a year depends on this profile as well as the damage accumulation to combine load case a,b,c and d in empty, full load and navigation conditions. Damage due to each load case for each load condition is accumulated according equations 4.10, 4.11 and 4.12. The three calculated damages are added up according their portion in the operational life of the dredger. The portions and number cycles are given in table 4.4.

Table 4.4: Operational profile hopper dredger

| | Symbol | Value |
|---|---|---|
| Sailing factor | $\alpha_{sailing}$ | 85% |
| Part in full load condition | $\alpha_{Fullload}$ | 40% |
| Part in empty condition | $\alpha_{Empty}$ | 40% |
| Part in navigation condition | $\alpha_{Navigation}$ | 20% |
| Number of wave cycles per year | $N_{waves}$ | 3.11E+06 |

$$D_{fl} = \frac{1}{6}D_{lca,fl} + \frac{1}{6}D_{lcb,fl} + \frac{1}{3}D_{lcc,fl} + \frac{1}{3}D_{lcd,fl} \tag{4.10}$$

$$D_{em} = \frac{1}{3}D_{lca,em} + \frac{1}{3}D_{lcb,em} + \frac{1}{3}D_{lcc,em} \tag{4.11}$$

$$D_{na} = \frac{1}{3}D_{lca,na} + \frac{1}{3}D_{lcb,na} + \frac{1}{3}D_{lcc,na} \tag{4.12}$$

The stress range of the dredging cycle is not based on a probability of occurrence and it is assumed that the hopper is filled four to six times a day when the dredger is operational. In practice it is possible that a dredger is filled more than six or less then four times a day and depending on the contribution of the dredging cycle this could have significant effect on the life length.

$$D_{dr} = N_{dr}\frac{\Delta\sigma_{dr}^{m}}{K_{97.7}} \tag{4.13}$$

Now the fatigue damage of all load components of the hopper dredger load profile have been determined and are now combined to calculated the total fatigue damage per year for each hot spot. Equation 4.14 combines the fatigue damages according their proportion in the fatigue life of a hopper dredger.

$$D_{total} = \alpha_{sailing}\left(\alpha_{fl}D_{fl} + \alpha_{em}D_{em} + \alpha_{na}D_{na} + D_{dr}\right) \tag{4.14}$$

Table 4.5: Fatigue damage in 20 year design life, life time prediction based on D = 1 and dredging cycle contribution all based on a minimum of four dredging cycles per day

| | Combined fatigue damage | Life time in years | Contribution dredging cycle |
|---|---|---|---|
| Longitudinal flange | 3.94 | 5.05 | 99.38 % |
| Transverse Flange | 1.85 | 10.38 | 95.61 % |
| Web plate | 4.57 | 4.30 | 98.17 % |
| Insert plate ellipse | 0.60 | 32.00 | 95.29 % |

The fatigue damage for a life time of 20 years is presented in table 4.5. The fatigue life in years is based the consideration of failure for $D \geq 1$. It is found that the dredging cycle has a major contribution in the fatigue damage. It even almost determines the entire fatigue life of the dredger at the location of the structural details of concern.

### 4.1.3. Low cycle fatigue

Wave stress ranges are low and considered high-cycle fatigue. The cyclic loading due to the dredging cycle however, does ask for further analysis considering the high stress ranges. The low-cycle fatigue region is determined by the number of cycle to failure of the hot spot according the applicable SN-curves and is considered low-cycle fatigue if the number of cycles is below a certain value. In this thesis a common value of $10^4$ is considered. It should be noted that failure of a specimen is called low cycle fatigue if it fails for limited amount of cycles. In this section conclusions regarding low cycle fatigue are only based on SN-curves and not on actual experimental data of the details of concern.

The number of cycles to failure of the details is presented in table 4.6. It shows that the hot spots in the longitudinal bulkhead and the web plate experience low-cycle fatigue where the stress range of the hot spot in the insert plate and the transverse bulkhead results in a number of cycle exceeding the $10^4$ threshold level. The probability of fatigue failure being low cycle fatigue is quantified to show too which extend it could be concluded that the cyclic loading is low-cycle fatigue assuming linear-elastic stresses.

Design SN-curves with a probability of survival of 97.7% are defined by the mean curve minus two times the standard deviation which is expressed in equation 4.15 substituted in equation 4.7. It means that there is a change of 2.3% that the structural detail will have an unacceptable amount of fatigue damage. The conclusion that fatigue failure is a low-cycle fatigue phenomenon is to bluntly. To see to which extend the probability of failure could be considered a probability of failure due to low-cycle fatigue the stress range of each detail is compared with the statistics of the SN-curve.

$$log_{10}(K) = log_{10}(K_{97.7}) + \beta\sigma_{stdv} \tag{4.15}$$

The 50% probability of survival mean stress SN-curve is computed with use of equations 4.7 and 4.15 and a standard deviation with a typical value of 0.2 [66] [52] [7] which is also used in DNV fatigue rules [79]. The SN-curves of the 97.7% and 50% probability are plotted in **figure 4.2** and the fatigue life at 50% probability is calculated for each hotspot in the cruciform joint and given in **table 4.6**. At this probability the fatigue lives at the hot spots are not in the low-cycle fatigue region. This means that there is a 50% probability of failure at this stress range but not all failures will be due to low-cycle fatigue assuming that this region stops at $10^4$ number of cycles to failure. The probability of survival at which all failures are due to low-cycle fatigue is calculated for each hot spot in the cruciform joint. This is done to see in which level of conviction the fatigue failure of the details could be seen as low-cycle fatigue.

Table 4.6: Cycles to failure 97.7% and 50% survival probability

| | $N_{97.7}$ | $N_{50.0}$ |
|---|---|---|
| Longitudinal flange | 5.1E+03 | 1.3E+04 |
| Transverse Flange | 1.1E+04 | 2.8E+04 |
| Web plate | 4.4E+03 | 1.1E+04 |
| Insert plate ellipse | 3.5E+04 | 3.5E+04 |

The SN-curve is shifted in direction of the stress range to find the $log_{10}(K)$ value at which fatigue failure is 100% due to low-cycle fatigue. First the amount of standard deviation $\beta\sigma_{stdv}$ at which the number cycles to failure is equal to $10^4$ is determined. Because the standard deviation is already known this amount is expressed in terms of factor $\beta$ by combining equations 4.7 and 4.15 and is given in equation 4.16.

$$\beta = \frac{log_{10}(N) - log_{10}(K) + m \cdot log_{10}(\Delta\sigma)}{\sigma_{stdv}} \tag{4.16}$$

The probability of survival is then calculated with use of the Gaussian cumulative density function expressed with equation 4.17. The probability of survival is $1 - CDF$ and the values are presented in table 4.7. The hot spot in the web shows that at a survival probability of 45%, 55% of the specimens will fail due to low cycle fatigue. The hot spot in the longitudinal bulkhead shows that almost half of the failures is due to low cycle fatigue if a 50% mean curve is used. If the hot spot in the transverse bulkhead may fail this would most likely be due to high cycle fatigue since the probability of survival in the low cycle fatigue range is 94%. In **figure 4.2** the 97.7% and the 50% SN-curves are plotted to show the range in which SN-curves are shifted

$$F(log_{10}(K)|log_{10}(K_{50}), \sigma_{stdv}) = \frac{1}{2}\left[1 + erf\left(\frac{log_{10}(K) - log_{10}(K_{50})}{\sigma_{stdv}\sqrt{(2)}}\right)\right] \tag{4.17}$$

Table 4.7: Probability of survival if cycles to failure is equal to 10000 cycles

| | $\beta$ | $log_{10}(K)$ | $P_{survival}$ |
|---|---|---|---|
| Longitudinal flange | 1.94 | 12.09 | 53% |
| Transverse Flange | 0.44 | 11.79 | 94% |
| Web plate | 2.14 | 12.13 | 45% |

## 4.2. Dredging data

The operational profile of a hopper dredger is specific for each individual hopper dredger. The contractor that operates these dredger receives orders that have different operating conditions. Different soil types result in different specific densities and loading times that will effect the frequency of loading and unloading. The frequency of the orders are also important factor in the design life of the hopper dredger. To validate the known average frequency of loading and unloading, which is four to six times a day, dredging data is analysed.

The author of this thesis is given dredging data by Jan de Nul, which is a contractor that is well known for using hopper dredgers for civil construction and maintenance projects. Data over a year, containing dredging dredging statuses of two sister ships, is acquired for analysis of the operational profile. The ships have

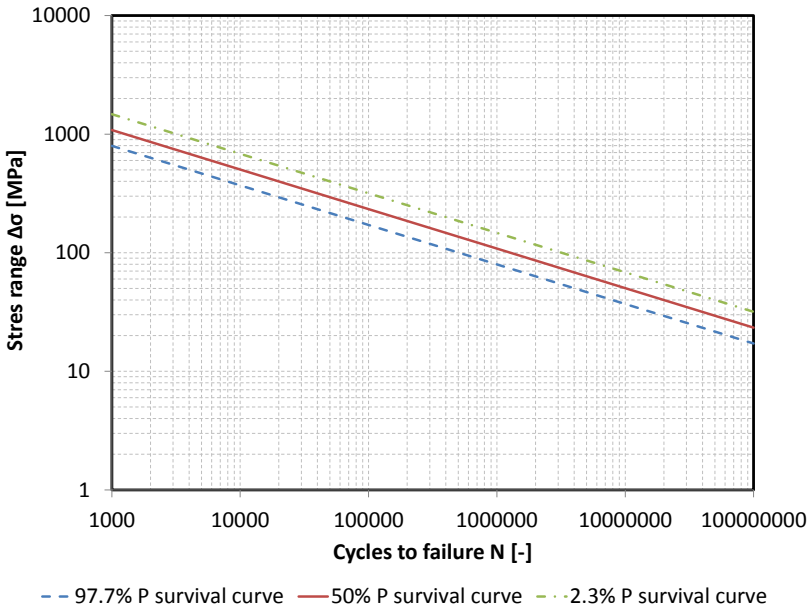


Figure 4.2: BV hot spot mean SN-curve

a length similar to that of the analysed hopper dredger so it is assumed that this data will provide a realistic view on the actual operating profile of a hopper dredger. Although the data covers one year it is expected that it is representative for the entire design life of the dredger if downtime due to maintenance and repair is not taken into account. One of variables in the dredging data is the status itself and these are:

- Discharging
- Dumping
- Sailing empty
- In between
- Dredging
- Sailing loaded

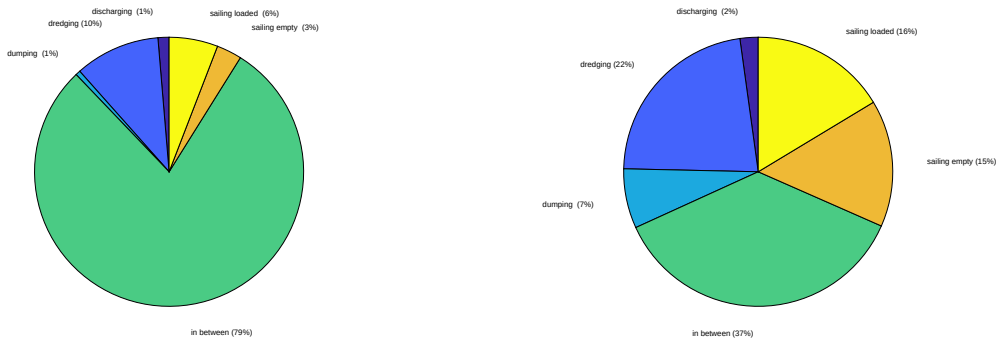


(a) (b)

Figure 4.3: **(a)** Ship status one year hopper dredger 1, **(b)** Ship status one year hopper dredger 2

Figures 4.3a and 4.3b show the distribution of the operating status of hopper dredger one and two, as they are now called. The in between status covers sailing in navigation and non operational conditions. The pie charts show that the distribution over a whole year does not correspond with the sailing factor which states that the dredger should be in between status 15% of the time. This however an average portion taken from the entire design life. Downtime due to required renewal surveys and repairs could span a longer period of time and still satisfy the sailing factor of 15% in its life time. It also does not conclude that there will be less cycles in a year. It depends on the type of operations the hopper dredger has performed in that year. The rainflow cycle counting method is applied on the draught and bottom door position data to count the amount of cycles with associated mean values and to see the magnitude of ranges and the proportion of the draught during operations. The results are presented in **figures 4.4a** to **4.5b**.

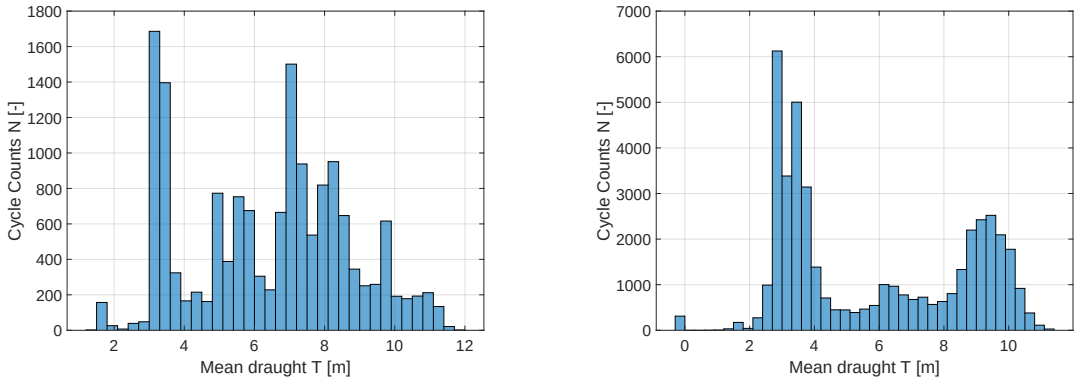


(a) (b)

Figure 4.4: **(a)** Mean cycles ship draught hopper dredger 1, **(b)** Mean cycles ship draught hopper dredger 2

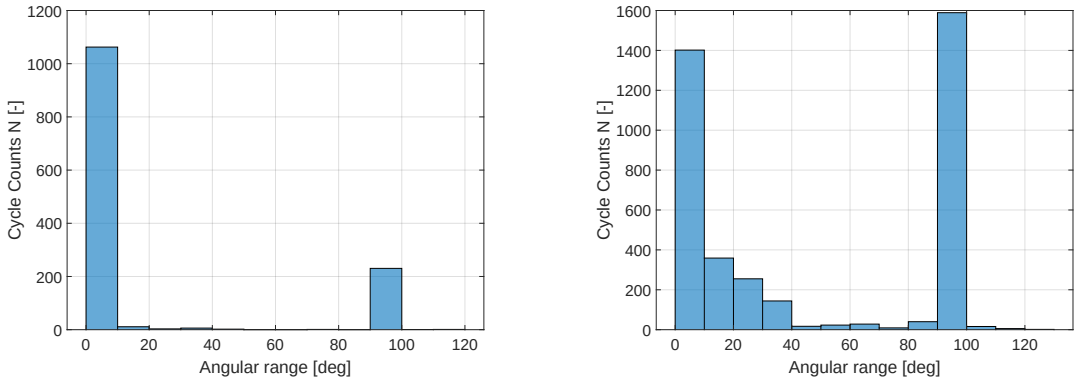


(a) (b)

Figure 4.5: **(a)** Angular range ship bottom door position (degrees) hopper dredger 1, **(b)** Angular range ship bottom door position (degrees) hopper dredger 2

The cycle ranges of the draught data are very small compared to the draught of the load condition and the large sample interval (one minute) compared to the wave period give reason for a conclusion that the calculated ranges could not be used for fatigue analysis. Hopper dredger 1 has a broad distributed operational draught which indicates that the dredger is not always working in fully loaded or empty hopper condition when operational. This could be if the hopper is loaded to a maximum overflow level with a low density spoil. The histogram of hopper dredger 2 shows two narrow banded distributions that clearly show that the majority of the waves is seen in the fully loaded and empty draught conditions. The distribution of the bottom door position is much more narrow and shows a clear amount of total cycles at a range of 90 degrees. A large

amount of cycles is found with a very low range close to zero which is considered to be due to small displacements when the bottom door is closed. It could be that the dredger is not always unloaded by using its bottom doors and discharge was performed with other methods such is pumping to shore. This is also indicated in figure 4.3a and 4.3b. The amount of the bottom door cycles could therefore not be used to count the amount of dredging cycles. To overcome this the sailing empty and sailing loaded dredging status are used to identify the amount of dredging cycles. The dredging status is adjusted so that sailing loaded equals one and sailing empty equals 0. Rainflow cycle counting is used to count the amount of fluctuations between these two conditions. The result are presented in table 4.8. It is found that the average amount of cycles of dredger one is significantly more than expected and hopper dredger two is near the upper bound of the assumed four to six cycles a day. If the proportional of operational time would be higher the amount of cycles each year would be much more than initially expected.

Table 4.8: Annual number of dredging cycles of analysed sister ships

| | Hopper dredger 1 | Hopper dredger 2 |
|---|---|---|
| Total number of cycles | 1762 | 426 |
| Operational time % | 63% | 21% |
| Average number of cycles a day | 7.66 | 5.57 |

## 4.3. Influences on fatigue life prediction

The dredging cycle has a significant effect on the fatigue damage and has a contribution which is on average 97%. The fatigue life and damage are calculated on the assumption that the SN-curve is applicable in the low cycle fatigue region. Taking into account the large contribution of the dredging cycle the methods to assess this cycle could have significant effect on the predicted fatigue life. The following main parameters in the procedure considered in this thesis are identified:

- Local geometry
- Wave Probability
- Residual stress
- Load ratio
- Damage accumulation

In the following sections the effect of these parameters is discussed by comparison with alternative methods which are deemed more applicable for hopper dredgers and parameters in the current assessment are varied for sensitivity analysis. Methods are selected which are suitable with the simplified hot spot stress method of this thesis and parameter variation is done within realistic range considerations.

### 4.3.1. Weld geometry

Due to the stress gradient of the stress at the structural discontinuity the size of the weld could have significant effect on the stress range and therefore the fatigue strength. The welded geometry has effect on the thickness effect in the welded joint as well. Changes in the weld size will change the through thickness stress distribution and therefore the effective thickness of the joint. According to the IIW [39] the governing parameters for fatigue failure at weld toes are:

- Weld transition angle.
- Toe radius.
- Weld throat size.
- Thickness of the welded plates.

The transition angle and toe radius are not accounted for in the hot spot assessment procedure due to the fact that stress induced by the shape of the notch is taken into account in the hot spot stress calculation [43]. The effective thickness of the welded plates is included with use of a correction factor which was presented in section 2.7.3. According the IIW the effect of the leg length cannot be assessed with use of the hot spot stress concept. It could however be estimated by the throat size of the weld. The hot spot stress calculation procedure used in the previous chapter does depend on the considered weld leg length.

Weld imperfections are taken into account in the hot spot stress SN-curve. Excessive corrosion due to the hopper dredger specific type of cargo reduces the throat size and weld leg length as discussed in section 2.7.4 of chapter 2. The sensitivity of the hot spot stress to the weld leg length is analysed by variation of the weld leg length proportional to the corrosion addition of the joint plates. Corrosion addition of the weld leg length according to the common structural rules for bulk carriers is given by equation 4.18 [7].

$$x_{wl,new} = x_{wl} - 0.7(t_{ca,1} + t_{ca,2}) \tag{4.18}$$

Weld corrosion addition is found to be up to $1.75mm$ and is used for variation of the weld leg lengths. The effect of the weld size on the annual fatigue damage in the hot spots at the joint are presented in **figure 4.6**.

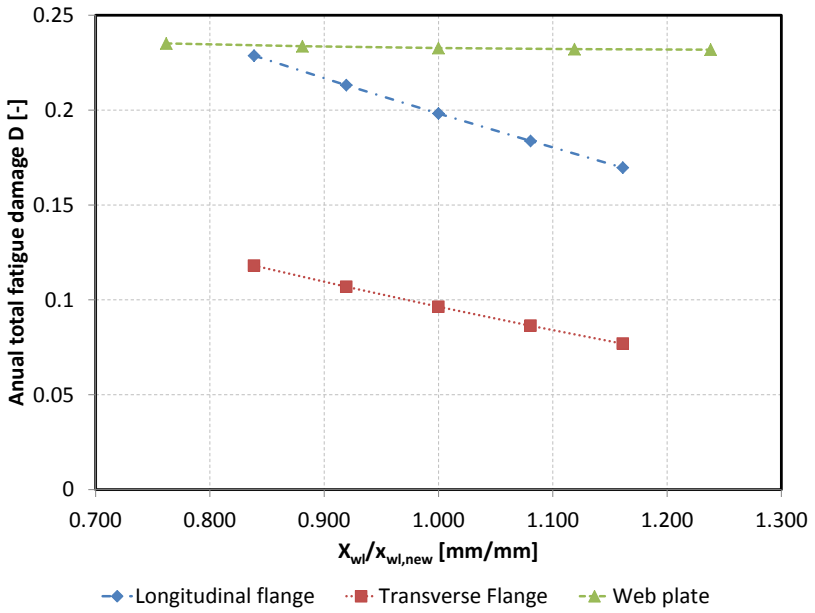


Figure 4.6: Effect of weld leg length on annual fatigue damage based on four dredging cycles a day

As expected the fatigue damage increases with decreasing weld leg length. The weld dimension considered in the analysis do not lead to thickness that require correction based on the reference thickness of the BV SN-curve. A thickness correction is required if the weld leg length is at least 17.5 mm or the welded plate has a thickness of $t = 25$. It appears that weld leg size has significant effect on the fatigue damage in the hot spots on the bulk heads. Calculated annual fatigue damage changes here between 8% and 13% per mm which is in the web plate only 1%. Here the stress is linear extrapolated diagonally toward the cruciform joint and has a lower stress gradient due to the structural discontinuity than uni-axial to the weld. Despite the fact that post weld treatment could decrease the effect of the notch at the weld toe, the geometry of the weld should be taken as a significant parameter in the simplified fatigue assessment when the structural hot spot stress is used based on the procedure described in section 3.5.

### 4.3.2. Probability of the dredging cycle wave

Wave cycle contribution based on $10^{-4}$ probability represents a wave that occurs once a day. It is estimated that the dredging cycle occurs between four to six times a day on average. The analysed data shows that the the dredging cycle has a higher frequency of occurrence when the hopper dredger is in dredging condition.

This causes suspicion that the probability of the dredging cycle wave could be increased to a wave that occurs every several hours. Taking the dredging cycle wave with a probability of $10^{-4}$ seems conservative because this type of wave is expected to occur once a day and will therefore not contribute to every dredging cycle. A probability of $10^{-3}$ could provide a more realistic wave amplitude contribution. The previous arguments to adjust the probability of the dredging cycle wave are all based on the assumption that the damage due to the dredging cycle and the wave loading is independent and linear accumulated to determine the total fatigue damage. The exact contribution of the wave is not known and experiments to determine this contribution is not within the scope of the project. To get an idea of the effect of the wave probability the fatigue damage associated with each probability is presented in **figure 4.7**.

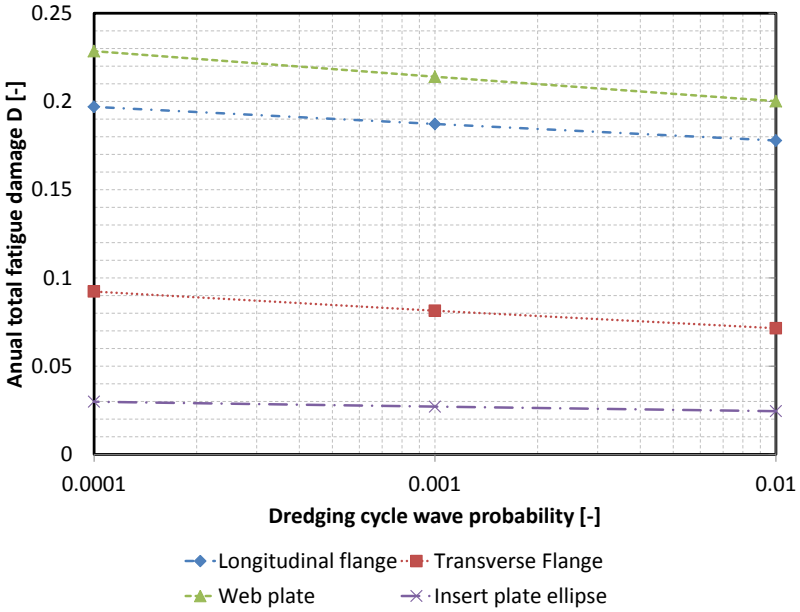


Figure 4.7: Effect of wave probability on fatigue life based on Miner's rule and four dredging cycles a day

Increase of the wave probability has significant effect on the fatigue damage and a decrease of the annual average fatigue damage is decreased by 9% if the a probability of $10^{-3}$ is considered. Although a significant reduction is seen in the annual damage of the dredging cycle with included wave contribution, the damage is still higher than the damage calculated by the LCF and HCF accumulation method proposed by Urm et al. 76 and is discussed in section 4.3.5.

### 4.3.3. Weibull shape parameter

The shape parameter is a difficult parameter to determine and it is seen that this parameter is important in the simplified fatigue assessment of steel ships. According to the Harmonised CSR of the IACS [7] the shape parameter has significant effect on the fatigue life if a wave probability other than $10^{-2}$ is used. The wave loading in this thesis is based on a probability of $10^{-5}$ which explains the effect of the shape parameter on wave induced fatigue. A range of typical shape parameter values is analysed on resulting fatigue damage. The results are presented in **figure 4.8a**

The shape parameter has little effect on the total damage as presented in **figure 4.8b**. This is explained by the fact that the wave stress ranges are low compared to the dredging cycle and the shape parameter only affects the fatigue damage due to wave loading. The load condition of the hopper dredger deviates the shape parameter of the wave load distribution. The assumption that the shape parameter could be taken equal for the fully loaded and ballast condition is justified considering the small effect of this parameter.

### 4.3.4. Load ratio

In chapter 2 the effect of residual stress relaxation is discussed ans is concluded that mean stress and residual stress cannot be assessed independently. This highly uncertain parameter could have significant effect on the predicted and actual fatigue life. The residual stress at the hot spots is unknown and is therefore included in SN-curves fto assure safe design. The BV mean stress correction is compared with the, in chapter 2 explained,

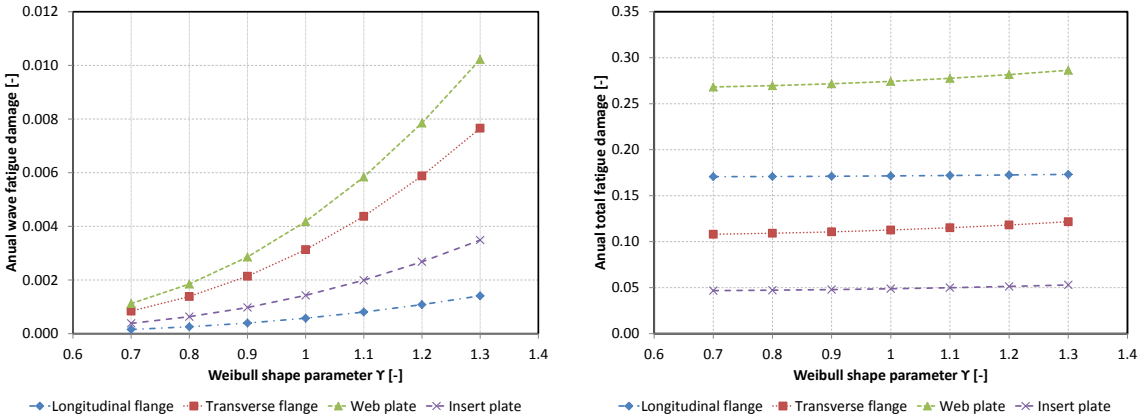


Figure 4.8: **(a)** Effect of shape parameter on wave induced fatigue, **(b)** Effect of shape parameter on total fatigue damage based on four dredging cycles a day

method of Zhang and Moan [86] which takes into account relaxation and mean stress effect simultaneously. Additional to this the mean stress correction proposed by walker is included in the analysis to see the independent effect of the load ratio. This correction method is a suitable mean stress correction method for welded steel plates [82] [27] and is deemed to give superior results.

The method proposed by Zhang and Moan calculates relaxation of residual stress if the maximum stress exceeds the yield stress of the material. Residual stress after this mechanical overloading is calculated with equation 4.19.

$$\sigma_{res,new} = \begin{cases} \sigma_{yield} - (\sigma_{mean} + \frac{\Delta\sigma}{2}) & \text{if } \sigma_{max} \geq \sigma_{yield} \\ \sigma_{res} & \text{otherwise} \\ -\sigma_{yield} - (\sigma_{mean} - \frac{\Delta\sigma}{2}) & \text{if } \sigma_{min} \leq -\sigma_{yield} \end{cases} \tag{4.19}$$

In which $\sigma_{res}$ is found according 4.20 in which initial residual stress $\sigma_{res,0}$ of 25% of the material yield stress should be used.

$$\sigma_{res} = \begin{cases} max\left[-\sigma_{yield}, min\left(\sigma_{yield}, \sigma_{res,0} + \sigma_{mean} + 0.6\Delta\sigma\right) - \sigma_{mean} - 0.6\Delta\sigma\right] & \text{if } \sigma_{mean} \geq 0 \\ min\left[\sigma_{yield}, max\left(\sigma_{yield}, \sigma_{res,0} + \sigma_{mean} - 0.24\Delta\sigma\right) - \sigma_{mean} + 0.24\Delta\sigma\right] & \text{if } \sigma_{mean} < 0 \end{cases} \tag{4.20}$$

This results in a new stress ratio that is used to determined a mean stress correction factor. The new stress ratio is given by equation 4.21.

$$R_{new} = \begin{cases} \frac{\sigma_{yield} - \Delta\sigma}{\sigma_{yield}} & \text{if } \sigma_{max} \geq \sigma_{yield} \\ \frac{\sigma_{mean} + \sigma_{res} - \frac{\Delta\sigma}{2}}{\sigma_{mean} + \sigma_{res} + \frac{\Delta\sigma}{2}} & \text{otherwise} \\ \frac{-\sigma_{yield} - \Delta\sigma}{-\sigma_{yield}} & \text{if } \sigma_{min} \leq -\sigma_{yield} \end{cases} \tag{4.21}$$

Walker proposes a completely reversed cycle amplitude by using the stress ratio and either the maximum stress or cycle amplitude. The walker mean stress correction accounts for the ineffectiveness of the compressive part of the cycle. This does not mean that this part is actually compressive for welded details since thermal residual stresses could be as high as the material yield strength. The completely reversed cyclic amplitude is half of the effective stress range with a load ratio of $R = -1$ which means zero mean stress. The effective stress range should be compared with an SN-curve based on the same load ratio.

The Walker mean stress correction is fitted to the material it is applied to. For steels equation 4.22 is applicable which uses the material ultimate strength [28]. The ultimate strength of AH-36 steel is between 490

and 560 MPa so an average value of 525 MPa is used as ultimate strength parameter. This results in a walker parameter equal to 0.7768 where a factor between 0.7 and 0.8 is common for high strength steels.

$$\gamma_w = -0.0002 \cdot \sigma_{ult} + 0.8818 \tag{4.22}$$

The equivalent fully reverse stress amplitude is then expressed with equation 4.23. The stress range is then two times this amplitude and this value will be compared with an adjusted SN-curve.

$$\sigma_{ar} = \sigma_{max} \left( \frac{1-R}{2} \right)^{\gamma_w} \tag{4.23}$$

The BV SN-curve is based on a load ratio of $R = 0.5$ which represents high tensile residual stress and is adjusted to a stress ratio of $R = -1$ so the fully reverse stress range can be assessed. The $\gamma$ exponent is applicable if the stress ratio is below zero. First the ratio is adjusted form a ratio of 0.5 to a ratio of -1 by equation 4.24. Then the effective stress range is determined with use of equation 4.24.

$$\Delta\sigma_{eff} = \begin{cases} \frac{\Delta\sigma}{(1-R)} & \text{if } R < 0 \\ \frac{\Delta\sigma}{(1-R)^{(1-\gamma)}} & \text{if } R \geq 0 \end{cases} \tag{4.24}$$

$$K_{R=-1} = K_{97.7} \cdot \frac{\Delta\sigma}{\Delta\sigma_{eff}} \tag{4.25}$$

The BV design SN-curve is shifted upwards by a factor of 2.33 to compute the fully reversed cyclic loading SN-curve with load ratio $R = 0$ which new characteristic SN-curve parameter is adjusted by equation 4.25. The dredging cycle and wave stress ranges are corrected with use of equation 4.23. The wave is considered to be in fully loaded hopper, empty hopper or ballast navigation condition and mean stress transition between empty and fully loaded hopper is ignored for simplicity reasons. According to the walker mean stress correction the stress ranges in the empty hopper condition do contribute to the fatigue damage since it is applicable for stress ratios between $-1 \geq R \leq 1$ [51]. The stress ratios of the wave loading in empty hopper condition are less than -1 and so these stress ranges are considered to be non-contributing to the fatigue damage. Note that this only holds assuming that residual stress relaxes. The wave loading in fully loaded condition has a high stress ratio of $R > 0.5$ which increases the contribution of the stress range to the fatigue damage. The dredging cycle itself is partly in compression and as a result has a negative stress ratio which reduces the effectiveness of the stress range.

The effect of mean stress in combination with residual stress relaxation is analysed at the four hot spots. In **figures 4.9a** to **4.9d** the annual fatigue damage is plotted for a variety of externally applied stress ratios. Hence this means that residual stress is included in the analysis method and not in the stress ratio. At each hot spot the stress range is kept constant assuming that this range is unaffected assuming this range is a function of the the hopper load capacity. The stress range is varied to see what the effect is of the dredging cycle load ratio on the fatigue damage. The comparison with the Zhang and Moan and Walker correction method is done to see what the effect is of the stress ranges and associated load ratios assuming BV mean stress correction does not sufficiently include residual stress relaxation due to static overload. The new residual stress after relaxation according equation 4.19 is included in the Walker mean stress correction to account for the actual mean stress.
It is shown in **figures 4.9a** to **4.9d** that the method proposed by Zhang and Moan seriously reduces the annual fatigue damage if residual stress relaxation is taken into account. The Walker mean stress correction, including the new residual stress according to Zhang and Moan, shows that the mean stress correction of the externally applied loading according to BV and Zhang and Moan include additional factors which result in higher fatigue damages. This is also observed in the hot spot located in the insert plate ellipse where the methods by BV and Zhang and Moan show similar results in terms of mean stress correction if residual stress is not included in the analysis. It is striking that Both BV and Zhang and Moan methods show that if the stress ratio is such that the maximum stress exceeds the yield stress the annual fatigue damage becomes independent of the applied load ratio.

The dredging cycle is mainly in the tensile region of loading which results in a tensile mean stress and a negative load ratio due to the compressive part of the cycle. In some cases the hopper dredger is filled with

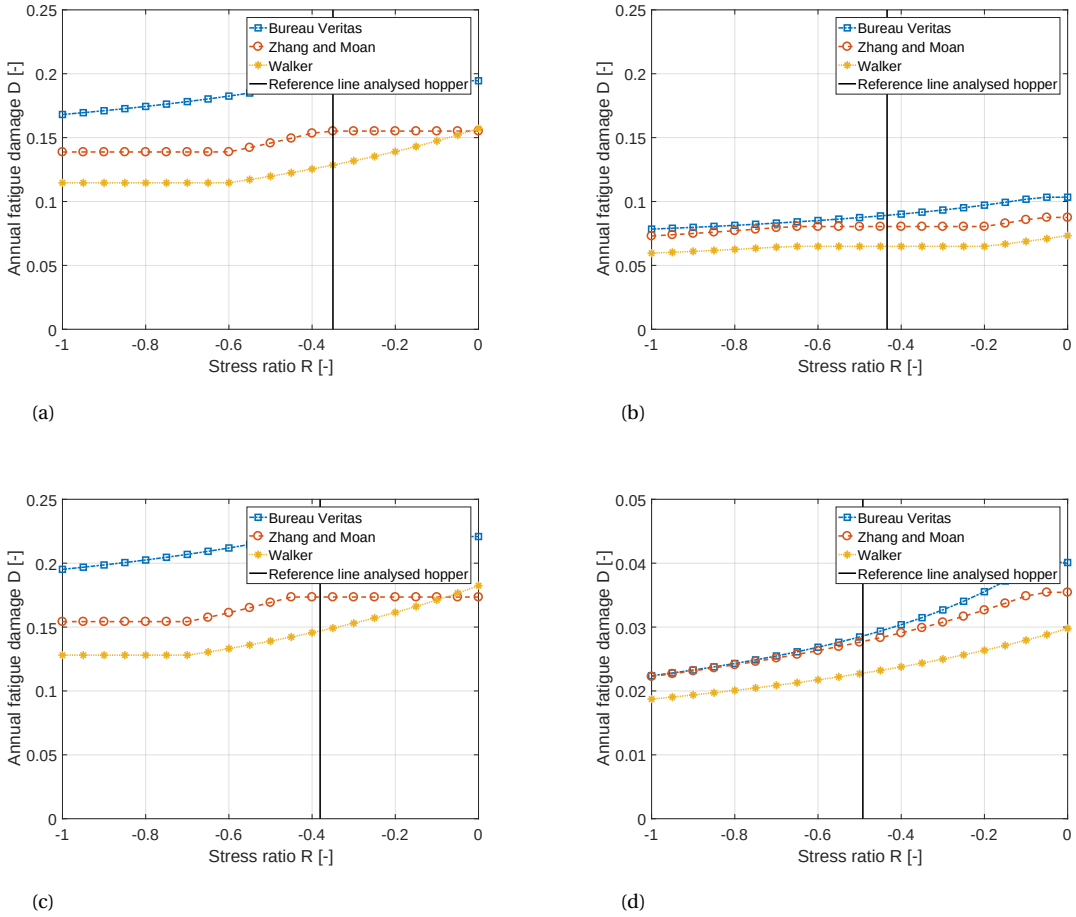


Figure 4.9: **(a)** Mean stress effect in longitudinal flange, **(b)** Mean stress effect in transverse flange,**(c)** Mean stress effect in web plate, **(d)** Mean stress effect in insert plate ellipse

ballast water when the load is dumped or discharged [61]. This will result in less hogging moment and therefore the minimum stress is increased resulting in a smaller stress range. This will shift the mean stress more into the tensile direction which could be expected to have a opposite effect than decreasing the stress range. The effect of increasing mean stress and decreasing stress range is given in **figures 4.10a** to **4.10d**.

The reduction of the stress range is governing and minor effect is seen due to the increasing load ratio. Decreasing the hogging moment by avoiding a completely empty hopper significantly reduces the annual fatigue damage and is unaffected by increasing mean stress.

### 4.3.5. Damage accumulation

The dredging cycle is described in this thesis by the still water stress range and a wave amplitude contribution to the total stress range. It would be interesting to see what the effect is of how the dredging cycle is included in the fatigue assessment. The current methodology included high and low cycle interaction in the form of wave contribution added to the still water cycle. According to Urm et al. [76] the still water and wave cycles could be assessed independently and the damage accumulation is adjusted to account for the contribution of the waves. Instead of including the wave contribution in the dredging cycle it is included in the damage accumulation based on the frequencies of the still water and wave loading. The combined low- and high cycle fatigue damage is calculated with use of equation 4.26. This method is suggested, however, for assessment of low cycle ranges that are corrected for cyclic plasticity. Equation 4.26 is a function of the damage due to the low cycle and not the range itself and is therefore deemed applicable.

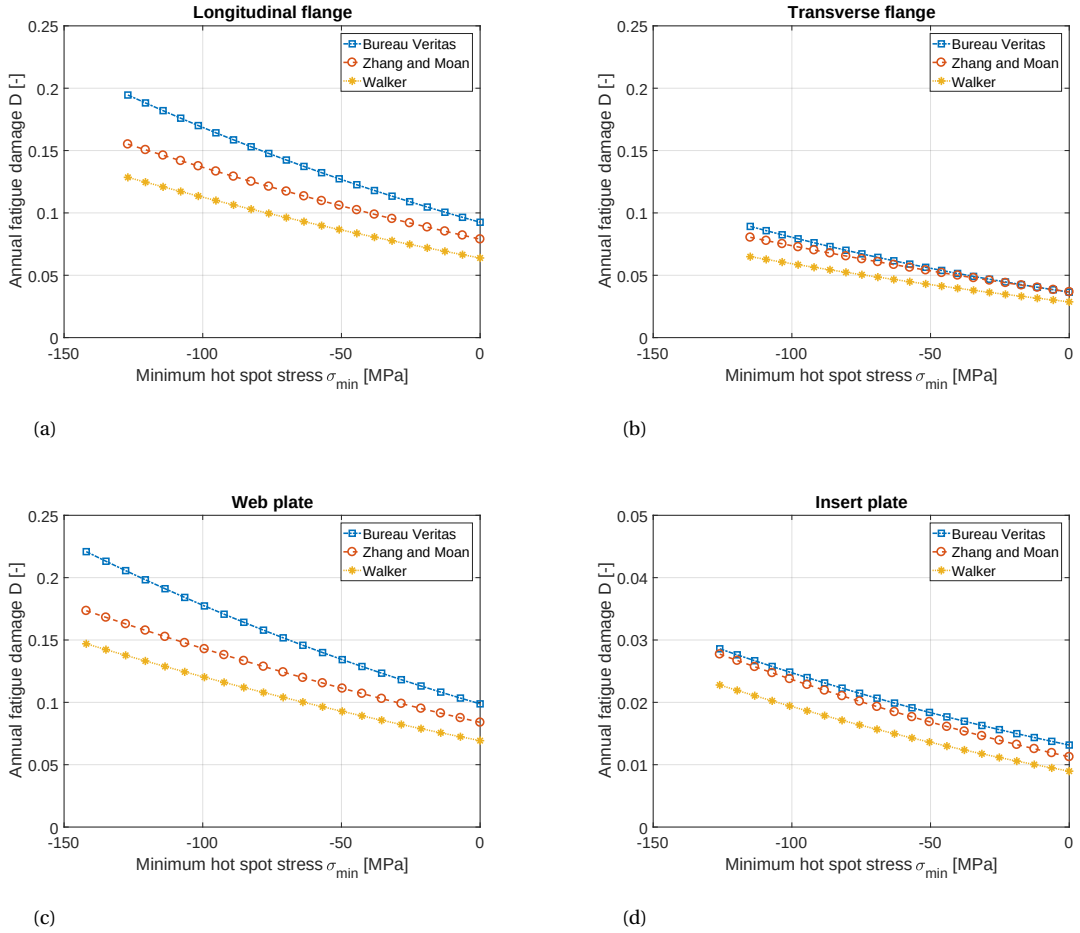


Figure 4.10: **(a)** Combined effect stress range reduction and increasing load ratio longitudinal flange, **(b)** Combined effect stress range reduction and increasing load ratio flange, **(c)** Combined effect stress range reduction and increasing load ratio web plate, **(d)** Combined effect stress range reduction and increasing load ratio insert plate ellipse

$$D_{combined} = D_{HCF}\left(1 - \frac{\nu_{LCF}}{\nu_{HCF}}\right) + \nu_{LCF}\left[\left(\frac{D_{LCF}}{\nu_{LCF}}\right)^{\frac{1}{m}} + \left(\frac{D_{HCF}}{\nu_{HCF}}\right)^{\frac{1}{m}}\right]^3 \tag{4.26}$$

Here are $D_{LCF}$ and $D_{HCF}$ the independent fatigue damages of still water and the wave loading respectively and $\nu_{LCF}$ and $\nu_{HCF}$ the frequencies of the loading. The low cycle frequency is based on the average amount of cycles per second and the wave frequency on the average wave period. To see the effect of the combined damage accumulation it is compared with the independently calculated fatigue damage of the still water stress range with- and without wave contribution and wave stress ranges. The results are plotted in **figure 4.11** which are based on four dredging cycles a day.

The combined annual damage proposed by Urm et al. is higher than the dredging cycle without wave contribution which was expected. On the other hand is the damage significantly lower compared to the still water cycle with added wave contribution. The annual fatigue damage is calculated for a variety of dredging cycle frequencies to see the effect of the frequency. It is found that the difference in annual fatigue damage between the the two damage accumulation methods is independent of the dredging cycle frequency. Significant difference arise when a ship experiences much lower frequencies such as weekly unloading. This is however not representative for the hopper dredger load profile.

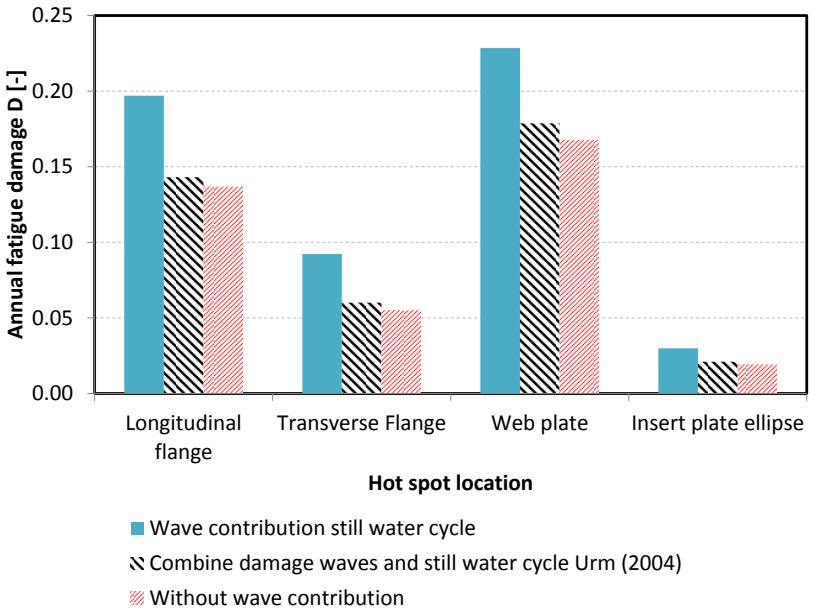


Figure 4.11: Effect of still water and wave loading on fatigue damage

## 4.4. Summary

In this chapter a base fatigue life is calculated according BV guideline methods and a analysis of the main parameters in the fatigue assessment are analysed on sensitivity and compared with alternative methods. The following statements summarize the findings of this chapter.

- The dredging cycle significantly contributes to the fatigue damage in the analysed details and determines at least on average 97% of the damage. Therefore, the fatigue life of the details in the bottom opening corner depend greatly on the accuracy of the dredging cycle description.

- Taking the probability of the BV SN-curve into account it is not said with certainty that in case of failure it is low cycle fatigue assuming $10^4$ cycles as clear separating limit between high- and low-cycle fatigue. The dredging cycle stress ranges are that close to this boundary limit that a conclusion if it is low cycle fatigue really depends on considerations regarding design SN-curves and mean stress corrections.

- The considered weld leg length in the structural hot spot stress calculation has major effect on the fatigue damage in the hot spots on the flanges of the cruciform joint. At these locations the stress gradient due to the geometric discontinuity is much larger compared to the web plate. These hot spots are located in the bottom opening corner and therefore prone to corrosion. The sensitivity of the stress range to the weld leg length leads to the conclusion that this dimension should be carefully determined based on average corrosion reduction of the leg length.

- The shape parameter of the Weibull distribution, used in wave cycle fatigue assessment, has little effect on the fatigue damage. This is explained by the low stress ranges of the waves since fatigue damage due to the waves depends on the Weibull distribution. The shape parameter of the distribution is an important factor in fatigue of ship structural details when using the simplified assessment method. If fatigue analysis of details in the studied area is executed a rough estimation of this parameter would not have significant effect on fatigue life prediction.

- The wave loading has the most effect contributing to the dredging cycle stress range and depends on the probability of the wave that is used. The wave amplitudes increase the dredging cycle stress range by an average of 15%. Increasing the probability from once a day to once every several hours leads to a fatigue damage reduction of 16% on average. This makes the consideration of the wave that could occur during empty or fully loaded condition an important parameter which depends on the time a dredger is in either of these conditions.

- If residual stress relaxation is taken into account this leads to a significant reduction of the fatigue damage according to the method proposed by Zhanga nd Moan. Measuring or monitoring of residual stress is not practical in a structure like a hopper dredger and therefore the residual stress is often unknown and correction methods are deemed to be conservative. In the low cycle region the effect of residual stress reduces significantly and supports the expectation that extension of the BV SN-curve to the low cycle fatigue region would lead to conservative results.
- If a hopper dredger maintains a certain water level during and after discharge this will reduce the fatigue damage significantly and is almost unaffected by the increase of the cyclic mean stress level. It is therefore concluded that if a certain weir level in the hopper is maintained this would greatly benefit the fatigue life of details in the bottom opening corners.
- An alternative method to account for high and low cycle fatigue damage is analysed and results in significantly lower calculated annual fatigue damages. Low and high cycle interactions are accounted for in the damage calculation and from it is concluded that reduction of the dredging cycle wave may be justified.

# 5

# Low cycle fatigue assessment

*In section 3.5.5 of chapter 3.2.3 the hotspot stress range of the dredging cycle including a wave contribution is established. The stress ranges have a relatively high value and fatigue failure could occur within* $10^4$ *cycles. As explained in chapter 2 this number of cycles to failure indicate low-cycle fatigue and this phenomenon is accompanied by cyclic plasticity. The finite element results are based on a linear-elastic analysis. In this section a procedure is proposed to adjust the stress range to account for this plasticity and associated applicable fatigue life predictions. Several aspects of the correction methods are analysed and the effect on the fatigue assessment is discussed.*

## 5.1. Analytical assessment

In this section three methods to take into account cyclic plasticity are presented. The methods to take into account the bi-axial loading are selected based on their proved close agreement to local principal stress and strains in notches [23] [28]

### 5.1.1. Principal stress range

It is seen that high structural stresses arise locally in the corners of bottom door openings. These stresses are based on a maximum principal hot spot stress range. It was shown by Wang et al. [83] that the hot spot stress could be used for a low cycle fatigue analysis, this has however only been proven for uni-axial loading. In the previous chapter the fatigue life is estimated by use of the principal hot spot stresses to account for the multi-axial nature of the loading. Methods of using the principal hot spot stresses are well known in case of linear plane stress states in plates on condition of the stress direction being within a certain angle perpendicular to the weld. In low cycle fatigue plasticity due to cyclic loading is considered significant and should be accounted for in the fatigue life assessment. Cyclic plasticity is usually assessed with the notch stress/strain approach and the strain amplitude, including elastic and plastic components, is assessed with a single strain life curve based on material properties. The hot spot stress, however, cannot be assessed with a single SN curve and therefore this stress concept is often not used in a low cycle fatigue analysis. Based on the finding that the uni-axial hot spot stress could be used to take into account cyclic plasticity, a proposal is made to use the hot spot stress for a bi-axial plane stress state as well.

Two methods to take into account biaxial stress states have been assessed and are based on the principal notch stresses. These are the generalized form of Neuber's correction [40], which uses a effective principal stress, and a method which is an adjustment of the cyclic stress strain curve based on principal stress ratio. The assumption is that these methods are also applicable for use with the principal hot spot stresses calculated in the previous chapters to obtain a pseudo hot spot stress. Pseudo hot spot stress methods are found in DNV and Norsok standard for high stress ranges in the low cycle fatigue region [79] [75]. This analysis focusses on the applicability and fitness of such an assessment approach in the fatigue assessment of the dredging cycle. The following aspects the low cycle fatigue assessment are identified and their effect on the stress range and fatigue life prediction are discussed:

- SN-curve selection for low-cycle fatigue region.

- Effect of principal stress direction and biaxiality ratio
- Combined effect of applied- and residual mean stress
- Stress range magnitude

## 5.2. Technical background

The correction of linear elastic stress is done with use of Neuber's rule in all methods. The distinction between the methods is the type of stress that is corrected or the cyclic stress strain curve that is used. In this section the technical background of the three analysed methods is elaborated. The equations used to correct the stress in the uni-axial case are applicable in the bi-axial methods as well.

### 5.2.1. Uni-axial

The correction method to correct the linear-elastic stress to account for plasticity based on Neuber's rule is explained in section 2.6.2 and given by equation 5.1.

$$\sigma\epsilon = \frac{\sigma_{1,le}^2}{E} \tag{5.1}$$

If plasticity is taken into account the local strain contains an elastic and a plastic component. The elastic component will disappear when the load is removed but the plastic part remains to some extent. To calculate the hot spot principal strain the cyclic stress strain curve is used. This curve is described by the Ramberg-Osgood equation and includes the elastic and plastic part as can be seen in equation 5.2.

$$\epsilon = \frac{\sigma}{E} + \left(\frac{\sigma}{K'}\right)^{\frac{1}{n'}} \tag{5.2}$$

Here are $K'$ and $n'$ the cyclic strength coefficient and cyclic strain hardening exponent of the material respectively. The dredging cycle stress range is computed from a maximum and minimum stress which represent the loaded and unloaded load conditions. At the first cycle the maximum stress is be reached on the linear elastic line and the associated stress and strain is corrected to a stress and strain on the cyclic stress-strain curve with use of Neuber's rule. This is done by solving equations 5.3 and 5.4 for $\sigma_{max}$ and $\epsilon_{max}$.

$$\epsilon_{max,eq} = \frac{\sigma_{max,le}}{E} + \left(\frac{\sigma_{max,le}}{K'}\right)\frac{1}{n'} \tag{5.3}$$

$$\frac{\sigma_{1,le}^2}{E} = \sigma_{max,le}\epsilon_{max,le} \tag{5.4}$$

From the local stress and strain point of the maximum stress the hot spot will be unloaded to a minimum stress and strain. To find these minimum values the linear-elastic stress amplitude is corrected with use of the cyclic stress strain curve and Neuber's rule. The stress and strain amplitudes of the cyclic loading are found by solving equation 5.5 and 5.6.

$$\epsilon_{amp,eq} = \frac{\sigma_{amp,le}}{E} + \left(\frac{\sigma_{amp,le}}{K'}\right)\frac{1}{n'} \tag{5.5}$$

$$\frac{\sigma_{1,le}^2}{E} = \sigma_{amp,eq}\epsilon_{amp,eq} \tag{5.6}$$

**Figure 5.1** illustrates Neuber's rule correction from the linear-elastic line onto the cyclic stress strain curve for AH-36 steel. The curved lines represent equation 5.6 in which the hot spot stress $\sigma_{hs}$ is kept constant on the amplitude of the elastic stress cycle of each hot spot in the bottom opening corner of the hopper dredger. To complete the cycle the minimum stress and strain are determined by extracting two times the amplitude from the maximum true stress and strain according equations 5.7 and 5.8.

$$\epsilon_{min,eq} = \epsilon_{max,eq} - 2\epsilon_{amp,eq} \tag{5.7}$$

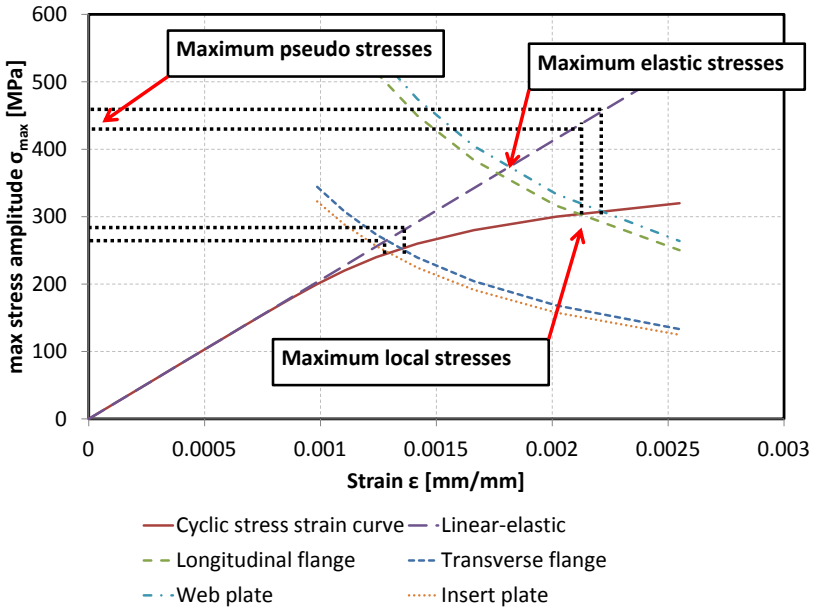


Figure 5.1: Illustration of using Neuber's rule to establish local stress and strain with use of the Ramberg-Osgood cyclic stress strain curve

$$\sigma_{min,eq} = \sigma_{max,eq} - 2\sigma_{amp,eq} \tag{5.8}$$

The first cycle is described and it is unknown if the cyclic loading has converged to a stable cyclic loading state. The cyclic loading is considered stable when the location of the cyclic loading hysteresis loop in the a stress-strain plane does not significantly change relative to the previous cycle. This means that the mean strain and stress of the cycle do not significantly change. The stress-strain behaviour of the next cycles is calculated with use of the cyclic stress-strain curve and the previously calculated maximum and minimum stress and strain assuming Masing-type behaviour. This means that the cyclic hysteresis loop follows the material stress-strain curve magnified by a factor two. The maximum and minimum values of the unloading and second loading is described by equations 5.9 and 5.10.

$$\frac{\epsilon_{max,eq} - \epsilon_{eq}}{2} = \frac{\sigma_{max,eq} - \sigma_{eq}}{2E} + \left(\frac{\sigma_{max,eq} - \sigma_{eq}}{2K'}\right)^{\frac{1}{n'}} \tag{5.9}$$

$$\frac{\epsilon_{eq} - \epsilon_{min,eq}}{2} = \frac{\sigma_{eq} - \sigma_{min,eq}}{2E} + \left(\frac{\sigma_{eq} - \sigma_{min,eq}}{2K'}\right)^{\frac{1}{n'}} \tag{5.10}$$

These steps show the sequence of actions to determine the local stress and strain from the linear elastic values obtained with FE analysis. The following sections describe similar procedures that take into account bi-axial stress states. The procedures have been validated for the effective notch stress concept.

### 5.2.2. Bi-axial method: Hoffmann and Seeger

To account for the influence of the bi-axial stress state that is found in chapter 3 the generalized Neuber's rule proposed by Hoffmann and Seeger is used. It is based on a equivalent stress which is computed with use of the principal stress and strains. The method is based on the assumption that the direction of the principal stresses are fixed and that the strain ratio remains constant during loading. The first assumption requires the loading to be proportional and the second assumption is based on experimental and numerical research on the ratio between principal strains during material yielding. The method is composed out of the following steps:

- Step 1: Identify linear-elastic principal stresses in minimum and maximum condition

- Step 2: Calculate the equivalent elastic stress and strain using Von Mises yield criterion

$$\sigma_{eq,le} = \sqrt{\sigma_{1,le}^2 - \sigma_{1,le}\sigma_{2,le} + \sigma_{2,le}^2} \tag{5.11}$$

- Step 3: Use Neuber's rule to determine the local equivalent stress and strain

$$\sigma_{eq}\epsilon_{eq} = \frac{\sigma_{eq,le}^2}{E} \tag{5.12}$$

- Step 4: Solve Hencky's flow equation to calculate local principal stresses and strains

$$a = \frac{\sigma_{2,eq}}{\sigma_{1,eq}} \tag{5.13}$$

$$\sigma_{1,eq} = \frac{\sigma_{eq}}{\sqrt{1-a+a^2}} \tag{5.14}$$

$$\epsilon_{1,eq} = \frac{\epsilon_{eq}(1-ua)}{\sqrt{1-a+a^2}} \tag{5.15}$$

$$\frac{\sigma_{2,eq}}{\sigma_{1,eq}} = -u\frac{(1+a)}{(1-ua)} \tag{5.16}$$

Where:

$$u = \frac{1}{2} - \left(\frac{1}{2} - \nu\right)\frac{\sigma_{eq}}{E\epsilon_{eq}} \tag{5.17}$$

The actual principal stress and strain are then used for further analysis. The equivalent elastic stress is found using step 1 and 2 and is used to determine the equivalent amplitude. The equivalent amplitude is adjusted with the same procedure to obtain the first principal minimum stress and strain so that the total range is computed.

### 5.2.3. Bi-axial method: Dowling

According to N.E. Dowling, stress in more than one direction has effect on the properties of the material in elastic and plastic state [28]. To account for the effect of the multi-axial stress state when material is yielding effective stress and strain variables are introduced based on the biaxiality ratio. The Ramberg-Osgood cyclic stress strain curve is determined by the plastic behaviour of the material and therefore the effective stress and strain values are used to adjust the curve based on state of stress at the notch of a detail. The method contains the following steps:

- Step 1: Determine the linear elastic principal stress ratio

$$\lambda = \frac{\sigma_{2,le}}{\sigma_{1,le}} \tag{5.18}$$

- Step 2: Calculate the linear-elastic effective stress

$$\sigma_{eq} = \sigma_{1,le}\sqrt{1-\lambda+\lambda^2} \tag{5.19}$$

- Step 3: Use generalized Hook's law, which is practically the same as equations 5.13 to 5.16, to determine elastic and plastic strain components

- Step 4: Substitute the elastic and plastic components into the Ramberg-Osgood equation to compute the bi-axial cyclic stress strain curve

$$\epsilon_{1,eq} = (1-\nu\lambda)\frac{\sigma_{1,le}}{E} + (1-0.5\lambda)(1-\lambda-\lambda^2)^{\frac{1-n'}{2n'}}\left(\frac{\sigma_{1,le}}{K'}\right)^{\frac{1}{n'}} \tag{5.20}$$

In which $\nu$ is the Poison's ratio and $\lambda$ is the ratio between the first and second principal stresses. The 0.5 in the second term originates from the assumption that plastic strains do not contribute to the volume change and the Poison's ratio is therefore replaced by 0.5. Note that this is done for a plane stress situation with principal stresses which means that this is valid when the shear stress equals zero and therefore shear stress is neglected.

The bi-axial influence of the loading is described by the ratio between the first and second principal stress in direction of the maximum principal stress range. The dredging cycle stress ranges with a wave contribution based on a probability of $10^{-4}$ are used as input of the three analysed methods. The principal stresses are corrected according the steps described. Using equations **??** and 5.20 the cyclic stress strain curve for uni-axial and bi-axial are plotted. The bi-axial curves show that positive biaxiality ratios raise the stress-strain curve where negative values lower it. Negative ratios enhance local strain due to the compressive second principal stress in combination with the Poisons's effect.

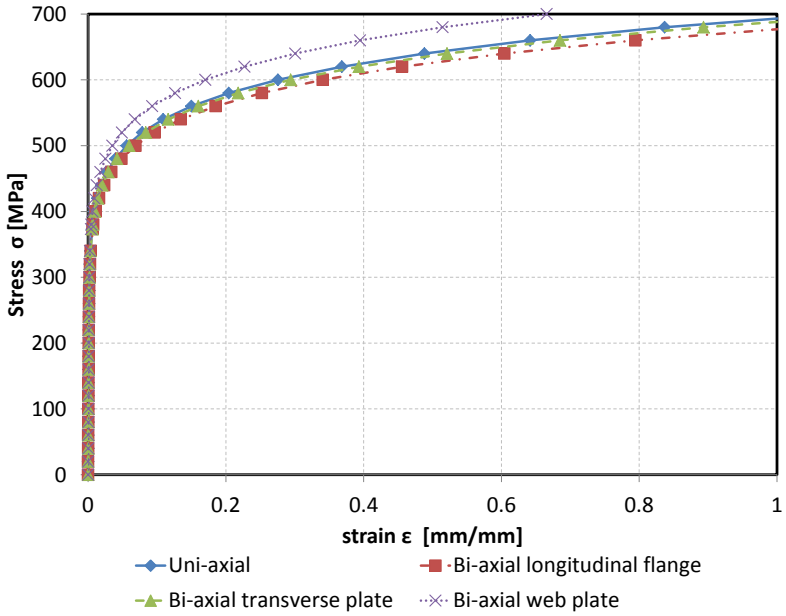


Figure 5.2: Uni-axial and bi-axial cyclic stress strain curves parent material AH-36 steel hot spots cruciform joint

### 5.2.4. Pseudo stress ranges

The pseudo stress range is computed to translate the plastic and elastic strains to the stress life domain and thereby preventing the need of a strain life curve. The strain difference between the maximum and minimum value represents the strain range which is used to determine the pseudo stress range. The new range is a projection of the local strain range on the linear-elastic line and is expressed by equation 5.21 and illustrated in figure 5.1. In which E is the Young's modulus and $\Delta\epsilon$ is two times the strain amplitude corrected by Neuber's rule. The pseudo stress ranges are presented in **table 5.21**.

$$\Delta\sigma_{pseudo} = E\Delta\epsilon \tag{5.21}$$

$$\Delta\epsilon = \epsilon_{max,eq} - \epsilon_{min,eq} \tag{5.22}$$

### 5.2.5. Low cycle SN-curves

In the previous chapter a conclusion was made that the initially used BV SN-curves may not representative in the low cycle region. On the assumption that residual stress would relax the SN-curve was shifted and compared with a method that taken residual and mean stress affect into account. It was concluded that the shifted SN-curve assuming zero mean stress leads to relatively long fatigue life estimations and may be too non-conservative compared to the method that takes into account residual stress relaxation. With this in

Table 5.1: Pseudo hot spot stress ranges of the three analysed methods for AH-36 steel material compared to linear elastic FE values

| | $\Delta\sigma_{le}$ [MPa] | $\Delta\sigma_{neuber}$ [MPa] | $\Delta\sigma_{HS}$ [Mpa] | $\Delta\sigma_{Dowling}$ [MPa] | Biaxial ratio [-] |
|---|---|---|---|---|---|
| Longitudinal plate | 489 | 504 | 513 | 510 | -0.047 |
| transverse plate | 379 | 382 | 383 | 383 | -0.015 |
| web plate | 514 | 535 | 509 | 521 | 0.116 |
| insert plate | 381 | 384 | 384 | 384 | - |

mind it may be that a SN-curve without accounted for residual stress is not applicable.

Actual data representative for hot spot stresses in a free corrosive environment is not known by the author which brings a lot of uncertainty in the fatigue life prediction. Two SN-curves have been found in DNV and ABS documentation [10] [5] in which the pseudo hot spot stress has been adopted as well. The methods associated with the pseudo hot spot stress curves state that mean stress should not be included in the fatigue analysis which leads to the conclusion that full relaxation of mean stress is assumed. These curves do also not take into account the presence of a corrosive environment and are therefore reduced by 30% to account for corrosion effects which is also done for the initially used BV SN-curve. The SN-curves are given in **table 5.2** and presented in appendix C.

Table 5.2: SN-curves considered for pseudo hot spot stress assessment

| SN-curve | Characteristic value | Slope | FAT |
|---|---|---|---|
| | $log(K_{97.7})$ | m | [MPa] |
| DNV low cycle fatigue [10] | 1.4588E+12 | 3 | 90 |
| DNV low cycle fatigue corrosive | 5.0037E+11 | 3 | 63 |
| ABS low cycle fatigue [3] | 3.5100E+10 | 2.4 | 59 |
| ABS low cycle fatigue corrosive | 1.4912E+10 | 2.4 | 41 |
| BV P-curve corrosive | 5.0652E+11 | 3 | 63 |
| BV P-curve $R = -1$ corrosive | 1.1826E+12 | 3 | 84 |

In **figures 5.3a** to **5.3d** the amount of cycles failure are presented calculated with use of the SN-curves which are presented in **table 5.2**. The fatigue lives are calculated with use of the pseudo stress ranges determined in section 5.2.4 and assuming AH-36 steel parent material. If a SN-curve for corrosive environment is used the amount of cycles to failure is much lower as expected. The stress range in the web is less damaging in case the Hoffmann and Seeeger method is used. The larger principal stress angle in the web plate leads to longer life predictions when taking taking bi-axiallity into account. The low-cycle fatigue SN curves specified by DNV and ABS, which are not corrected for corrosion, show that the amount of cycles is still above the $10^{-4}$ limit. The shifted BV curve to zero mean stress shows result in between and below the low-cycle fatigue limit level.

Comparing the DNV and ABS corrosion curves with the shifted BV corrosion curve by walker to a stress ratio of -1, the calculated fatigue lives are much shorter. This could indicate that mean stresses are included in the DNV and ABS pseudo hot spot stress SN-curves or that the assumption that the curve could be reduced by 30% is too conservative. Wang et al. Concluded that the use of a extended D-curve into the low cycle fatigue region is applicable although it is rather conservative. Due to the uncertainty of which SN-curve should be selected the use of the initial BV corrosion curve seems suitable in this case.

## 5.3. Effect of material type

To determine the non-linear strains associated with the high stress levels a cyclic stress-strain is computed in all three methods. The curve is described by the commonly used Ramberg-Osgood equation. Wang et al. [83] studies the application of low-cycle fatigue assessment in marine structures and provides material parameter $K'$ and $n'$ which are based on DSME test results and are presented in **table 5.3**.
Note that these are material properties of parent materials. Welded joint have a heat affected zone that changes the material properties locally. If local plasticity in welded joints is analysed the heat-affected zone should be taken into account [38]. According to Lotsberg [52] for the heat-affected zone the material prop-

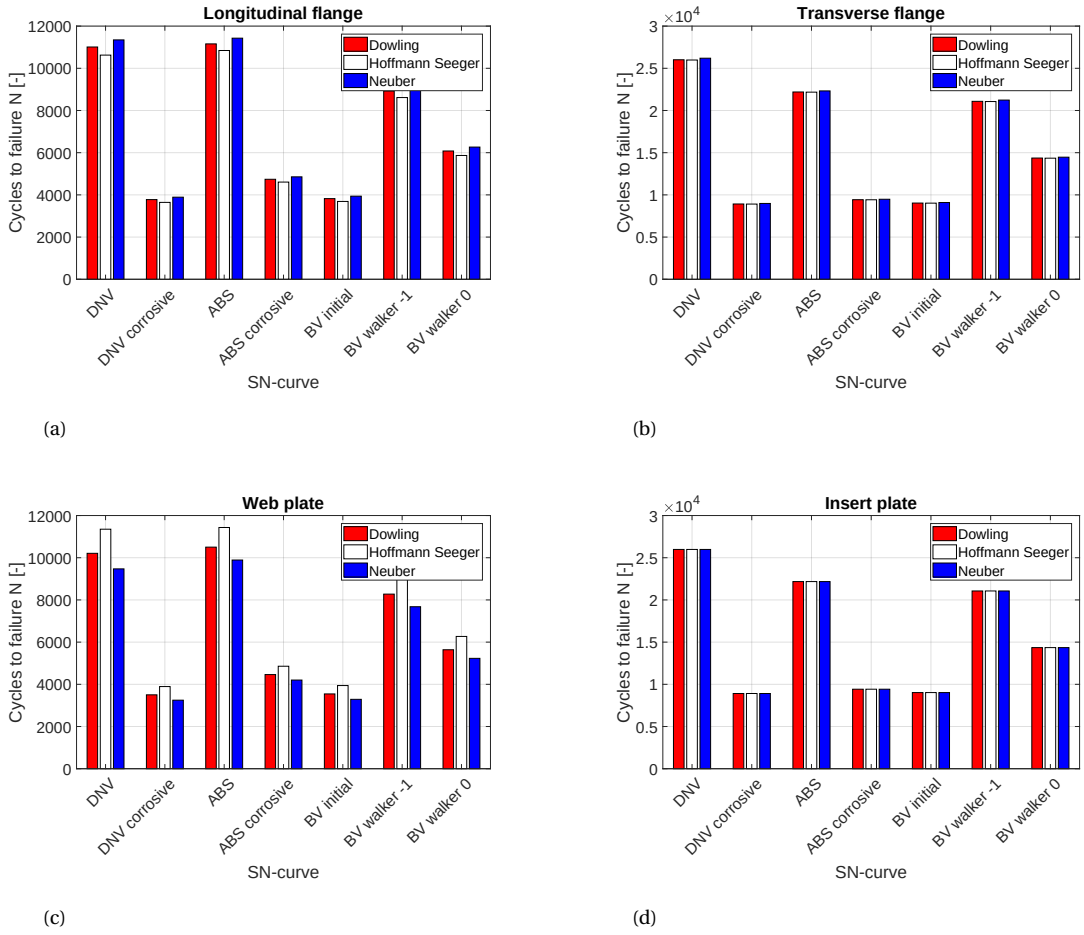


Figure 5.3: **(a)** Cycles to failure different stress ranges according to the three analysed methods on longitudinal flange, **(b)** Cycles to failure different stress ranges according to the three analysed methods on transverse flange, **(c)** Cycles to failure different stress ranges according to the three analysed methods on web plate, **(d)** Cycles to failure different stress ranges according to the three analysed methods on insert plate

Table 5.3: Cyclic stress strain material properties ship building steels [83]

| Material constant | Mild steel | AH-32 | AH-36 | DH-36 |
|---|---|---|---|---|
| K' | 592 | 669 | 694 | 739 |
| n' | 0.114 | 0.108 | 0.112 | 0.106 |

erties of the weld material is recommended. The properties of the weld consumables are found by Heo et al. with monotonic tensile tests with incremental steps. The cyclic material properties of three weld consumables are given in **table 5.4**.

Table 5.4: Cyclic stress strain material properties welding consumables [38]

| Material constant | A | B | C |
|---|---|---|---|
| K' | 1073.4 | 1070.1 | 958.5 |
| n' | 0.159 | 0.133 | 0.120 |

Wang et al. [83] did not mention that a heat-affected zone should be taken into account for the pseudo hot spot stress range and this is also not addressed in the DNV pseudo hot spot analysis. This could be justified due to fact that the hot spot stress is used and not the effective notch stress. This stress is in almost all cases

lower than the actual stress at the notch due to the non-linear surface peak stress. The effect of the material choice is analysed in terms of fatigue lives and because the difference bewteen elastic and pseudo elastic stresses are small it is compared with material effects at higher stress ranges. The effect of the material type is plotted in **figures 5.4a** to **5.4c.**

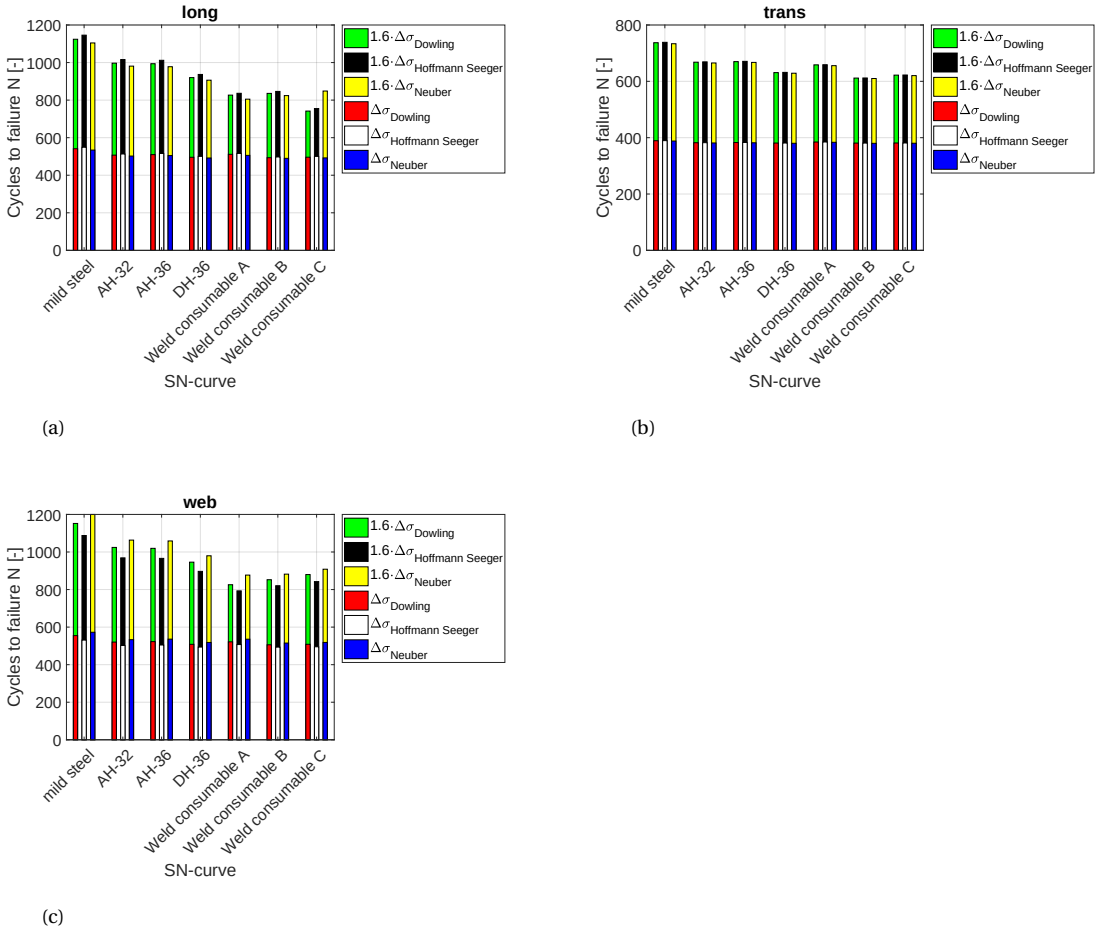


Figure 5.4: **(a)** Pseudo hot spot stress ranges according to the three analysed methods on longitudinal flange, **(b)** Pseudo hot spot stress ranges according to the three analysed methods on transverse plate, **(c)** Pseudo hot spot stress ranges according to the three analysed methods on web plate

The effect of material on the insert plate is not included since the focus is on the difference between parent material and HAZ and the pseudo hot spot stress difference in the insert plate is small. The influence of material choice is affected by the magnitude of the elastic stress range. In case of a higher elastic stress ranges a serious reduction of the pseudo stress range is seen if material specifications of a weld consumable would be considered. This effect is small in case of the stress levels that are found in the analysed hopper dredger.

## 5.4. Principal stress direction

Both methods that take into account bi-axial stresses depend on the ratio between the first and second principal stress. Up to this point it is assumed that the maximum principal stress range with associated direction is the dominant load range in the fatigue assessment and the influence of the second principal stress is not included. To see what the effect is of the chosen direction on the pseudo stress range the direction of the principal stress range is adjusted with use of the stress components in the maximum and minimum conditions. The angle of the principal stress direction is varied between zero and 45 degrees to satisfy the angular sector requirements of the SN-curves. The pseudo stress ranges as function of the considered principal stress angle are presented in **figures 5.5a** to **5.5c**.
The maximum pseudo hot spot stress is indeed found in the direction of the maximum elastic principal stress

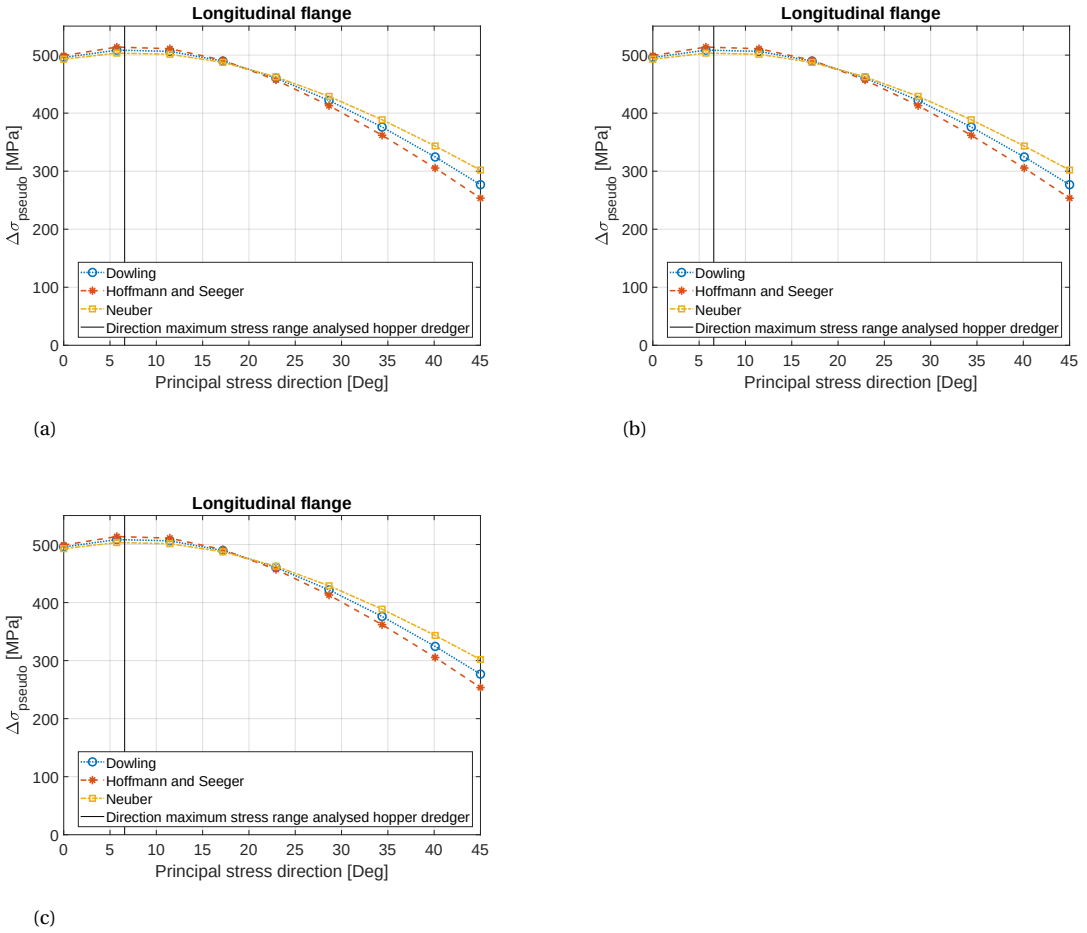


Figure 5.5: **(a)** Effect of bi-axiality ratio on pseudo hot spot stress range on longitudinal flange, **(b)** Effect of bi-axiality ratio on pseudo hot spot stress range on transverse plate, **(c)** Effect of bi-axiality ratio on pseudo hot spot stress range on web plate

range and all three methods show close agreement in all directions. In the BV fatigue assessment procedure the second principal stress is only considered if fatigue damage due to this stress component is more compared to the first principal stress range. The second principal stress is in all analysed hot spots much lower than the first principal stress and is therefore considered insignificant. The two bi-axial local stress methods show dependency to the bi-axiality ratio. It is therefore interesting to see what the effect is of the second principal stress is if it would have a larger proportion compared to the first component. The effect of the ratio on the pseudo stress range is plotted in **figure 5.6a** to **5.6c** for a varying ratio between -1 and 1. From a pure shear state to a pure biaxial stress state respectively.
According to **figures 5.6a** to **5.6c** increase shear state of stress increases the pseudo hot spot stress significantly according to both biaxial methods. This is explained by the compressive second principal stress that enhances the strain in direction of the first principal stress based on the Poisson's effect. This effect is stronger when using the method proposed by Hoffmann and Seeger which also leads to lower pseudo stress ranges if the ratio is positive. Application of either of the two methods instead of uni-axial Neuber's rule has shown little effect in the hot spots in the analysed hopper dredger. If absolute first and second principal stresses would have been more of the same magnitude the consideration for a bi-axial assessment method would be more in place due to this.

## 5.5. Residual stress effect

The analysis in the previous sections was done including residual stress that was assumed to be equal to the yield stress and included in the linear elastic maximum stress. To see if this assumption has effect on the strain range that is found it is compared to the strain range if residual stress is not included in the hot spots

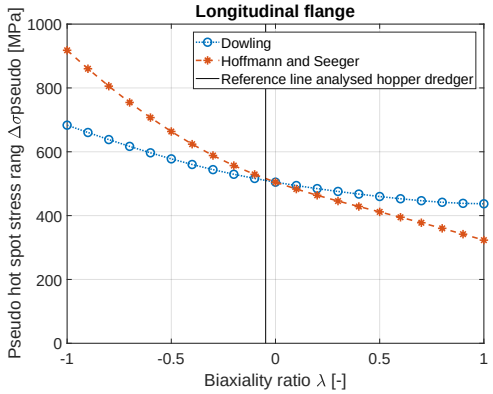


(a)

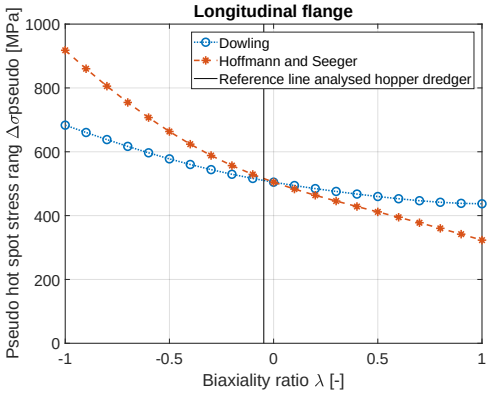


(b)

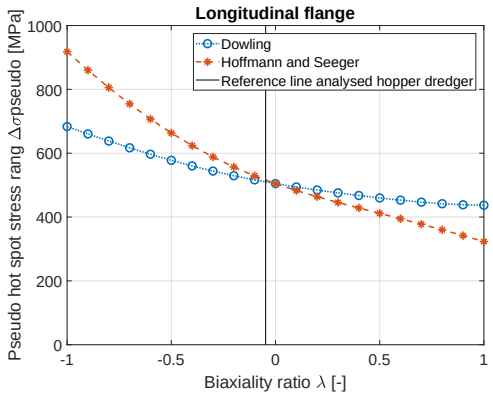


(c)

Figure 5.6: **(a)** Effect of bi-axiality ratio on pseudo hot spot stress range on longitudinal flange, **(b)** Effect of bi-axiality ratio on pseudo hot spot stress range on transverse plate, **(c)** Effect of bi-axiality ratio on pseudo hot spot stress range on web plate

at the welded joint. The mean stress stress is increased from zero up to a mean stress equal to the yield stress which is recommended to use if the actual residual stress is unknown [52]. The mean stress is implemented by increasing the maximum and minimum elastic stresses with a mean stress. In case of the Hoffmann and Seeger method this is added to the effective stress range.

As shown in **figures 5.7a** to **5.7c** the residual stress has negligible effect in all cases. The cyclic stress-strain curve has, however, an upward trend after the cyclic yield point due to hardening behaviour of the material. Increasing the elastic initial stress range with residual stress will increase the local maximum stress and therefore also the mean stress considering the fact that the pseudo stress range is unaffected. There is little cyclic plasticity concluding form the small difference between linear elastic and pseudo elastic stress ranges and full relaxation of the mechanical applied mean stress is not likely.

Cyclic mean stress in terms of increasing residual stress is given in figures 5.8a to 5.8c. It is shown that the mean stress increases if more tensile residual stress is considered in the first cycle. There is little known about the use of mean stress correction in the pseudo hot spot assessment procedure. It is difficult to physically interpreted the pseudo hot spot stress and therefore the meaning of mean stress as well. DNV and ABS [10] [5] mention that mean stress effect should not be included in the pseudo hot spot stress procedure. According to **figures 5.8a** to **5.8c** the local mean stress could turn out higher than the remote mechanical mean stress if residual stress is included in the initial linear elastic stress amplitude. It is however not known if stable cyclic loading is the case after the first cycle. Cyclic softening of the material could also relax this mean stress again. With this in mind, and the assumption that cyclic plasticity is small, this mean stress could have influence on the fatigue strength of the welded joint and should be taken into account.

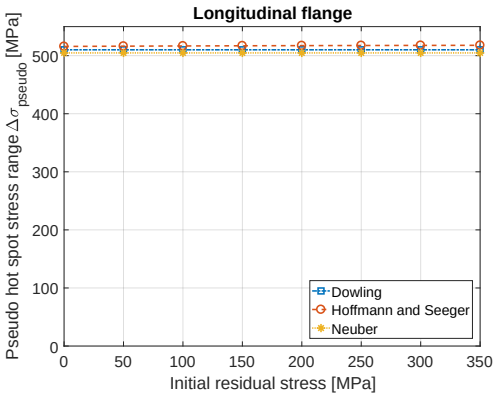


(a)

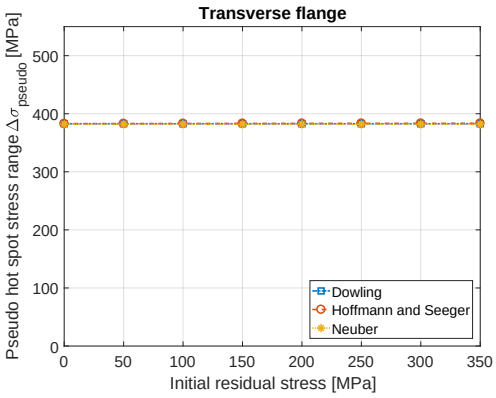


(b)

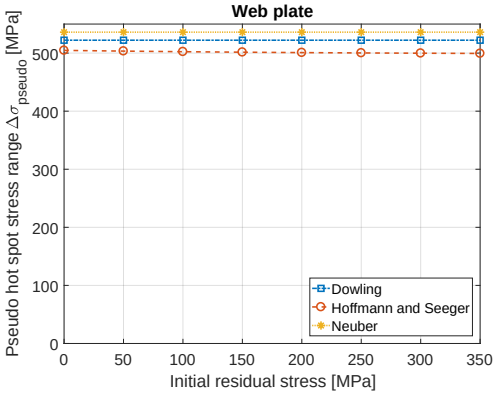


(c)

Figure 5.7: **(a)** Effect initial residual stress on pseudo hot spot stress longitudinal flange, **(b)** Effect initial residual stress on pseudo hot spot stress transverse flange, **(c)** Effect initial residual stress on pseudo hot spot stress web plate

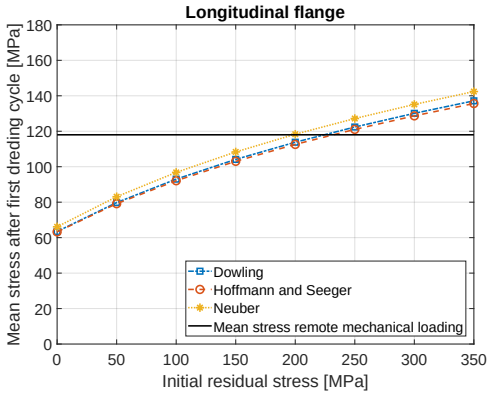


(a)

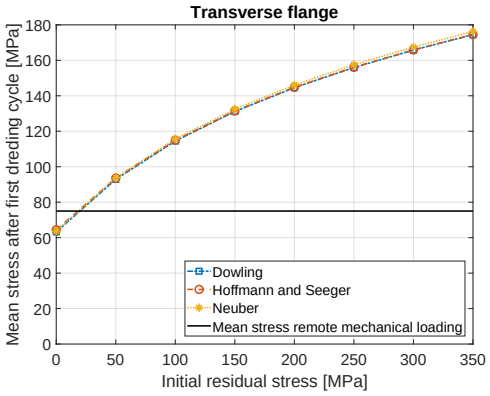


(b)

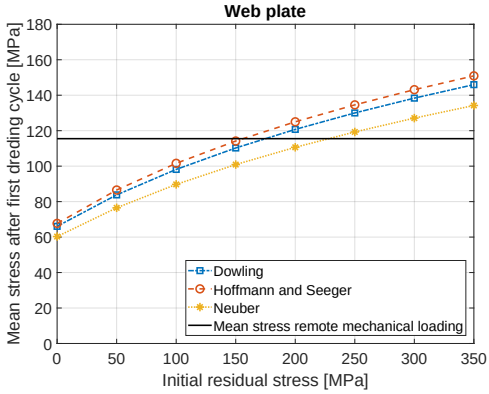


(c)

Figure 5.8: **(a)** Effect initial tensile residual stress on cyclic mean stress longitudinal flange, **(b)** Effect initial tensile residual stress on cyclic mean stress transverse flange, **(c)** Effect initial tensile residual stress on cyclic mean stress web plate

## 5.6. Effect of stress range

The magnitudes of the dredging cycle stress ranges are relatively low in low-cycle fatigue terms. It is possible that the stress range in other details, or dredgers, reaches higher levels and that will result in higher pseudo stress ranges. It is expected that the two methods that are analysed here show more difference if higher stress ranges are found. To see what the effect is of the stress range magnitude increasing elastic stress range is plotted against its associated pseudo stress range in **figures 5.9a** and **5.9b**. This is done by scaling the initially established elastic ranges in the analysed hopper dredger.

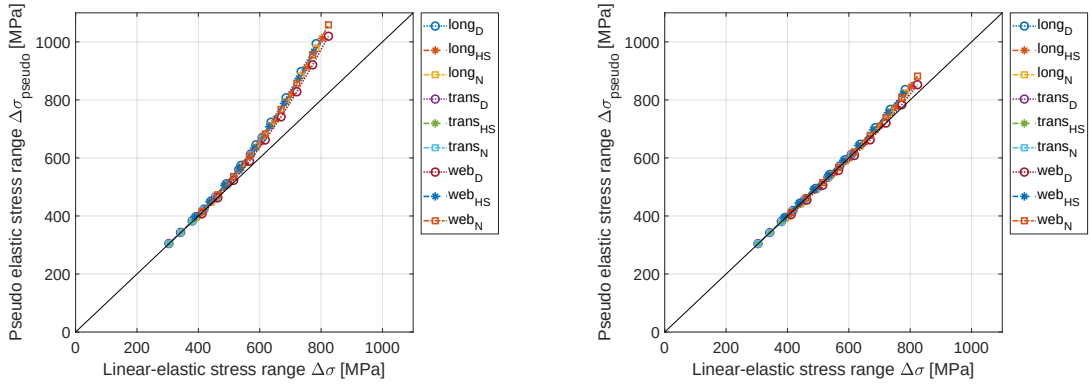


(a) (b)

Figure 5.9: **(a)** Effect increasing linear-elastic stress ranges on pseudo hot spot stress ranges AH-36 steel, **(b)** Effect increasing linear-elastic stress ranges on pseudo hot spot stress ranges weld consumable

It seems that in case the parent material is considered, elastic stress ranges of at least 500 MPa are required palsticity correction effects. Lower stress ranges could be considered equal to the elastic stress range. For HAZ material the minimum elastic stress range is much higher until the pseudo stress ranges becomes significant. This complies with the findings of the analysis in section 5.3. Note that this is analysis is done with initial linear elastic bi-axial stress ratios.

## 5.7. Validation

An attempt is made to validate the equivalent stresses and strains found with the three plasticity correction methods using a fine mesh sub-model of the cruciform joint modelled with shell elements as presented in **figure 5.10**. Nodal loads that are subtracted from the cargo hold model analysis are applied on the boundaries. A non-linear analysis is performed with Femap and NX Nastran solver and stress and strain is measured for comparison with the calculated equivalent stress and strains. Stress and strain where calculated in the hot spot on the web plate of the cruciform joint with use of the stress extrapolation technique discussed in section 3.5.1 of chapter 3. Three limitations arose form this analysis:

- Hot spot stress is a linearisation through the thickness of the plate and this cannot be captured with use of shell elements. Surface extrapolation cannot be used due to the non-linear behaviour between the shell elements which is not included in the hot spot stress calculation. The stress at the hot spot should therefore be determined with the through thickness stress distribution of the plate at the location of the hot spot. This is not possible using shell elements.
- The second limitation is the fact that Femap's material model uses a monotonic stress-strain which does not capture the cyclic behaviour of the material. Adjustment of the material model is possible but results in additional limitations such as difficulties in the description of the curve by taking into account different bi-axial stress states.
- A third discrepancy is determination of the applied load. Plasticity changes the stress distribution in the plate and it is unknown what the effect is on the applied loading on the boundaries. Also, modelling of realistic thermal induced residual stress is limited.

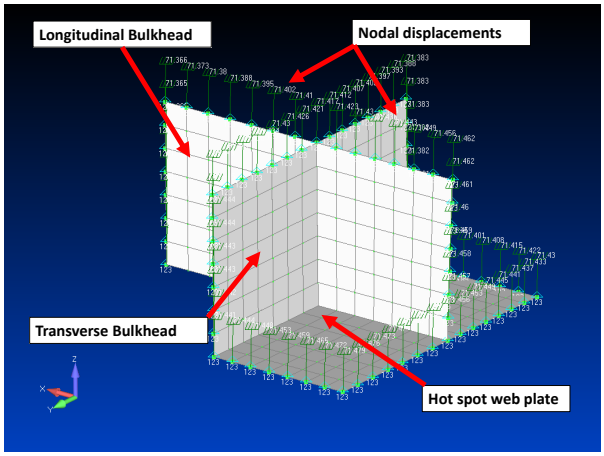


Figure 5.10: Sub-model of cruciform joint used for non-linear finite element analysis

## 5.8. Summary

One uni-axial and two bi-axial plasticity correction methods are assessed in this chapter and the use of the principal hot spot stress is proposed. The linear elastic stress ranges are corrected to pseudo stress ranges which could be used for stress based fatigue analysis. A study on the effect of the parameters of the correction procedures has led to the flowing findings:

- The difference between elastic and pseudo-elastic stress ranges is small and depending on the selected design curve will have little effect on fatigue life prediction. This indicates that very little cyclic plasticity occurs and that pseudo hot spot stress assessment would not be applicable or necessary for the analysed details.
- A major uncertainty is the selection of a suitable SN-curve for the pseudo hotspot stress. There is no data available that could be used to compute a SN-curve applicable with the pseudo principal hot spot stress. Although it might be too conservative, the initial BV corrosion curve could used as a base case.
- Increasing the first loading with residual stress does not have effect on the calculated pseudo stress range which means that the pseudo stress range depends fully on the amplitude of the mechanical applied loading. The mean stress does increase if the residual stress is included which leads to the conclusion that mean stress should be taken into account in the assessment procedure. However, if mean stress relaxation is assumed after a relatively small number of cycles the effect of mean stress dissipates.
- The material properties that are used in the cyclic stress strain curve have significant effect on the pseudo stress range if cyclic elastic stress amplitudes levels are near the static material yield point and beyond. Considering the stress ranges in the hopper, the type of material has little effect. In combination with the small difference between elastic and pseudo elastic stress ranges leads to the conclusion that the stress ranges in the analysed hopper dredger are too low for the proposed procedure.
- The previous statement only holds if the bi-axial stress ratios are small. If higher absolute values of this ratio are found the applicability of the bi-axial correction methods is in place. A more shear dominated stress state increases the pseudo stress range and a more bi-axial stress state seems to be beneficial. The pseudo hot spot stress ranges found in the hopper dredger could be underestimated if the level of bi-axial stress is not taken into account.
- Non-linear finite element analysis to validate bi-axial hot spot plasticity correction cannot be done using the current model. This means that more detailed numerical modelling methods or even experimental validation is required.

The proposed correction methods in combination with all fatigue assessment aspects discussed in the previous chapters is summarized and a recommended procedure is elaborated and presented in figure 5.11. Note that this is a global procedure that generally describes the steps and things that to pay attention to when

performing a fatigue assessment of a hopper dredger using a finite shell element model. Note that, due to uncertainties, conservative methods are selected to assure safe design.

**Step 1:** Use ship specifications, hopper tables and still water bending moment documents to describe the dredging cycle as is done in 3. Then calculate hull girder and pressure loads with use of the ship specifications and dredging cycle load steps.

**Step 2:** Use beam theory to do a simplified calculation of the nominal transverse and longitudinal stresses in the analysed cross section. Tune and validate the FE model and identify its accuracy.

**Step 3:** Perform a coarse mesh analysis to check for high stressed areas close to the tuned cross sections. Make a fine mesh according required procedures and calculate the principal hot spot stresses with applicable extrapolations methods. Establish the maximum load conditions and determine the maximum dredging cycle stress range including wave contribution based on a probability of $10^{-4}$. Assure that loading is proportional. Otherwise plasticity correction methods are not applicable.

**Step 3:** Perform a coarse mesh analysis to check for high stressed areas. Make a fine mesh according required procedures and calculate the pricipal hot spot stresses according applicable extrapolations methods. Establish the maximum load conditions and determine the maximum dredging cycle stress range including wave contribution based on a probability of $10^{-4}$. Assure that loading is proportional, otherwise plasticity correction methods are not applicable.

**Step 4:** Confirm that the maximum stress exceeds the yield stress and if the hot spot is in uni-axial, or considerable bi-axial stress state. In this chapter it is seen that at least the maximum stress excluding residual stress should exceed the material yield stress to see an effect of the correction methods and that a negative bi-axial ratio enhances the pseudo stress magnitude. If the stress is considered uni-axial the amplitude should exceed the yield stress and the mean stress should be at least zero. Satisfaction of the plasticity correction requirements result in pseudo hot spot stresses that should be assessed with BV hot spot stress SN-curves.

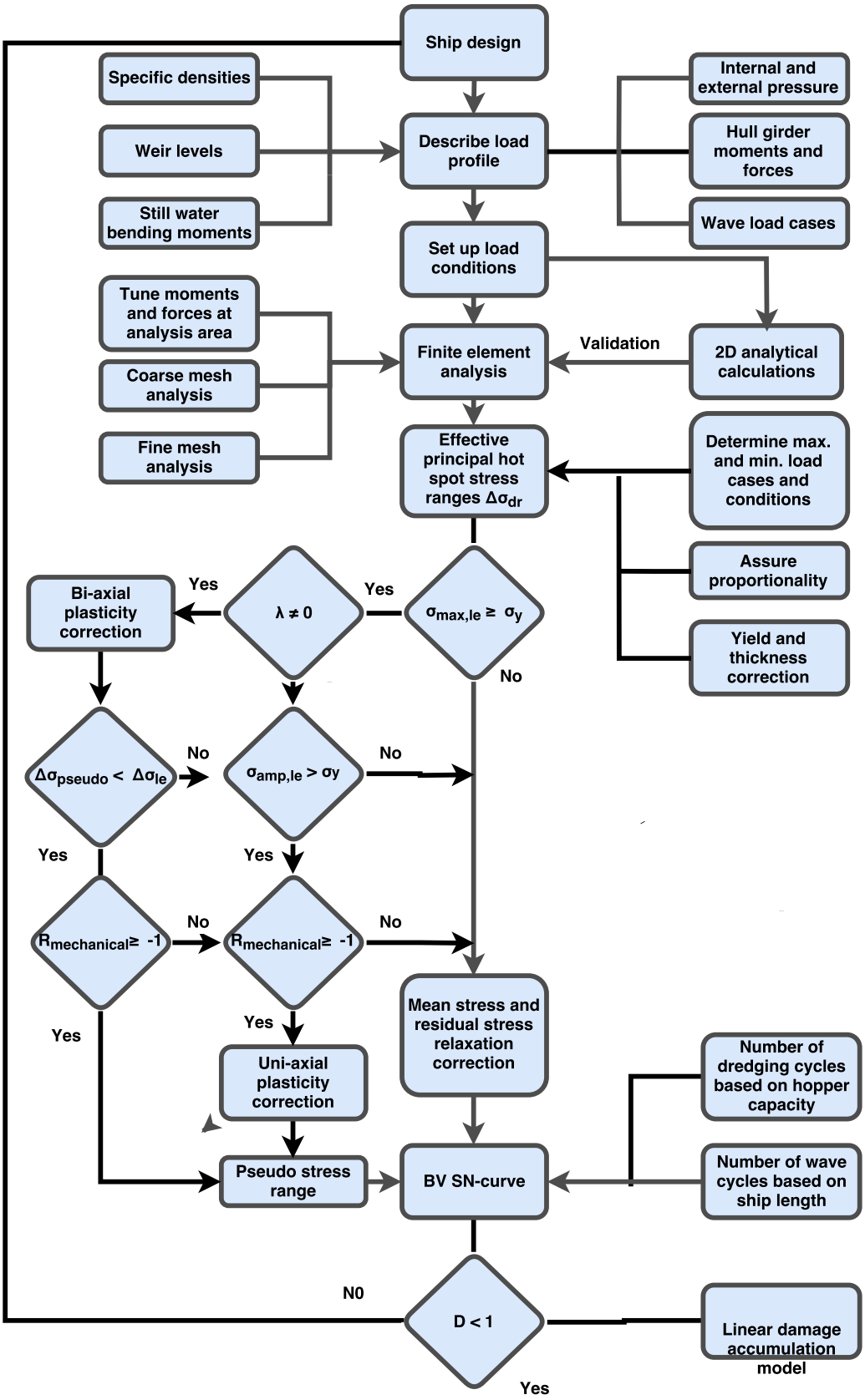


Figure 5.11: Low-cycle fatigue assessment procedure hopper dredger

# 6

# Conclusion

## 6.1. Conclusions

The aim of this research is to obtain better understanding of fatigue crack initiation in hopper dredger hull designs and assessment methods applicable for the specific load profile of such a ship. Especially the effect of the loading and unloading cycle of the hopper on fatigue life prediction is thoroughly investigated. Documented damage cases of cracks in hopper dredgers are studied to get an indication of the fatigue problem in these hull designs. A representative hopper dredger is selected and analysed with use of a finite element model to obtain hot spot stresses in the bottom opening corners where fatigue damages have been found. Main parameters in the current assessment procedure are identified and their sensitivity is examined and compared to alternative methods which are assumed suitable for fatigue assessment of hopper dredgers. The load profile in combination with high stress ranges indicate that fatigue failure is due to low-cycle fatigue and therefore a low-cycle fatigue assessment procedure is proposed. Three methods to correct cyclic behaviour to a pseudo stress domain are analysed and compared. These steps led to the following main conclusions:

- A significant amount of cracks are found in hopper dredgers with a length $L < 170m$ and appeared within the minimum required 20 year fatigue life time. If fabrication flaws or operational misuse are neglected it is concluded that fatigue strength is not covered sufficiently in the strength assessment of the shorter hopper dredgers.

- Primary loads contributing to fatigue damage are identified. The local transverse still water pressure difference of cargo and sea pressure has a significant contribution to the fatigue stress range in structural details located in the bottom opening corner compared to the hull girder loads. Wave stress ranges are small compared to the still water stress range but have a substantial contribution in the overall description of the total dredging cycle by increasing the stress range on average by 15%.

- The load condition with maximum specific cargo density is not necessarily the condition with maximum hot spot stress. A load condition with a specific density of $1600 kg/m^3$ is found to result in a maximum principal stress range. The multi-axial load path of normal stress is found to be proportional to the shear stress component of the loading.

- Actual dredging data of two hopper dredger show that the proportion of time in a year that a hopper dredger is operational is much shorter than initially concluded from literature. Despite this the average amount of cycles a day is higher than the initially assumed four to six cycles and also a higher amount of cycles are experience per year. Although this is data of only two dredgers this shows that it is possible that the dredging cycle frequency is underestimated according to current knowledge. This also contributes to the suspicion that the wave probability of the dredging cycle wave is too low. Considering a wave that occurs every several hours reduces the fatigue damage by 16%. When using an frequency based alternative damage accumulation method for ships that experience loading and unloading cycles the annual fatigue damage is even reduced by 28%.

- The shape parameter of the Weibull long term stress distribution has little effect on fatigue damage in the structural details located in bottom opening corners. This is a result of the small stress ranges in-

duced by the wave loading. A rough estimation of this difficult to determine parameter would therefore not have significant effect on the fatigue life prediction in the bottom opening corners.

- The maximum stress of the dredging cycle is close to, and even exceeds, the material yield stress. This static overload leads to relaxation of the thermally induced residual stress due to fabrication welding. The stress ratio of the total loading is therefore significantly lowered and high cycle stress life curves become inappropriate for use. Methods that account for this relaxation show reduced annual fatigue damage compared to current methodology.

- Due to the large contribution of the dredging cycle, in combination with high stress ranges, the fatigue lives of the welded details in the bottom opening corners are below the required minimum of 20 years. With an average contribution to the fatigue damage of 97% it is concluded that the dredging cycle is the sole cause for this damage in the bottom opening corners of the hopper dredger. The main contribution of the wave loading is its 15% addition to the still water loading and unloading cycle.

- The stress in the hot spots is found to be bi-axial and loading is proportional. This multi-axiality in combination with the high stress ranges is analysed with three plasticity correction models which are used to calculate pseudo-elastic equivalent stress ranges. It is concluded that the use of such methods has little effect on fatigue life prediction and introduces a lot of additional uncertainties. This concerns selection of a suitable SN-curve for pseudo hot spot stresses and implementation of mean stress corrections. The stress ranges are too low to see a distinct difference between linear-elastic and pseudo elastic stress ranges considering either uni-axial or bi-axial stress states. Pseudo principal hot spot stress ranges are found to be on average 5% higher relative to the elastic stress ranges. If higher hot spot stresses where to be found, the difference between linear elastic and pseudo elastic stresses increase exponentially and the use of a plasticity correction method is required to avoid overestimation of fatigue life prediction. The use of this stress in combination with initial considered BV corrosion curves is deemed to give conservative fatigue life predictions but assures safe design.

- The magnitude of the bi-axiallity ratio makes the application of the proposed bi-axial plasticity correction methods much more significant even if the same stress ranges as found in the analysed hopper dredger are considered. Negative ratios lead to a serious increase of the pseudo hot spot stress range and makes uni-axial Neuber's relatively non-conservative.

- A decisive conclusion on whether the dredging cyclic loading could be seen as a low-cycle fatigue phenomenon cannot be made. The cycles to failure off all hot spot exceed the low-cycle fatigue limit if the mean SN-curve with a survival probability of 50% is used. The small difference between pseudo- and linear-elastic stresses adds up to this.

The performed research leads to the overall conclusion that the dredging cycle is an important parameter in the assessment of the structural integrity of a hopper dredger design. Fatigue life prediction greatly depends on the dredging cycle description and effect of the wave loading. Alternative methods and considerations to the current assessment procedure suggest that current methodology is too conservative. However, calculated fatigue life of the welded joint is still below the desired period. Strong indications that the dredging cycle could be seen as low-cycle fatigue are not confirmed and specific assessment approaches for such a phenomenon do not seem to be required in case of the analysed hopper dredger.

## 6.2. Recommendations

Analysis of the survey reports has shown that fatigue damage cases are not that well documented in practice. Often a crack is reported without additional information of the type of detail nor the type of failure. Pictures are made of the repairs but not the cracked damage before repair. If certain specific damages are repetitive and if research is done to prevent these damages in future designs, it would greatly improve the process and understanding of the problem if these damages would be reported in more detail. Quick reparation is better for continuity of operations but a damage database with detailed reports would improve the overall evolution of ship design. Also, further research should be done on the actual operating profile of the hopper dredging in practice. Analysed dredging shows that dredging cycle frequency could be underestimated in fatigue assessment.

The fatigue assessment done in this thesis is based on the simplified approach which uses deterministic wave

load cases to describe the long term stress range distribution. A spectral fatigue analysis could give a more detailed description of the cyclic response of the ship in different sea states. A hydrodynamic analysis of the entire ships leads to a direct calculation between the wave loading and the stresses in the structure. This analysis, in the frequency domain, will give better understanding of the relation between the structural response and the wave loading and could even lead to more suitable deterministic wave load cases for hopper dredgers specifically.

It is found that the weir level is an important parameter in the description of the dredging cycle. This is due to the dependency of the cargo pressure on the level in the hopper. The behaviour of the soil inside the dredger is however not precisely known and a more detailed analysis of the density distribution though the hopper would provide a more accurate calculation of pressures on the inner hopper plating. A lot is known about settling of the soil particles and the speed at which the hopper is full but the effect of this on the structure still lacks knowledge.

It could be interesting to see what the effect is of erosion on the edge of the insert plate and which SN-curve curve is best suitable to calculate the service life of the insert plate. Erosion causes critical notches in the material which could propagate as cracks and negatively influence the fatigue life.

Weld root failure has not been addressed in this thesis due to the choice of using the hot spot stress concept which requires complex structural stress methodology to determine weld root structural stress. In case of partial penetration or filled welds the weld root has usually a higher stress concentration factor compared to the weld toe which suggest that the change of crack initiation at the weld root is considerably higher than at the weld toe. The residual stress in the root is however often compressive due to the thermal influence of the weld. This lowers the mean stress and therefore it is not self-evident that root failure is dominant [26]. In this thesis the residual stress is taken into account by assuming relaxation. If this magnitude of relaxation is also found at the weld root this could make root failure more likely. Therefore it would be interesting to research what the material behaviour at the weld root is due to the load profile of the dredging cycle.

Further research on the application of different damage accumulation models could provide a more accurate total damage estimation of combined still water and wave loading. Real time strain measurements at hot spots in the bottom opening corners of an operational hopper dredger will result in load time series data which could be evaluated with rainflow cycle counting. This data could be used for validation of the plasticity correction of the principal hot spot stress range and the effectiveness of the wave contribution to the dredging cycle in terms of probability.

It is recommended to extend the low cycle fatigue analysis to area where cracks have been found at the connection between the cross beams and the coaming. It would also be interesting to apply the fatigue assessment methods to other V- and W-shaped hopper dredger. The structural behaviour of a w-shaped hopper is expected to be different due to the greater number of discharge openings and a cellular keel that will contribute to the longitudinal strength of the ship. Despite the fact that the cross section is about 85% effective it is expected to have a significant effect on the stress levels in the connection of the transverse and longitudinal bulkheads due to the vertical displacement relative to the bottom plating.

Validation of using the principal hot spot stress range in combination with multi-axial strain estimation methods is not included in this thesis. However, validation should be done so that the procedures could be implemented in the hot spot stress fatigue assessment of the dredging cycle in case of low-cycle fatigue. This could be done using numerical tools such as non-linear finite element analysis or by experimental low-cycle fatigue testes of welded and non-welded details. Finite element analysis has been proven to give accurate results regarding non-linear fatigue analysis and takes into account plane stress and strain behaviour. Experiments are not practical on a 1:1 scale and testing of small scale specimens introduces additional uncertainties. It is therefore recommended to use a solid model analysed with the finite element method.

Analysis of the effect of the dredging cycle on crack propagation after initiation would provide knowledge on the severity of the initiated crack. Knowing the crack propagation behaviour, the severity of an initiated crack could be quantified when the hopper dredger is operational and the classification society could approve continuation of operations until its next survey.

# 7

# Discussion

The focus of this thesis is on the role of the dredging cycle and the aim is to determine the effect of the dredging cycle according its fatigue damage relative to the fatigue damage induced by the waves. The executed research provides an overall description of which parameters are important in fatigue assessment of a hopper dredger and is a step closer to a procedure tailored for such a ship. It is shown that the dredging cycle is the main parameter that determines the entire fatigue life of the hot spots in the bottom opening corner. It cannot be concluded that cyclic loading of the dredging cycle is a low cycle fatigue phenomenon due to the magnitude of its stress range. This is however concluded from one hopper dredger design and it cannot be expected that the values found in this hopper are the upper bound stresses in all hoppers. It may very well be that higher stresses are found in the hopper dredgers that have shown cracks in the hull structure. A distinct explanation for fatigue cracks in hopper dredgers hull structures is therefore not found. Considerations of alternative methods of mean stress correction and damage accumulation even increase the expected fatigue life relative to the current methodology. The stress ranges at the hot spots in the welded joint do however result in short fatigue life predictions within the desired 20 year design life while the ship does not require fatigue analysis according to BV rules due to its length. This dredger is not equal to the dredgers that are damaged but the short fatigue lives in combination with the higher than expected dredging cycle frequency suggest that underestimation of the dredging cycle is the cause.

The fatigue assessment in this thesis is based on a simplified approach due to the static nature of the dredging cycle. Wave loading in the dredging cycle however, significantly increase the stress range used for calculation and a more detailed description of the wave loading based on spectral or time domain analysis could result in a more accurate description of the dredging cycle. Also, the wave contribution to the dredging cycle range is based on a shape parameter $\gamma = 1$. This parameter does have effect on the wave stress range individually and it could therefore result in a slightly under- or over estimation of the total dredging cycle stress range. Wave loads during loading time of the hopper is not taken into account in the fatigue calculation. It may be possible that structural behaviour of the hull to wave loading is different when the hopper not entirely filled when the soil is considered to behave as a fluid. Wave stress ranges are small and therefore it is assumed that that this assumption is not significantly affects the fatigue calculation.

The single tuning point limits the analysis to the area amidships. It is therefore not possible to exclude that higher stressed areas are present in the hopper dredger. The vertical bending moment is however maximum at the tuning point and is of much larger order of magnitude compared to the wave induces hull girder loads. Also, the local transverse pressure difference is equal along the length of the hopper area and a increase of cross sectional loading is not expected.

The significant contribution of the local pressure difference in combination with the effect of the weir level makes the use of specific densities to the describe the cargo questionable. Particle settling in the hopper could divide the cargo into a solid and a liquid part that results in additional sloshing behaviour that could increase the maximum stress due to wave induced inertial loads.

Despite the fact that the use of the hot spot stress in low-cycle fatigue should be validated some other limita-

tions are associated with the selection of this stress concept. Low-cycle fatigue is a strain-based phenomenon that is most accurately described by the stress-strain relation in the notch. The hot spot stress is a method to linearise the stress and strain at a notch and could be seen as a somewhat fictive entity to simplify the complex stress distribution. It is therefore difficult to relate the local hot spot stress and strain, which are found with Neuber's rule, to more realistic stresses and strains used in the strain-life curve. If mean stress effects are an issue and the stress range requires significant plasticity correction, the notch stress concept is more suitable and a strain life curve including morrow mean stress correction as presented in chapter 2 should be deployed.

# A

# Appendix A

## A.1. Dredging cycle properties

Table A.1: Detailed dredging cycle specifications of analysed hopper dredger

| Load condition | Cargo weight [tonnes] | Cargo volume [$m^3$] | Weir level [mm] | Draught [mm] | Specific density [$kg/m^3$] | Vertical SWBM [Nmm] |
|---|---|---|---|---|---|---|
| 1 | 0 | 0 | 0 | 4529 | 0 | -5.04E+11 |
| 2 | 5222 | 4017 | 6142 | 5628 | 1300 | -9.49E+10 |
| 3 | 10444 | 8034 | 8742 | 6728 | 1300 | 3.14E+11 |
| 4 | 15666 | 12051 | 10642 | 7827 | 1300 | 7.24E+11 |
| 5 | 20888 | 16068 | 15142 | 8926 | 1300 | 1.13E+12 |
| 6 | 22495 | 16068 | 15142 | 9337 | 1400 | 1.26E+12 |
| 7 | 24102 | 16068 | 15142 | 9689 | 1500 | 1.35E+12 |
| 8 | 25709 | 16068 | 14792 | 10041 | 1600 | 1.45E+12 |
| 9 | 25238 | 15067 | 14042 | 10041 | 1675 | 1.46E+12 |
| 10 | 25238 | 14021 | 12792 | 10043 | 1800 | 1.46E+12 |
| 11 | 25238 | 13283 | 12192 | 10045 | 1900 | 1.47E+12 |
| 12 | 25238 | 12619 | 11692 | 10047 | 2000 | 1.47E+12 |

# B

# Appendix B

## B.1. Finite element results

### B.1.1. Model calibration accuracy

Forces in y- and z-direction and moments in all three directions are applied at the aft side of the cargo hold model to realise accurate hull girder loads at the tuning point. At the fore side of the cargo hold model is constraint in translation and rotation in all directions as it is clamped. A rigid body element RBE2 is modelled at this side which is a single node that is connected to all nodes in the cross section at the fore side and the clamped constraint is applied on this node. Similar to the fore side, a rigid body element is connected to all nodes at the cross section at the aft side without any constraint. The nodes are located only in the y-z plane so the rigid body element inhibits rotation of the individual nodes and prohibits translation in all directions.

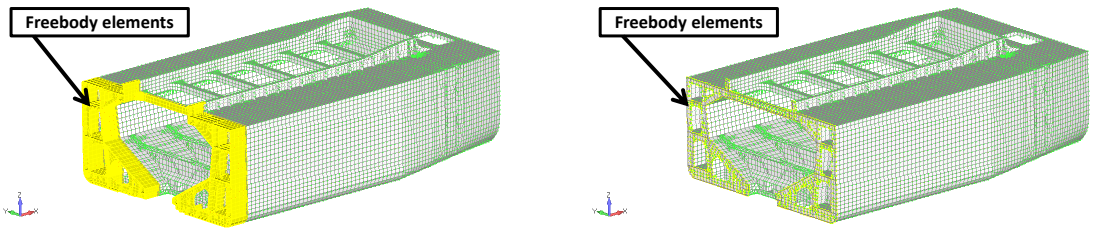


(a) (b)

Figure B.1: **(a)** Modelled freebody elements used for tuning of the model, **(b)** Modelled freebody nodes used for tuning of the model

Femap freebodies are used to measure the hull girder loads at the tuning point. The total summation of the nodal forces and moments is calculated in the centre of the freebody cross section which represent the shear forces and moments of still water and wave loading.

$$F_{tuning,y} = F_{shear,horizontal} - \sum_{n=1}^{k} F_{y,n} \tag{B.1}$$

$$F_{tuning,z} = F_{shear,vertical} - \sum_{n=1}^{k} F_{z,n} \tag{B.2}$$

$$M_{tuning,x} = M_{torsion} - \sum_{n=1}^{k} F_{y,n}(z_n - z_{neutral}) + F_{z,n}(y_n - y_{neutral}) \tag{B.3}$$

$$M_{tuning,y} = M_{vertical} - \sum_{i=1}^{k} F_{x,i}(z_i - z_{neutral}) \tag{B.4}$$

$$M_{tuning,z} = M_{horizontal} - \sum_{i=1}^{k} F_{x,i}(y_i - y_{neutral}) \tag{B.5}$$

Table B.1: Tuning point accuracy dredging cycle load steps

| | $F_x$ | | $F_y$ | | $F_z$ | |
|---|---|---|---|---|---|---|
| Load condition | Model [N] | Error [%] | Model[N] | Error [%] | Model[N] | Error [%] |
| 1 | -5.49E+05 | - | 1.31E+00 | 0.00% | 3.43E+03 | 0.03% |
| 2 | 1.44E+06 | - | 9.47E-01 | 0.00% | -3.96E+03 | -0.04% |
| 3 | 4.51E+06 | - | 1.61E+00 | 0.00% | 4.13E+03 | 0.04% |
| 4 | 7.93E+06 | - | 9.51E-01 | 0.00% | -1.52E+04 | -0.15% |
| 5 | 1.97E+07 | - | 7.52E-01 | 0.00% | -2.38E+02 | 0.00% |
| 6 | 2.09E+07 | - | 1.11E+00 | 0.00% | -2.91E+03 | -0.03% |
| 7 | 1.88E+07 | - | 6.87E-01 | 0.00% | -2.89E+03 | -0.03% |
| 8 | 1.54E+07 | - | 1.37E+00 | 0.00% | -4.32E+04 | -0.43% |
| 9 | 1.39E+07 | - | 1.20E+00 | 0.00% | 1.14E+04 | 0.11% |
| 10 | 1.27E+07 | - | 6.30E-01 | 0.00% | -6.79E+03 | -0.07% |
| | $M_x$ | | $M_y$ | | $M_z$ | |
| 1 | -4.49E+04 | 0.04% | 5.04E+11 | 0.09% | 6.67E+04 | 0.07% |
| 2 | 1.33E+05 | 0.13% | 9.52E+10 | 0.36% | -3.57E+04 | 0.04% |
| 3 | -5.51E+03 | 0.01% | -3.15E+11 | 0.13% | -2.44E+04 | 0.02% |
| 4 | 4.61E+04 | 0.05% | -7.20E+11 | 0.42% | -4.14E+04 | 0.04% |
| 5 | -8.67E+03 | 0.01% | -1.13E+12 | 0.03% | -3.38E+04 | 0.03% |
| 6 | -3.57E+04 | 0.04% | -1.45E+12 | 0.09% | 9.86E+03 | 0.01% |
| 7 | -3.16E+04 | 0.03% | -1.46E+12 | 0.13% | 1.94E+05 | 0.19% |
| 8 | -6.35E+03 | 0.01% | -1.46E+12 | 0.05% | -9.98E+03 | 0.01% |
| 9 | -3.19E+04 | 0.03% | -1.47E+12 | 0.07% | 2.43E+03 | 0.00% |
| 10 | 2.25E+04 | 0.02% | -1.47E+12 | 0.10% | 6.62E+04 | 0.07% |

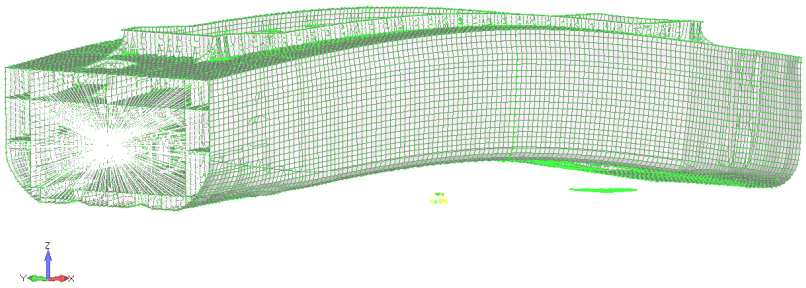

Figure B.2: Deformed cargo hold model due to maximum hogging moment

## B.1.2. Contour plots

Table B.2: Tuning point accuracy wave loads empty hopper

| | | $F_x$ | | $F_y$ | | $F_z$ | |
|---|---|---|---|---|---|---|---|
| Load case | | Model [N] | Error [%] | Model[N] | Error [%] | Model[N] | Error [%] |
| a | max | -7.28E+05 | - | 3.72E-01 | 0.00% | 1.83E+03 | 0.02% |
| | min | -3.76E+05 | - | 3.74E-01 | 0.00% | -1.05E+03 | -0.01% |
| b | max | - | - | - | - | - | - |
| | min | - | - | - | - | - | - |
| c | max | -6.00E+05 | - | 1.88E-01 | 0.00% | -3.49E+03 | -0.03% |
| | min | -6.03E+05 | - | 3.95E+02 | 0.00% | -2.71E+03 | -0.03% |
| d | max | -5.68E+05 | - | 2.54E-01 | 0.00% | 1.15E+03 | 0.01% |
| | min | -5.68E+05 | - | 4.29E+02 | 0.00% | -1.58E+03 | -0.02% |
| | | $M_x$ | | $M_y$ | | $M_z$ | |
| Load case | | Model [Nmm] | Error [%] | Model[Nmm] | Error [%] | Model[Nmm] | Error [%] |
| a | max | 2.69E+04 | 0.03% | 5.11E+11 | 0.03% | 4.69E+05 | 0.47% |
| | min | -3.50E+04 | 0.03% | 4.96E+11 | 0.08% | -5.46E+04 | 0.05% |
| b | max | - | - | - | - | - | - |
| | min | - | - | - | - | - | - |
| c | max | -3.91E+10 | 0.00% | 5.11E+11 | 0.03% | -1.03E+11 | 0.00% |
| | min | 3.91E+10 | 0.00% | 4.97E+11 | 0.04% | 1.02E+11 | 0.00% |
| d | max | -4.42E+07 | 0.44% | 5.11E+11 | 0.01% | -1.03E+11 | 0.00% |
| | min | 8.89E+05 | 0.89% | 4.96E+11 | 0.09% | 1.03E+11 | 0.00% |

Table B.3: Tuning point accuracy wave loads fully loaded hopper

| | | $F_x$ | | $F_y$ | | $F_z$ | |
|---|---|---|---|---|---|---|---|
| Load case | | Model [N] | Error [%] | Model[N] | Error [%] | Model[N] | Error [%] |
| a | max | 2.07E+07 | - | 1.26E+00 | 0.00% | -1.17E+02 | 0.00% |
| | min | 2.11E+07 | - | 1.32E+00 | 0.00% | -2.22E+00 | 0.00% |
| b | max | 2.38E+07 | - | 1.25E+00 | 0.00% | -3.49E-01 | 0.00% |
| | min | 1.80E+07 | - | 1.54E+00 | 0.00% | -4.48E+03 | -0.04% |
| c | max | 1.91E+07 | - | -4.04E-02 | 0.00% | 2.35E+02 | 0.00% |
| | min | 1.97E+07 | - | -4.25E+02 | 0.00% | 1.21E+02 | 0.00% |
| d | max | 1.90E+07 | - | -3.65E+02 | 0.00% | -1.06E+02 | 0.00% |
| | min | 1.91E+07 | - | -8.31E-01 | 0.00% | -2.58E+02 | 0.00% |
| | | $M_x$ | | $M_y$ | | $M_z$ | |
| Load case | | Model [Nmm] | Error [%] | Model[Nmm] | Error [%] | Model[Nmm] | Error [%] |
| a | max | 3.26E+04 | 0.03% | -1.46E+12 | 0.02% | -2.12E+04 | 0.02% |
| | min | -2.91E+04 | 0.03% | -1.47E+12 | 0.02% | 4.08E+06 | 4.08% |
| b | max | -3.20E+04 | 0.03% | -1.47E+12 | 0.03% | -8.39E+05 | 0.84% |
| | min | -1.94E+04 | 0.02% | -1.46E+12 | 0.20% | 2.94E+04 | 0.03% |
| c | max | -3.91E+10 | 0.00% | -1.46E+12 | 0.02% | -1.03E+11 | 0.00% |
| | min | 3.91E+10 | 0.00% | -1.47E+12 | 0.00% | 1.03E+11 | 0.00% |
| d | max | 6.01E+04 | 0.06% | -1.46E+12 | 0.03% | -1.03E+11 | 0.00% |
| | min | 3.85E+07 | 0.39% | -1.47E+12 | 0.25% | 1.03E+11 | 0.00% |

Table B.4: Tuning point accuracy wave loads hopper in ballast navigation condition

| | | $F_x$ | | $F_y$ | | $F_z$ | |
|---|---|---|---|---|---|---|---|
| | Load case | Model [N] | Error [%] | Model[N] | Error [%] | Model[N] | Error [%] |
| a | max | 3.35E+06 | - | 1.41E+00 | 0.00% | 3.27E+03 | 0.03% |
| | min | 2.85E+06 | - | 9.41E-01 | 0.00% | 2.70E+03 | 0.03% |
| b | max | 3.87E+06 | - | 1.10E+00 | 0.00% | 2.60E+02 | 0.00% |
| | min | 2.06E+06 | - | -4.64E+02 | 0.00% | 9.89E+02 | 0.01% |
| c | max | 2.16E+06 | - | 3.42E+03 | 0.03% | 8.06E+03 | 0.08% |
| | min | 4.87E+06 | - | 5.85E+01 | 0.00% | 1.29E+04 | 0.13% |
| d | max | 1.83E+06 | - | 1.46E+02 | 0.00% | -2.63E+04 | -0.26% |
| | min | 1.72E+06 | - | 2.54E+02 | 0.00% | -1.40E+03 | -0.01% |
| | | $F_x$ | | $F_y$ | | $F_z$ | |
| | Load case | Model [N] | Error [%] | Model[N] | Error [%] | Model[N] | Error [%] |
| a | max | 3.35E+06 | - | 1.41E+00 | 0.00% | 3.27E+03 | 0.03% |
| | min | 2.85E+06 | - | 9.41E-01 | 0.00% | 2.70E+03 | 0.03% |
| b | max | 3.87E+06 | - | 1.10E+00 | 0.00% | 2.60E+02 | 0.00% |
| | min | 2.06E+06 | - | -4.64E+02 | 0.00% | 9.89E+02 | 0.01% |
| c | max | 2.16E+06 | - | 3.42E+03 | 0.03% | 8.06E+03 | 0.08% |
| | min | 4.87E+06 | - | 5.85E+01 | 0.00% | 1.29E+04 | 0.13% |
| d | max | 1.83E+06 | - | 1.46E+02 | 0.00% | -2.63E+04 | -0.26% |
| | min | 1.72E+06 | - | 2.54E+02 | 0.00% | -1.40E+03 | -0.01% |

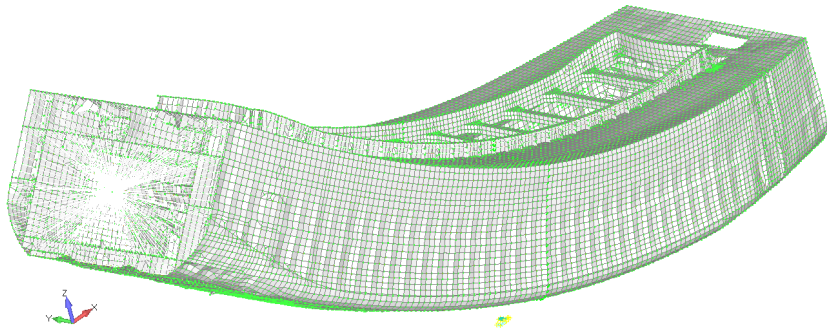

Figure B.3: Deformed cargo hold model due to maximum sagging moment

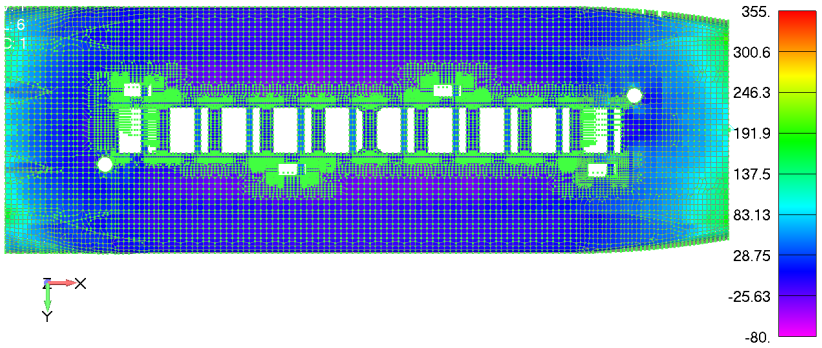


Figure B.4: Bottom view major principal stress hopper in empty hopper condition

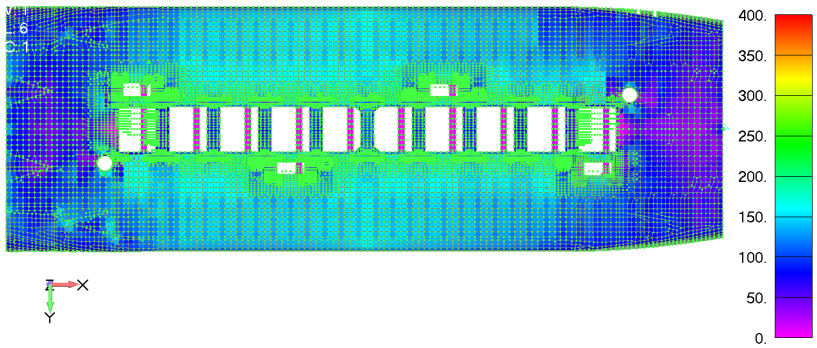


Figure B.5: Bottom view major principal stress hopper in fully loaded hopper condition

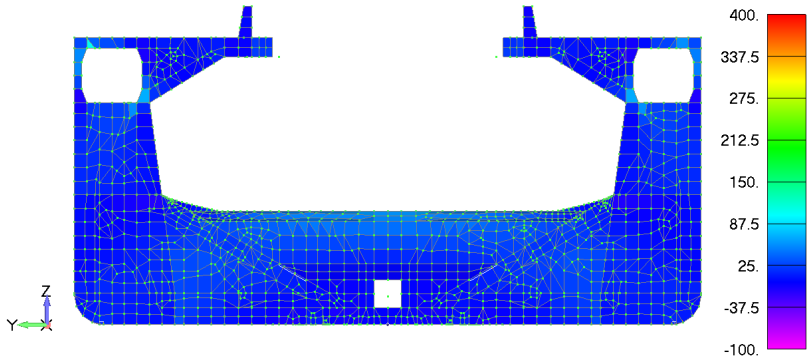


Figure B.6: Mid ship cross section major principal stress empty hopper

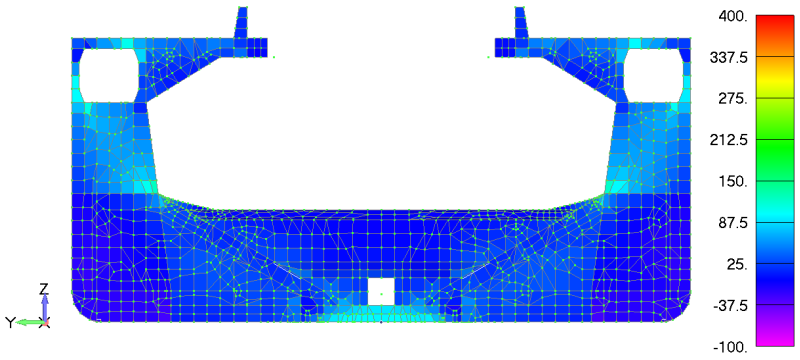


Figure B.7: Mid ship cross section major principal stress fully loaded hopper

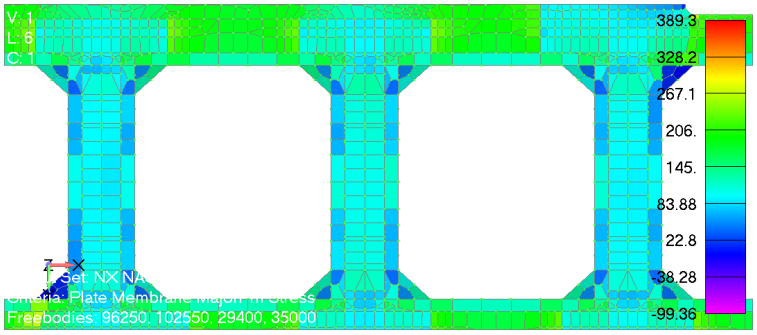


Figure B.8: Bottom view major principal stress maximum load condition bottom door opening amidships

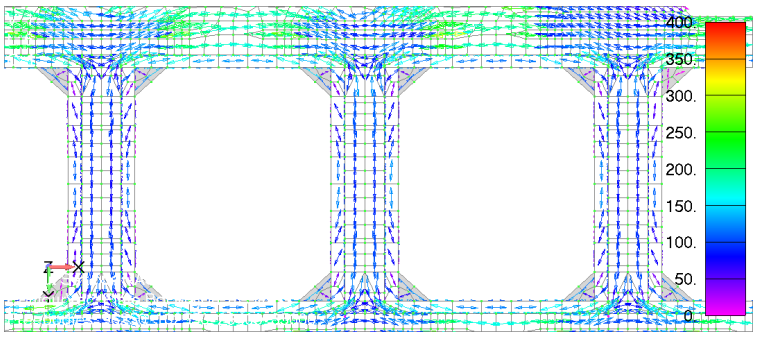


Figure B.9: Bottom view major principal stress directions maximum load condition bottom door opening amidships

# C

# Appendix C

## C.1. Plotted SN-curves

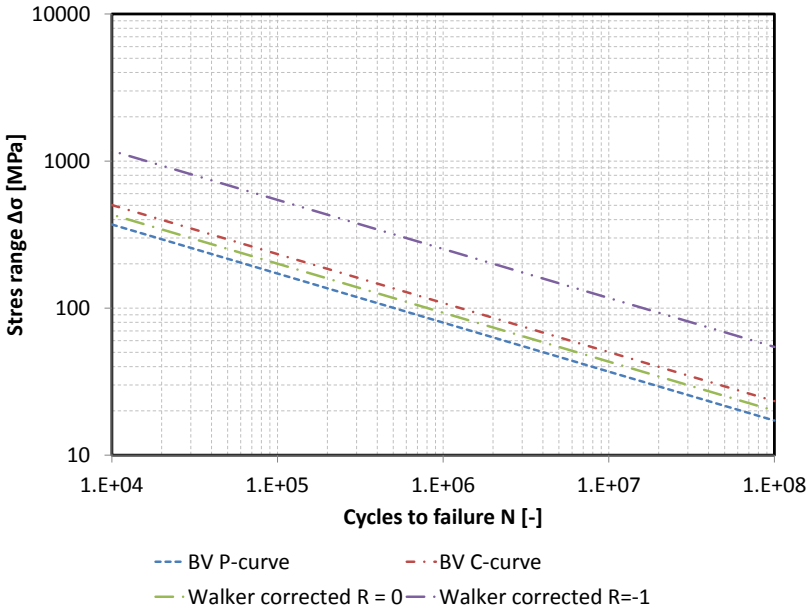


Figure C.1: Walker corrected SN-curves to R = 0 and R = -1

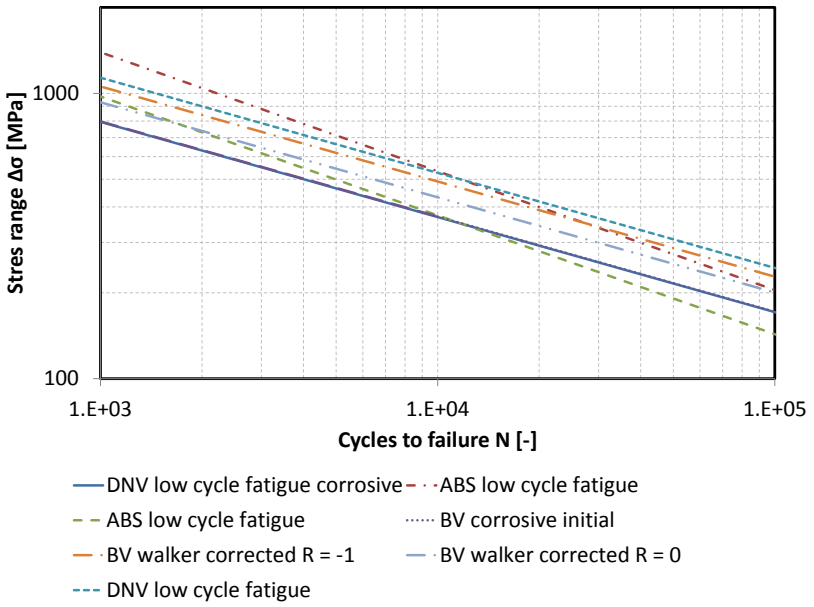


Figure C.2: Low-cycle SN curves used for pseudo hot spot stress proposal

# Bibliography


[1] Ssc-418 compensation for openings in primary ship structures. resreport, Ship structure committee 2002, 2002.

[2] Rules for the classification of steel ships part a, January 2013.

[3] Spectral-based fatigue analysis for floating production, storage and offloading (fpso) installations, February 2014.

[4] Fatigue assessment of offshore structures, February 2014.

[5] Spectral-based fatigue analysis for floating production, storage and offloading (fpso) installations, February 2014.

[6] Common structural rules for bulk carriers and oil tankers, January 2014.

[7] technical background report harmonised csr, June 2014.

[8] Rules for the classification of steel ships part b, July 2014.

[9] Rules for the classification of steel ships part d, July 2014.

[10] Fatigue assessment of ship structures, October 2015.

[11] Guidelines for fatigue assessment of steel ships and offshore structures, September 2016.

[12] Mika Bäckström. Multiaxial fatigue life assessment of welds based on nominal and hot spot stresses. 2003.

[13] Yong Bai. *Marine structural design*. Elsevier, 2003.

[14] Giulio Ballio and Carlo A Castiglioni. A unified approach for the design of steel structures under low and/or high cycle fatigue. *Journal of Constructional Steel Research*, 34(1):75–101, 1995.

[15] OH Basquin. The exponential law of endurance tests. In *proc. ASTM*, volume 10, page 625, 1910.

[16] Stig Berge. On the effect of plate thickness in fatigue of welds. *Engineering Fracture Mechanics*, 21(2): 423–435, 1985.

[17] P Biasotto, V Bonniol, P Cambos, et al. Selection of trading tankers for fpso conversion projects. In *Offshore Technology Conference*. Offshore Technology Conference, 2005.

[18] Branko Blagojević and Želko Domazet. Simplified procedures for fatigue assessment of ship structures. In *IMAM Congress*, 2002.

[19] J Braaksma, R Babuska, JB Klaassens, and C De Keizer. A computationally efficient model for predicting overflow mixture density in a hopper dredger. *Terra et Aqua*, 106:16, 2007.

[20] M W Brown and K J Miller. A theory for fatigue failure under multiaxial stress-strain conditions. *Proceedings of the Institution of Mechanical Engineers*, 187(1):745–755, 1973.

[21] Ionel Chirică, Ștefan Giuglea, and Elena-Felicia Beznea. Fatigue analysis of a ship structural detail. 2009.

[22] L Fo Coffin Jr. A study of the effects of cyclic thermal stresses on a ductile metal. *trans. ASME*, 76:931–950, 1954.

[23] Ademar de Azevedo Cardoso and Silvio Castro Alano. Multiaxial stress in the fatigue life of mechanical parts. Technical report, SAE Technical Paper, 2011.

[24] Gijsbert DE JONG. Classification of dredgers–technical & regulatory developments, 2010.

[25] JH Den Besten. *Fatigue resistance of welded joints in aluminium high-speed craft: A total stress concept*. PhD thesis, TU Delft, Delft University of Technology, 2015.

[26] Y Dong and C Guedes Soares. On the fatigue crack initiation point of load-carrying fillet welded joints. *Towards Green Marine Technology and Transport*, page 407, 2015.

[27] NE Dowling, CA Calhoun, and A Arcari. Mean stress effects in stress-life fatigue and the walker equation. *Fatigue & Fracture of Engineering Materials & Structures*, 32(3):163–179, 2009.

[28] Norman E Dowling. *Mechanical behavior of materials: engineering methods for deformation, fracture, and fatigue*. Pearson, 2012.

[29] BS EN. 1-9 (2005): Design of steel structures. part 1.9: Fatigue. *British Standards Institution, London*, 1993.

[30] Ali Fatemi and Nima Shamsaei. Multiaxial fatigue: An overview and some approximation models for life estimation. *International Journal of Fatigue*, 33(8):948–958, 2011.

[31] Ali Fatemi and Darrell F Socie. A critical plane approach to multiaxial fatigue damage including out-of-phase loading. *Fatigue & Fracture of Engineering Materials & Structures*, 11(3):149–165, 1988.

[32] P Ferreira, J Pinho-da Cruz, and F Teixeira-Dias. Finite element and local strain approach stress-strain predictions in notched alcu4. 5mn specimens. *Iberoam. J. Eng. Mech*, 10(1):93–110, 2006.

[33] Ernest P. Fortino. New approaches to the design of hopper dredges. *Marine Technology*, 17(4):371–384, October 1980.

[34] Ernest P Fortino. New approaches to the design of hopper dredges. *Marine Technology Society Journal*, 17(4), 1980.

[35] Wolfgang Fricke and Adrian Kahl. Comparison of different structural stress approaches for fatigue assessment of welded ship structures. *Marine structures*, 18(7):473–488, 2005.

[36] G Glinka. Residual stresses in fatigue and fracture: Theoretical analyses and experiments. *Advances in Surface Treatments*, 4:413–454, 2014.

[37] TR Gurney. Some comments on fatigue design rules for offshore structures. *INTEGRITY OF OFFSHORE STRUCTURES., 1981,*, pages 219–233, 1981.

[38] Joo-Ho Heo, Joong-Kyoo Kang, Yooil Kim, IS Yoo, KS Kim, and HS Urm. A study on the design guidance for low cycle fatigue in ship structures. In *Proceedings of the 9th Symposium of Practical Design of Ships and Other Floating Structures*, 2004.

[39] Adolf Hobbacher et al. *Recommendations for fatigue design of welded joints and components*. Springer, 2009.

[40] M Hoffmann and T Seeger. A generalized method for estimating multiaxial elastic-plastic notch stresses and strains, part 1: Theory. *Journal of Engineering Materials and Technology*, 107(4):250–254, 1985.

[41] Wenbo Huang. The frequency domain estimate of fatigue damage of combined load effects based on the rain-flow counting. *Marine Structures*, 52:34–49, 2017.

[42] K Hussain and ER De Los Rios. Monotonic and cyclic stress-strain behaviour of high strength steel. *Metallurgical Science and Tecnology*, 11(1), 1993.

[43] Bertil Jonsson, Gerd Dobmann, AF Hobbacher, M Kassner, and Gary Marquis. *IIW guidelines on weld quality in relationship to fatigue strength*. Springer, 2016.

[44] ML Kaminski et al. Sensing and understanding fatigue lifetime of new and converted fpsos. In *Offshore Technology Conference*. Offshore Technology Conference, 2007.

[45] Kamal Karunan, Mitao Ohga, Ranjith Dissanayake, and Sudath Siriwardane. A combined high and low cycle fatigue model to estimate life of steel bridges. *Journal of Engineering and Technology Research*, 2 (8):144–160, 2010.

[46] David P Kihl and Shahram Sarkani. Mean stress effects in fatigue of welded steel joints. *Probabilistic engineering mechanics*, 14(1):97–104, 1999.

[47] Young-Hoon Kim, Ji-Ho Song, and Jun-Hyub Park. An expert system for fatigue life prediction under variable loading. *Expert Systems with Applications*, 36(3):4996–5008, 2009.

[48] Christian Lalanne. *Mechanical vibration and shock analysis, fatigue damage*, volume 4. John Wiley & Sons, 2010.

[49] Kwang-Soo Lee and Ji-Ho Song. Estimation methods for strain-life fatigue properties from hardness. *International Journal of Fatigue*, 28(4):386–400, 2006.

[50] Yung-Li Lee. *Fatigue testing and analysis: theory and practice*, volume 13. Butterworth-Heinemann, 2005.

[51] Yung-Li Lee, Mark E Barkey, and Hong-Tae Kang. *Metal fatigue analysis handbook: practical problem-solving techniques for computer-aided engineering*. Elsevier, 2011.

[52] Inge Lotsberg. *Fatigue design of marine structures*. Cambridge University Press, 2016.

[53] Kenneth Macdonald. *Fracture and fatigue of welded joints and structures*. Elsevier, 2011.

[54] Takao KAMATA Jiho SONG Haruo HIMURO Makoto KIKUKAWA, Masahiro JONO. Low-cycle fatigue under varying strain conditions : Effects of the mean plastic strain and the stress factor. *Bulletin of JSME*, 20(140):145–152, 1977.

[55] M Malikoutsakis and G Savaidis. Fatigue assessment of thin-welded joints with pronounced terminations. *Fatigue & Fracture of Engineering Materials & Structures*, 37(7):782–799, 2014.

[56] Samuel S Manson. Behavior of materials under conditions of thermal stress. 1954.

[57] A Mansour and A Thayamballi. Probability based ship design; loads and load combinations. Technical report, MANSOUR ENGINEERING INC BERKELEY CA, 1993.

[58] John P. Martin and Louis J. Mauriello. Hopper dredgers and certain aspects of their design. *Marine Technology*, 20(2):164–176, April 1983.

[59] M Matsuishi and T Endo. Fatigue of metals subjected to varying stress. *Japan Society of Mechanical Engineers, Fukuoka, Japan*, 68(2):37–40, 1968.

[60] Ahmed Megharbi. Low cycle fatigue of fpso ship structure. 2015.

[61] Dr.ir. Sape A. Miedema. Dredging processes, January 2013.

[62] SA Miedema. A sensitivity analysis of the scaling of tshd's. *WEDA XXIX & Texas A&M*, 40:14–17, 2009.

[63] M A Miner. 'cumulative damage in fatigue'. *Trans ASME*, 1945.

[64] Said Fawad Mohammadi, Nelson Szilard Galgoul, Uwe Starossek, and Paulo Mauricio Videiro. An efficient time domain fatigue analysis and its comparison to spectral fatigue assessment for an offshore jacket structure. *Marine Structures*, 49:97–115, 2016.

[65] Krzysztof Molski and Grzegorz Glinka. A method of elastic-plastic stress and strain calculation at a notch root. *Materials Science and Engineering*, 50(1):93–100, 1981.

[66] Arvid Naess and Torgeir Moan. *Stochastic dynamics of marine structures*. Cambridge University Press, 2012.

[67] Naoki Osawa, Norio Yamamoto, Tetsuji Fukuoka, Junji Sawamura, Hiroshi Nagai, and Shingo Maeda. Study on the preciseness of hot spot stress of web-stiffened cruciform welded joints derived from shell finite element analyses. *Marine Structures*, 24(3):207–238, 2011.

[68] Jeom Kee Paik, Anil K Thayamballi, P Terndrup Pedersen, and Young Il Park. Ultimate strength of ship hulls under torsion. *Ocean Engineering*, 28(8):1097–1133, 2001.

[69] Dieter Radaj. *Design and analysis of fatigue resistant welded structures*. Elsevier, 1990.

[70] Dieter Radaj, Cetin Morris Sonsino, and Wolfgang Fricke. *Fatigue assessment of welded joints by local approaches*. Woodhead publishing, 2006.

[71] Jaap Schijve et al. *Fatigue of structures and materials*. Springer, 2001.

[72] C Guedes Soares and T Moan. Model uncertainty in the long-term distribution of wave-induced bending moments for fatigue design of ship structures. *Marine Structures*, 4(4):295–315, 1991.

[73] C Guedes Soares, Y Garbatov, and H Von Selle. Fatigue damage assessment of ship structures based on the long-term distribution of local stresses. *International Shipbuilding Progress*, 50(1, 2):35–55, 2003.

[74] Darrell Frederick Socie, Michael R Mitchell, and Edward M Caulfield. *Fundamentals of modern fatigue analysis*. College of Engineering, University of Illinois, 1978.

[75] NORSOK Standard. Assessment of structural integrity for existing offshore load-bearing structures. *NORSOK Standard N-006, March*, 2009.

[76] HS Urm, IS Yoo, JH Heo, SC Kim, and I Lotsberg. Low cycle fatigue strength assessment for ship structures. In *Proc. of 9th Int. Symp. on Pract. Design of Ships and Floating Struct.(PRADS'2004), Schiffbautech. Ges., Seehafen Verlag, Hamburg*, 2004.

[77] PS van Lieshout, JH den Besten, and ML Kaminski. Comparative study of multiaxial fatigue methods applied to welded joints in marine structures. *Frattura ed Integrità Strutturale*, (37):173–192, 2016.

[78] Bureau Veritas. Guidance on fatigue check of dredgers. 2015.

[79] Det Norske Veritas. Fatigue design of offshore steel structures. Technical report, DNV-RP-C203, 2010.

[80] Norske Veritas. *Fatigue assessment of ship structures*. Det Norske Veritas, 2001.

[81] Wim J Vlasblom. *Design of dredging equipment*. 2005.

[82] K Walker. The effect of stress ratio during crack propagation and fatigue for 2024-t3 and 7075-t6 aluminum. In *Effects of environment and complex load history on fatigue life*. ASTM International, 1970.

[83] Xiaozhi Wang, Joong-Kyoo Kang, Yooil Kim, and Paul H Wirsching. Low cycle fatigue analysis of marine structures. In *25th International Conference on Offshore Mechanics and Arctic Engineering OMAE2006, Hamburg, Germany*, 2006.

[84] T Wehner and A Fatemi. Effects of mean stress on fatigue behaviour of a hardened carbon steel. *International Journal of Fatigue*, 13(3):241–248, 1991.

[85] BK Yuen, TS Koko, H Polezhaeva, and L Jiang. Mean stress assessmen in fatigue analysis and design. *Washington, Ship Structure Committee*, 2013.

[86] Bin Zhang and Torgeir Moan. Mean stress effect on fatigue of welded joint in fpsos. *stress*, 2:2, 2006.

[87] Chen Zhanglan, Ye Jiawei, Wang Dongjiao, and Yuan Hongli. The numerical prediction of draghead motion of trailing suction hopper dredger in time domain. *Ocean Engineering*, 91:146–151, 2014.